



TECNOLÓGICO  
NACIONAL DE MÉXICO®

Instituto Tecnológico de Pabellón de Arteaga



**“Design and Characterization of an Advanced pH Instrument  
Using Artificial Intelligence Algorithms For Vertical Farming  
Applications”**

TESIS

Para Obtener el Grado de:

Maestro en Ciencias en Ingeniería Mecatrónica

PRESENTA:

Ing. Rolando Moisés Hinojosa Meza

TUTORES:

Dr. Paulino Vacas Jacques

Dra. Nivia Iracemi Escalante García

Dr. Martín Montes Rivera

Pabellón de Arteaga, Ags., mayo del 2023



**INSTITUTO TECNOLÓGICO DE PABELLÓN DE ARTEAGA**  
**SUBDIRECCIÓN ACADÉMICA**  
**MAESTRÍA EN CIENCIAS EN INGENIERÍA MECATRÓNICA**

Tesis:

**“Design and Characterization of an Advanced pH Instrument Using Artificial Intelligence Algorithms For Vertical Farming Applications”**

Presenta:

Ing. Rolando Moisés Hinojosa Meza

Dirigida por:

Dr. Paulino Vacas Jacques

Dra. Nivia Iracemi Escalante García

Dr. Martín Montes Rivera

Sinodales:

Dr. José Ernesto Olvera González

M. en C. José Guillermo Batista Ortiz

Pabellón de Arteaga, Ags., mayo del 2023

## **AGRADECIMIENTOS**

Agradezco a mi director de tesis, Dr. Paulino Vacas Jacques y a mis codirectores de Tesis, Dra. Nivia Iracemi Escalante García y Dr. Martín Montes Rivera por su guía, apoyo y orientación durante todo el proceso de investigación. Sus conocimientos y experiencia han sido fundamentales para el éxito de este trabajo.

Agradezco a mi familia y amigos por su incondicional apoyo emocional durante esta etapa. Sus palabras de aliento y motivación me han impulsado a seguir adelante y superar los obstáculos.

Agradezco al Dr. José Ernesto Olvera González por creer en mí y darme la oportunidad de realizar mis estudios en el Laboratorio de Iluminación Artificial.

Agradezco a mis profesores por sus valiosos aportes y consejos durante mi formación. Sus conocimientos y sugerencias han enriquecido el trabajo y me han ayudado a mejorar como investigador.

Finalmente, agradezco a todos aquellos que, de una forma u otra, han contribuido a que este proyecto se haya llevado a cabo. Este logro es también suyo y espero poder seguir contando con su apoyo en el futuro.



TECNOLÓGICO  
NACIONAL DE MÉXICO®



INSTITUTO TECNOLÓGICO  
de Pabellón de Arteaga

**ITEC**

Pabellón de Arteaga, Ags.,

**14/abril/2023**

**MES. EDGAR ZACARÍAS MORENO  
SUBDIRECTOR ACADÉMICO**

**PRESENTE**

Por medio del presente doy el visto bueno a la Tesis de Maestría titulada **“DESIGN AND CHARACTERIZATION OF AN ADVANCED PH INSTRUMENT USING ARTIFICIAL INTELLIGENCE ALGORITHMS FOR VERTICAL FARMING APPLICATIONS”** del estudiante **ROLANDO MOISÉS HINOJOSA MEZA** con numero de control M151050126 de la Maestría en Ciencias en Ingeniería Mecatrónica. Dicho trabajo ya fue revisado por cada uno de los miembros del comité tutorial y el estudiante ya realizo los cambios sugeridos, por lo que autorizamos su impresión.

Sin otro particular, aprovecho la ocasión para enviarle un cordial saludo, quedo de Usted.

**ATENTAMENTE**

*Excelencia en Educación Tecnológica®  
Tierra Siempre fértil®*

**DR. PAULINO VACAS JACQUES  
MIEMBRO DE COMITÉ TUTORIAL**

**DRA. NIVIA IRACEMI ESCALANTE GARCÍA  
MIEMBRO DE COMITÉ TUTORIAL**

**DR. MARTÍN MONTES RIVERA  
MIEMBRO DE COMITÉ TUTORIAL**



TECNOLÓGICO  
NACIONAL DE MÉXICO®



INSTITUTO TECNOLÓGICO®  
de Pabellón de Arteaga

**ITEC**

Pabellón de Arteaga, Ags.,

**2/mayo/2023**

**ING. ROLANDO MOISÉS HINOJOSA MEZA**  
**ESTUDIANTE DE LA MAESTRÍA EN CIENCIAS EN INGENIERÍA MECATRÓNICA**  
**NO. DE CONTROL M151050126**

**PRESENTE**

Por medio de este conducto me permito comunicar a Usted que habiendo recibido los votos aprobatorios de los revisores de su trabajo de Tesis titulado: **“DESIGN AND CHARACTERIZATION OF AN ADVANCED PH INSTRUMENT USING ARTIFICIAL INTELLIGENCE ALGORITHMS FOR VERTICAL FARMING APPLICATIONS”**, hago de su conocimiento que puede imprimir dicho documento y continuar con los trámites para la presentación de su examen de grado.

Sin otro particular, aprovecho la ocasión para enviarle un cordial saludo, quedo de Usted.

**ATENTAMENTE**

*Excelencia en Educación Tecnológica®*

*Tierra Siempre fértil®*

**MES. EDGAR ZACARÍAS MORENO**  
**SUBDIRECTOR ACADÉMICO**

## ABSTRACT

### “Design and Characterization of an Advanced pH Instrument using *Artificial Intelligence Algorithms for Vertical Farming Applications*”

By: Ing. Rolando Moises Hinojosa Meza

Global Vertical Farming (VF) applications with characteristic Industry 4.0 connectivity will become more and more relevant as the challenges of food supply continue to increase worldwide. A cost-effective and portable instrument that enables accurate pH measurements for VF applications is presented. We demonstrate that by performing a well-designed calibration of the sensor, a near Nernstian response, 57.56 [mV/pH], ensues. The system is compared to a ten-fold more expensive laboratory gold standard, and is shown to be accurate in determining the pH of substances in the 2–14 range. The instrument yields precise pH results with an average absolute deviation of 0.06 pH units and a standard deviation of 0.03 pH units. The performance of the instrument is ADC-limited, with a minimum detectable value of 0.028 pH units, and a typical absolute accuracy of  $\pm 0.062$  pH units. By meticulously designing bias and amplification circuitry of the signal conditioning stage, and by optimizing the signal acquisition section of the instrument, a (minimum) four-fold improvement in performance is expected. In addition, we proposed an advanced filtering scheme based on Recurrent Neural Networks (RNNs) and Deep Learning to enable efficient control strategies for Vertical Farming (VF) applications. We demonstrate that the best RNN model incorporates five neuron layers, with the first and second containing ninety Long Short-Term Memory neurons. The third layer implements one Gated Recurrent Units neuron. The fourth segment incorporates one RNN network, while the output layer is designed by using a single neuron exhibiting a rectified linear activation function. The RNN models are contrasted with conventional digital Butterworth, Chebyshev I, Chebyshev II, and Elliptic Infinite Impulse Response (IIR) configurations. The RNN digital filtering schemes avoid introducing unwanted oscillations, which makes them more suitable for VF than their IIR counterparts. Finally, by utilizing the advanced features of scaling of the RNN model, we demonstrate that the RNN digital filter can be pH selective, as opposed to conventional IIR filters. Temperature affects pH measurement, producing inaccurate readings. More complex sensors integrate Automatic Temperature Compensation (ATC) because they accurately adjust the electrode calibration for pH when the temperature changes. However, ATC cannot correct for the pH/temperature effects of unknown samples. For this reason, a fuzzy interference system is also proposed to compensate for the temperature effects on pH measurements through a Mamdani interference system, in addition to genetic algorithms to adjust the vertices in the output matrices.

Directed by:

Dr. Paulino Vacas Jacques

Dra. Nivia Iracemi Escalante García

Dr. Martín Montes Rivera

## CONTENTS

	Pág.
<b>I. INTRODUCTION</b> .....	1
1.1 State of the art.....	2
1.2 Problem Definition.....	3
1.3 Objectives.....	4
1.3.1 General.....	4
1.3.2 Specifics.....	4
1.4 Justification.....	4
<b>II. METHODOLOGY</b> .....	4
2.1 Design and Characterization of the Instrument .....	4
2.1.1 Materials.....	5
2.1.1.1 Perception Layer—Sensing Stage.....	6
2.1.1.2. Perception Layer—Signal Conditioning and Signal Acquisition Stages.....	6
2.1.1.3. Network Layer—Bluetooth Wireless Communications Stage.....	8
2.1.1.4. Integration of the Portable pH Instrument.....	8
2.1.2 Methods.....	9
2.1.2.1 pH Sensor Characterization.....	9
2.1.2.2 Preparation of Signal Conditioning, Acquisition, and Transmission.....	10
2.1.2.3. Methodology to Assess the pH of Arbitrary Solutions.....	10
2.2 Comparative Analysis of RNN versus IIR Digital Filtering to Optimize Resilience to Dynamic Perturbations.....	10
2.2.1 Materials.....	10
2.2.1.1 Instrumentation.....	10
2.2.2 Methods.....	11
2.2.2.1 Generation of Dataset.....	12
2.2.2.2 Dataset Augmentation and Splitting.....	12
2.2.2.3 Training Datasets.....	13
2.2.2.4 IIR Digital Filter Designs.....	14
2.2.2.5 RNN Digital Filter Design.....	15
2.3 Design of a fuzzy inference system to compensate for the effect of temperature on pH measurements using genetic algorithms.....	18

2.3.1 Methods.....	18
<b>III. CONCLUSIONS .....</b>	<b>19</b>
<b>IV. BIBLIOGRAPHY .....</b>	<b>21</b>
<b>ANNEX 1. Cost-Effective and Portable Instrumentation to Enable Accurate pH Measurements for Global Industry 4.0 and Vertical Farming Applications .....</b>	<b>24</b>
<b>ANNEX 2. Comparative analysis of RNN versus IIR digital filtering to optimize resilience to dynamic perturbations in pH sensing for Vertical Farming .....</b>	<b>42</b>
<b>ANNEX 3. Temperature compensation of pH measurements using a Fuzzy inference system and genetic algorithms .....</b>	<b>61</b>
<b>ANNEX 4. Second place certificate for best paper MICA I 2021 Workshop on Hybrid Intelligent Systems.....</b>	<b>72</b>

## LIST OF FIGURES

Figure	Pág.
1 Three-layer IoT architecture.....	5
2 Schematic of the pH sensor.....	6
3 Stage of the signal conditioning circuitry.....	7
4 The pH instrumentation for global VF applications.....	8
5 The operational block diagram of an optimal closed-loop control system.....	11
6 Block diagram and experimental setups of the pH instrumentation utilized to generate training and testing datasets.....	12
7 The training dataset without mechanical perturbations and exhibiting intrinsic and extrinsic disturbances.....	14
8 The Butterworth, Chebyshev I, Chebyshev II, and Elliptic IIR digital filter designs.....	15
9 The best model trained.....	17



## LIST OF TABLES

Table		Pág.
1	IIR digital filter designs for the Butterworth, Chebyshev I, Chebyshev II, and Elliptic configurations .....	15
2	Training metrics for the best model trained with MSE loss function at the maximum step reached.....	17
3	Validation metrics for the best model trained with MSE loss function at the maximum step reached.....	17
4	Testing metrics in the test dataset for the best model trained with MSE loss function.....	18
5	Electrode voltage values at different temperatures.....	19

## I. INTRODUCTION

Agriculture has been one of the greatest advancements for humanity, providing the ability to have access to food and resources when needed, which had a significant impact, changing the life of nomads to a sedentary one. Over the years, new elements were introduced; iron tools appeared to facilitate tasks, civilizations emerged - a group of people with a common goal to survive, trade was invented and products could now be shared. Later in 1760, the industrial revolution brought the introduction of machines for planting, harvesting, and spraying. Fertilizers were invented for pests, modified foods and pesticides emerged. In 1960, the green revolution began, bringing mechanization to the field and with it, many improvements for increased agricultural production. Advances in genetics allowed for the creation of improved foods, which began to spread across most of the world. All these technological advancements created new opportunities and allowed for a better quality of life and satisfaction of basic human needs.

Currently, traditional agriculture is no longer capable of fully meeting the demand for food, due to population growth, high demand for resources, city growth, migration of farm workers, adverse crop conditions due to climate change, etc.

Recent predictions reveal that the world will not have the capacity to meet the requirements of food production and other alimentation products to ensure adequate nutrition for the entire population. Precision Agriculture (PA) is the set of technological tools implemented to optimize crop-yield and -quality in plant production. Also, an essential resource for sustainable agriculture is water. Today, water use is inefficient: 65-70% of the freshwater is utilized for non-essential human activity. Our research group focuses on developing novel PA techniques to maximize natural resources through Vertical Farming (VF). Furthermore, the effective use of this production style allows optimizing the space in which different crops, such as fruits, vegetables, fine herbs, and flowering plants, can be grown in the same area by locating them in different production levels. Hydroponic VF is the most common method to cultivate plants. The salient features of hydroponic VF systems reside in their capacity to enable crop growth whilst minimizing water, CO<sub>2</sub>, energy, and fertilizer consumption. This is enabled by virtue of quantifying key growth parameters, such as conductivity, temperature, light exposure, and especially pH.

Several studies have reported where hydroponic systems are automated and make use of IoT technology that provides the system with a wide variety of new functions compared to traditional hydroponic systems, making it increasingly less dependent on human intervention. To build these systems, it is necessary to have reliable instrumentation that allows for proper control of all variables involved in crop growth. An essential aspect of any instrument intended for PA or VF use, is that such instrumentation must meet availability, portability, and cost-effectiveness constraints to enable global adoption. Furthermore, the global food supply chain, which by 2050 will have to increase its capacity by 60-70% due to the growth of the world population, would benefit greatly if connected (characteristic of Industry 4.0 solutions) pH sensors were available. In this work, we describe the

implementation of a portable, cost-effective, and connected instrument that enables accurate pH measurements for PA/VF and, more generally, Industry 4.0 applications.

## 1.1 STATE OF THE ART

Globally, numerous industries employ the pH level for multiple purposes. For instance, the pH is recurrently used as a central metric to determine the alkalinity. Furthermore, by controlling the pH, an efficient coagulation of sludge in wastewater can be guaranteed [1–3]. Similarly, pH serves as a reference to monitor and prevent corrosion in pipes and boilers [4,5]. In fermentation processes, continuous quantification of the pH is relevant to avoid the generation of unwanted and harmful by-products [6–8]. In the brewing industry, the pH serves to determine aging, increments in hop hardness, and bittering concentrations [9–11]. For perishable products, such as meat and fish, the pH level reveals shelf life and freshness [12–15]. Finally, the pH is central to determine ripening stage, as a function of ethylene concentration, of fruits and vegetables [16–18].

In the past, several groups have reported the construction of instrumentation to enable pH measurements. For example, Jin et al. [19] developed a pH potentiometer applicable to teaching in a chemistry laboratory setting. Moreover, a pH sensor to assess the changes in cementitious materials, through a sol-gel process with an alizarin yellow as meter, has been developed [20]. Additionally, portable chemical sensors, requiring specialized processes for manufacturing, have been reported for non-invasive real-time monitoring of parameters for medical care and disease diagnosis [21,22]. Manjakkal et al. [23] integrated an electrochemical pH sensor, applicable to several industries, with a screen printed on flexible substrates through CuO nanostructures exhibiting nanorods morphology. The measurement range was established to be 5–8.5 pH units. Dang et al. [24] developed a wireless system for monitoring pH of sweat, integrated by a pair of serpentine-shaped stretchable interconnects. The authors constructed a reference electrode using graphite-polyurethane composites for biological applications. Cordoba et al. [25] reported the development of an optical sensor, which requires a high-cost external instrument to determine the pH level. Rasheed et al. [26] designed a multilayer (ZnO/Ag/ZnO) film pH sensor, which was tested as an extended gate field effect transistor. The pH detection range was demonstrated to be 2–12 pH units.

Lastly, solutions using ISFET (Sensitive Field Effect Transistors) sensors, which have the advantage of being small, have been proposed. Nonetheless, with ISFET sensors, samples under study must be small, and the measuring range is limited to 10 pH units (1.5 to 11.5 pH) [27]. An essential aspect of any instrument intended for use in PA is that such instrumentation must meet the constraints of availability, portability, and cost-effectiveness to enable global adoption.

On the other hand, this instrumentation must ensure optimal crop yields. As a starting point for controlling pH in PV applications, an efficient and simple to implement on-off control scheme can be used.

However, to implement a good control system, it is essential to have properly conditioned signals of the parameter of interest. Predictable filtering can be achieved, on the one hand, using traditional techniques such as Butterworth,

Chebyshev and Elliptic filters (analog or digital) [28-31]. On the other hand, when unpredictable disturbances are present, it is challenging to design an electronic circuit that can handle these unpredictable and random behaviors. However, Artificial Intelligence (AI) has shown that it can cope with imprecise and unexpected conditions. Recurrent Neural Networks (RNNs) are ANNs utilized when behaviors depend on time sequences, which allows the resolution of problems with unexpected behaviors, like detecting malware affecting cloud systems [32]. Natural language processing also employs RNNs for translation because these solutions must consider time sequences to maintain context [33]. Forecasting of power demand also uses RNNs to predict energy consumption depending on time sequences [34]. Finally, RNNs serve to predict concrete dam deformation based on previous deformation or time sequences [35].

## **1.2 PROBLEM DEFINITION**

In particular, a VF hydroponic system is being constructed in our laboratory, which consists of three distinct vertical racks where various plants can be grown. Each variety is exposed to a specific light recipe depending on the plant characteristics. Ambient humidity and temperature sensors are distributed along the racks to monitor plant parameters. The nutrients come from a reservoir that incorporates a pump, as well as water level, temperature, total dissolved solids, and pH sensors. As a starting point to control pH for VF applications, an efficient and simple-to-implement on-off control scheme can be utilized. Nonetheless, in order to implement such a control system, it is indispensable to have appropriately conditioned signals of the parameter of interest. Because the pH level is critical to VF as it influences the chemical, physical and biological properties of the soil, affecting factors such as plant growth, denitrification, plant toxicity, bacterial activity and soil nutrients, it is necessary to have a portable, accurate and disturbance-immune pH measurement instrument to ensure optimal crop performance. Additionally, generally speaking, plants are more vulnerable whenever alkalinity conditions are present. For example, crops are more susceptible to being attacked by insects when the alkalinity increases. Meanwhile, whenever an acid behavior is present, plants tend to more frequently suffer diseases. Furthermore, alkaline environments are correlated with deficiencies of nitrogen, phosphorus, and sulfur; whereas calcium, magnesium, potassium, and sodium deficiencies ensue in acidic conditions. This implies that latent risks exist with respect to deficient ion distributions, vulnerability, and crop disease, which need to be detected and controlled. Therefore, depending on the plant or crop of interest, the pH must be controlled (normally in the range of 4 to 8 units [8,10–12]), in order to ensure optimal environments for growing and, thus, yield. However, the pH measurement is no longer linear in behavior when the temperature changes. Automatic temperature compensation (ATC) is built into some sensors, allowing precise calibration adjustments of the pH electrode when the temperature changes. However, ATC cannot correct for unknown sample pH/temperature effects. When the behavior of a sensor is known, the ATC works adequately to perform the calibration of some sensors.

## 1.3 OBJECTIVES

### 1.3.1 General

Design and characterize of a portable, cost-effective, and connected instrument that enables accurate pH measurements for VF and, more generally, Industry 4.0 applications. As well as to design and evaluate the performance of an advanced signal conditioning and filtering stage, utilizing RNN and Deep Learning, to account for intrinsic and extrinsic temporal perturbations that ensue in real-world VF settings. To propose a fuzzy system tuned by genetic algorithms to compensate for the effect of temperature on pH measurements.

### 1.3.2 Specific

- Design and implementation of a portable, cost-effective, and connected instrument that enables accurate pH measurements for PF/VF and, more generally, *Industry 4.0* applications.
- Evaluate the effect of temporal intrinsic and extrinsic (mechanical) perturbations, as applicable to the sensing and controlling of pH values, by using conventional digital filtering, and comparing it to a more resilient solution based on RNN.
- Apply fuzzy inference system to compensate for the temperature changes in pH measurements, using a genetic algorithm to tune the best vertices of the membership functions to obtain the desired behavior, specially adapted for the sensor used.

## 1.4 JUSTIFICATION

An essential aspect of any instrumentation intended for use in PV is that such instrumentation must meet the constraints of availability, portability, and cost-effectiveness to enable global adoption. Furthermore, the global food supply chain, which by 2050 will need to increase its capacity by 60-70% due to global population growth, would benefit greatly from the availability of connected pH sensors capable of filtering unpredictable disturbances, which are difficult to design with electronic circuitry. Through the application of Artificial Intelligence (AI) it is possible to cope with imprecise and unexpected conditions by solving complex problems without deterministic solution, especially when using Artificial Neural Networks (ANN) and Deep Learning.

## II. METHODOLOGY

### 2.1 Design and Characterization of the Instrument

Internet of Things (IoT) is a key enabling technology for Industry 4.0 applications. No unified or standardized agreement has been reached with respect to IoT architectures. Nonetheless, every IoT architecture should implement at least three layers. More complex architectures, including four- or five-layered ones, have also been

proposed. The instrument described in this work is unique, compared to other pH sensing devices, because it incorporates a three-layer IoT architecture with Perception, Network, and Application Layers.

### 2.1.1 Materials

In Figure 1, we depict the block diagram of the cost-effective and portable instrument to enable accurate pH measurements for global VF and, more generally, Industry 4.0 applications, as proposed and implemented by our group. The instrument described in this work is unique, compared to other pH sensing devices, because it incorporates a three-layer IoT architecture with Perception, Network, and Application Layers.

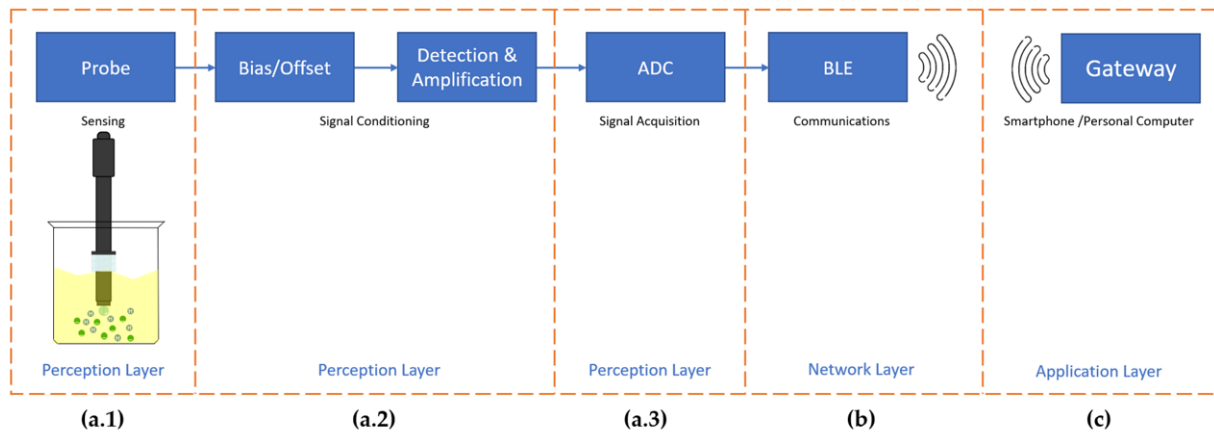


**Figure 1.** The cost-effective and portable pH instrument has been implemented in a three-layer IoT architecture, consisting of (a) Perception, (b) Network, and (c) Application Layers. The Perception Layer is further divided into: (a.1) Sensing, (a.2) Signal Conditioning, and (a.3) Signal Acquisition stages. The Network Layer has been enabled by means of a Bluetooth (BLE) Communications stage. The Application Layer utilizes a gateway, in the form of a Smartphone or a Personal Computer, for user interaction.

As illustrated in Figure 1, the three-layer architecture of the instrument incorporates: (a) Perception Layer, (b) Network Layer, and (c) Application Layer. The Perception or Physical Sensor Layer is further divided into: (a.1) Sensing, (a.2) Signal Conditioning, and (a.3) Signal Acquisition stages. Meanwhile, the Network Layer, used to connect the pH sensor to other sensors, network devices, or servers, is implemented through a Wireless Bluetooth (BLE) Communications stage. Finally, the Instrument Application Layer, which is in charge of providing useful information to the user, is enabled by means of a smartphone or a personal computer. Hereafter, we describe the materials necessary to implement the sections of the accurate, cost-effective, and portable instrumentation for pH measurements.

### 2.1.1.1 Perception Layer—Sensing Stage

We employ a silver|silver-chloride, Ag|AgCl, glass electrode in a potentiometric arrangement, which is readily available and cost-effective. The implemented sensor (Hinotek, Ningbo, China, E201-BNC) consists of a working electrode in the form of a glass ball, filled with a well-known buffer solution, which is in contact with the sample under study. The reference electrode also interacts with the solution of unknown pH. The sensor is protected by a cover and maintained in a storage solution, which is central to ensure sensor performance over time. A schematic of the pH sensor is depicted in Figure 2.

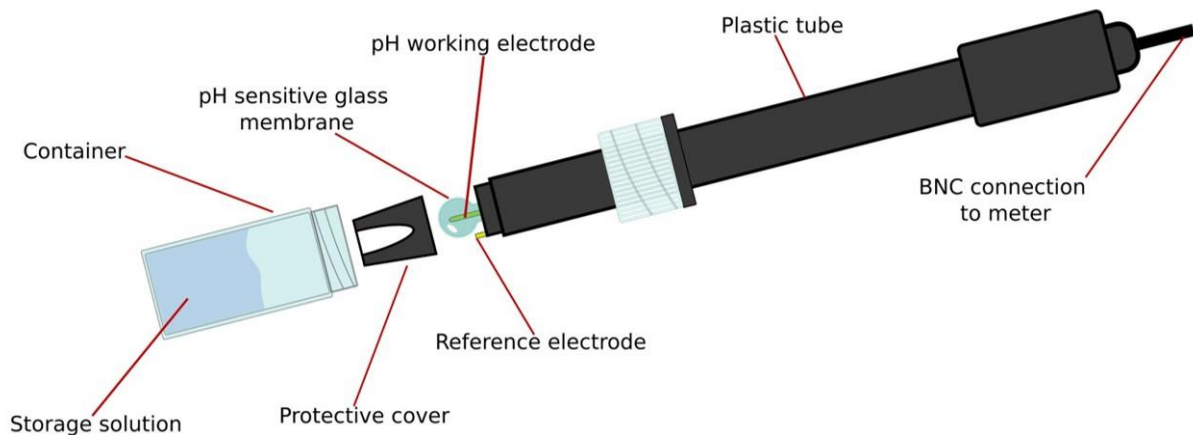


**Figure 2.** The implemented sensor consists of: a. Working electrode in contact with sample under study; b. Reference electrode interacting with solution of unknown pH; c. Protective cover; d. Storage solution; and e. Standard BNC connector for interoperability.

Any other pH detector (including those implementing novel materials) in a potentiometric arrangement would, despite accessibility and/or availability constraints, be compatible with the instrument described in this work, provided it has a standard BNC connector. Such a connector was selected to ensure interoperability and to facilitate signal conditioning interfacing.

### 2.1.1.2. Perception Layer—Signal Conditioning and Signal Acquisition Stages

Alkaline solutions tend to generate negative potential differences. Meanwhile, acidic solutions will have a positive trend, in terms of the voltage generated by the sensor. Therefore, in order to ensure that the electrical waveform is adequate for analog to digital conversion (ADC), an offset voltage must be implemented in the signal conditioning stage. As illustrated in Figure 3, a divider network with a stable voltage input (Texas Instruments, Dallas, TX, USA, TL431) of 2.5 V defines the bias voltage. This offset voltage can be varied by means of a potentiometer (RV1). In this work, we present key modifications to the passive components of this bias stage of the signal conditioning circuitry, which serve to optimize pH detection.





### 2.1.1.3. Network Layer—Bluetooth Wireless Communications Stage

The Network Layer enables the pH sensor to connect to other devices such as gateways (e.g., in the form of smartphones or personal computers) or even other sensors. Such connectivity is characteristic of Industry 4.0 applications. In the instrument described in this work, a Bluetooth radio version 2.0 (Linvor, Jinan city, Shandong, China, LV-BC-2.0) enables wireless transmission of pH data, and serves as the Network Layer. The radio, implemented in a breadboard (Olimex, Plovdiv, Bulgaria, BLE HC-06) for ease of integration, is a Class 2 device, and exhibits a maximum communication range of 10 m. This range is sufficient for isolated VF applications. However, for distributed VF applications or, more generally, other Industry 4.0 applications, a Class 1 Bluetooth device can be employed to yield a range of 100 m. In fact, for conventional farming, the Bluetooth technology enables a very desirable feature: Mesh Networks. In such a topology, a rather large area (e.g., 1000 m<sup>2</sup>) can be covered with a handful of Bluetooth radios. Any gateway, functioning as part of the Application Layer, which supports Bluetooth communications, as specified in this section, can interface with the instrumentation, potentially minimizing deployment challenges encountered in global Industry 4.0 applications.

### 2.1.1.4. Integration of the Portable pH Instrument

Figure 4 displays the layout and a representative picture of our portable pH instrument, as well as the integration required to enable accurate pH measurements for global VF applications. To integrate the overall solution six main components are needed: 1. Glass electrode for pH sensing with standard BNC connector; 2. Signal conditioning module; 3. Bluetooth communications module; 4. Integration breadboard; 5. Signal acquisition and processing module; and 6. Power supply.

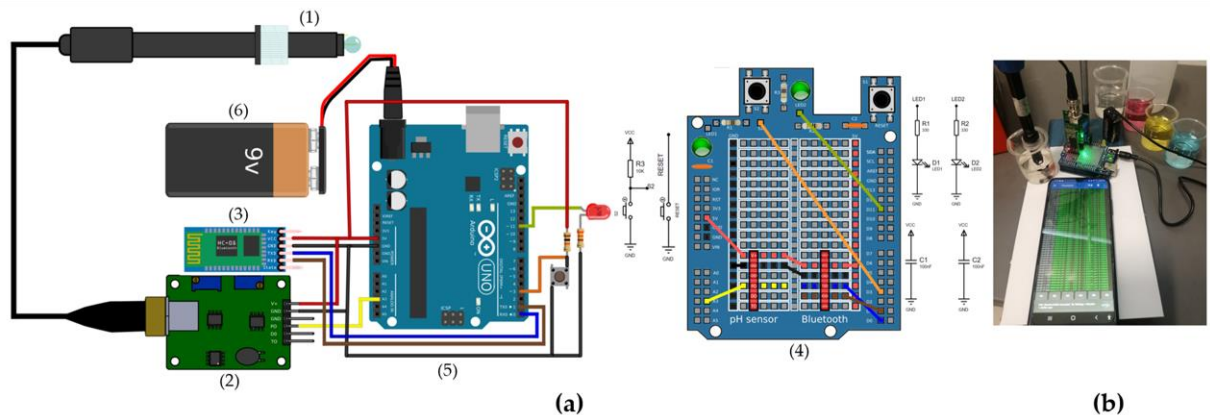


**Figure 4.** (a) The pH instrumentation for global VF applications consists of six main components: (1) Glass electrode; (2) Signal conditioning module; (3) Bluetooth communications module; (4) Integration breadboard; (5) Signal acquisition and processing module; and (6) Power supply. (b) Representative photo.

Figure 4a provides a detailed integration (i.e., wiring) diagram to ensure adequate signal processing, as well as the intermediate breadboard needed to assemble the components that constitute the instrument. Finally, Figure 4b presents a representative picture of the portable instrument for pH measurements.

## 2.1.2 Methods

### 2.1.2.1 pH Sensor Characterization

The pH of a solution under study can be determined after a meticulous calibration. In order to characterize the pH sensor, the potential difference over the two electrodes must be measured, and related to the hydrogen-ion activity of reference solutions.

Three pH buffer solutions (Mallinckrodt Baker, Hampton, NJ, USA, manufacture date 31 August 2020) with a 2-year validity certification (at 25 °C) and traceable to NIST standards were used. The standard buffer solutions employed in the calibration of our instrument were: 1. Biphthalate; 2. Phosphate; and 3. Borate. Correspondingly, the pH and certified range values for the buffer solutions were 4 [3.96, 4.04]; 7 [6.96, 7.04]; and 10 [9.99, 10.01]. Utilizing the batch information of our buffer solutions, the pH reference values for our calibration procedure were: 3.99, 6.98, and 10.00.

The characterization method is divided into two phases. In phase one, the sensitivity of the pH sensor is determined with a conventional voltage meter, such as a multimeter. It is important to note that the instrument input impedance should be high, and the noise performance optimally below the mV range for accurate calibration. In phase two, the signal conditioning stage, as described in this work is employed, in order to quantify the modified (i.e., including bias and amplification effects) sensitivity of the pH sensor. Hereafter, the methods for both phases are described. Phase I does not include the signal conditioning stage. First, the pH sensor is attached to the measuring device using the BNC connector. For this phase, a multimeter (Steren, Ciudad de México, Mexico, MUL-605) is employed to determine the voltage, irrespective of polarity, as a function of buffer solution. Next, the calibration curve that describes the linear behavior of the sensor is calculated by using regression techniques. The derived slope will serve to relate pH as a function of (sensor) voltage. In Phase II, the signal conditioning stage is included. Nonetheless, the above methodology remains practically the same. One of the differences is that in the first step, the pH sensor is attached to the signal conditioning module using the BNC connector. Then, the circuitry of Figure 3 is employed to measure the voltage as a function of buffer solution. Next, the calibration curve that describes the linear behavior of the sensor is obtained by employing regression techniques. Here another difference is in place. The pH is still related to a modified potential difference, which includes the effects of the signal conditioning stage: bias and amplification. The modified potential difference is obtained by dividing the output voltage by the gain and subtracting the bias voltage. The derived slope will serve to relate pH as a function of (instrument) voltage. Finally, it is important to note that, irrespective of the calibration method, the overall cleanliness and mechanical stability, while measuring, of the working electrode are key factors to obtain accurate calibration results.

### 2.1.2.2 Preparation of Signal Conditioning, Acquisition, and Transmission

The procedure implemented to utilize the signal conditioning, acquisition, and transmission stages is as follows. First, the wiring of the instrument is performed, as shown in Figure 4a. It is relevant to note that this step defines the performance of the signal acquisition stage, if an external voltage is used. In our case, this parameter was set to 5 V using the microcontroller code. Then, the offset voltage of the instrument is tuned by cautiously adjusting the potentiometer, RV1 in Figure 3, thus accounting for the ADC configuration previously mentioned. Finally, BLE transmission of sensed data is facilitated by means of the microcontroller code, which implements two modalities: Calibration and Measurement. In calibration mode, the user is enabled to characterize the sensor (refer to Section 2.1.2.1) by employing the three buffer solutions. The resulting parameters are stored in the instrument memory for future use. In measurement mode, the instrument acquires arbitrary voltage values, and converts such information to pH values. pH information is then sent serially to the Bluetooth radio, which transmits wirelessly the data to a gateway (i.e., personal computer or smartphone) for further processing.

### 2.1.2.3. Methodology to Assess the pH of Arbitrary Solutions

The first step to measure the pH of a selected sample is to perform the calibration of the probe, refer to Section 2.1.2.1. Here, sensor cleanliness is crucial. Second, the sensor is connected to the instrument, and the signal conditioning, acquisition, and transmission stages are prepared as mentioned in Section 2.1.2.2. Once this has been performed, the instrument is ready for measurements. Nevertheless, the sample must be prepared and the chemical integrity of the same must be ensured. In order to perform pH evaluation, mechanical stability must be guaranteed. In this work, we elaborate further on the implications of unstable systems, which are likely to occur in global VF settings. A simple-to-use interface was implemented, by means of a push-button (S2), to select the operation modality. A light emitting diode (LED2) is used to indicate operation mode, and for general user interaction. Once instrument and sample are ready, the user selects an operation mode, by means of S2, and performs the pH measurement. Such measurement is then transmitted to the gateway of interest. Furthermore, calibration code may be found in the Supplementary Materials section of this work, go to Annex 1.

## 2.2 Comparative Analysis of RNN versus IIR Digital Filtering to Optimize Resilience to Dynamic Perturbations.

### 2.2.1 Materials

#### 2.2.1.1 Instrumentation

For the purpose of generating reference and output datasets ( $r$  and  $y$  in Figure 5), we utilized the designed pH instrumentation. Once the data is obtained, the computing entity performs the IIR and RNN digital filtering. For IIR digital filtering, we employed the Signal Processing Toolbox of MATLAB (MathWorks, Natick, United States,

MATLAB) running on a Windows 10 Dell G3 3500 computer with a 4-core Intel i5-10300H 2.50GHz processor with 16GB of RAM. The RNN analysis was performed with the TensorFlow, Sklearn, and other conventional python libraries of JupyterLab (NumFOCUS, Austin, United States, Jupyter) running on a Windows 10 Desktop Computer with an Intel i7-6700 3.40GHz processor with 16GB of RAM and NVIDIA GeForce RTX 2060 GPU.

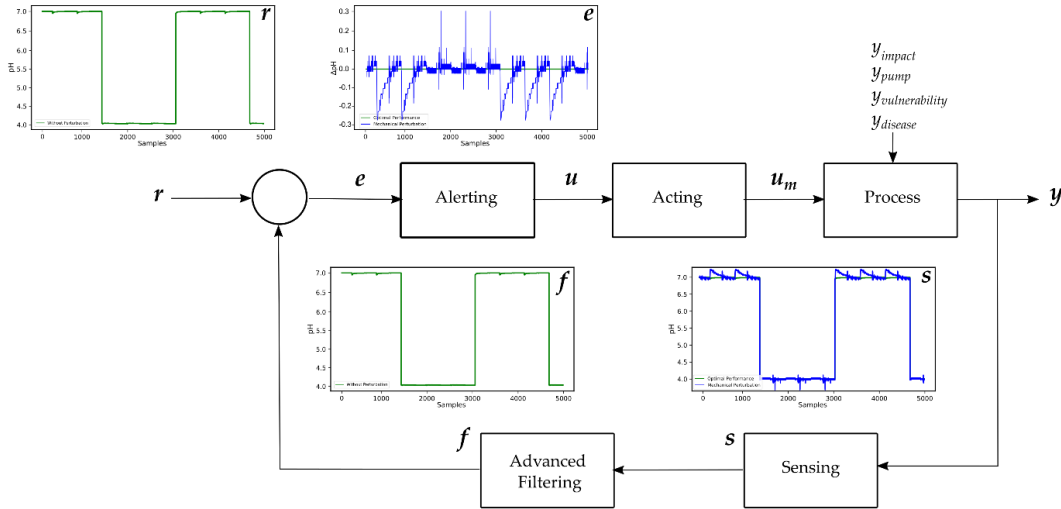


**Figure 5.** The operational block diagram of an optimal closed-loop control system to ensure that a VF setup is exposed to appropriate pH values includes: Sensing, (Advanced) Filtering, Alerting, Acting, and Processing sections. The most critical step of the control system is the filtering section because unpredictable perturbations occur in real-life VF implementations. In this diagram,  $r$  denotes eference signal,  $e = f - r$  and stands for error signal,  $u$  symbolizes process input,  $u_m$  is manipulated variable,  $y_{impact}$  demarcates extrinsic mechanical perturbations,  $y_{pump}$  represents intrinsic movement effects,  $y_{vulnerability}$  refers to intrinsic crop vulnerability,  $y_{disease}$  denotes intrinsic crop disease,  $s$  stands for sensed signal,  $f$  symbolizes filtered signal, and  $y$  is controlled output.

## 2.2.2 Methods

Figure 6 displays (a) the block diagram and (b) the experimental setup that are needed to generate the training and testing waveforms, in order to assess the deep-learning RNN and IIR digital filters. The training dataset is created by using an ideal pH sensing setup without mechanical perturbations, see the central section of Figure 6(b). Meanwhile, the intrinsic mechanical perturbations are enacted by exposing the instrument to a laboratory stirrer, refer to the left section of Figure 6(b), which mimics the use of conventional pumps in VF systems for circulation purposes. Finally, the extrinsic mechanical perturbations were created by impacting the utilized setup, at different locations, as depicted in the right-most portion of Figure 6(b)

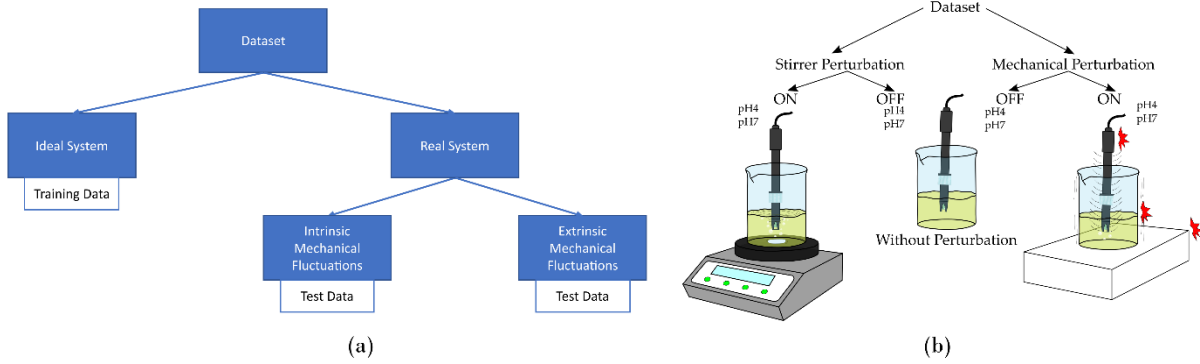


**Figure 6.** (a) Block diagram and (b) experimental setups of the pH instrumentation utilized to generate training and testing datasets, in order to assess the advanced filtering proposed in this work. We utilized different arrangements to create the intrinsic and extrinsic mechanical perturbations that are common in real-life VF applications.

### 2.2.2.1 Generation of Dataset

Reliable solutions (Mallinckrodt Baker, Hampton, New Jersey, USA) were utilized to ensure accurate pH values ( $pH_{signal} = 3.99$  and  $pH_{reference} = 6.98$ ) for the measurements, refer to section 2.1.2.1 above.

We performed two sets of pH measurements for ideal and real scenarios, corresponding to mechanical perturbations being absent and present, respectively. In addition to pH values, we recorded the raw ADC temporal voltage values for redundancy and better control of the datasets. Thus, the dataset samples ( $n$ ) included: input temporal indices,  $t_i$ , ADC voltages,  $v_i$ , and pH values,  $pH_i$ , for (a) ideal  $input_i=(t_i, v_i, pH_i)$  and (b) real  $output_i=(t_i, v_i, pH_i)$  scenarios, for every sample  $i=[1 \dots n]$ . It is worth noting that the aforementioned datasets have a periodic behavior, in order to emulate the characteristic on-off cycle necessary to ensure optimal crop growth and yield.

### 2.2.2.2 Dataset Augmentation and Splitting

Specifically with respect to the RNN analysis, we utilized both datasets to train the model and suppress perturbations. As depicted in Figure 2 in Annex 2, the RNN is based on a supervised-learning model, which requires knowledge of the input signals, as well as the desired output for training purposes. Since after RNN filtering, we are interested in obtaining pH signals free of perturbations, we solely utilized the signal without perturbations as the desired output dataset to train the model. Thus, the training input and output datasets were  $X = \{x_1, x_2, x_3, \dots, x_n\}$  and  $Y = \{y_1, y_2, y_3, \dots, y_n\}$ , where  $x_i$  and  $y_i$  were pH values for the signals with perturbations and without them, respectively. Furthermore, we employed a data augmentation mechanism to increase the dataset samples and the representativity without the need for new measurements. The data augmentation in this work considered that the pH instrumentation will record values in the range 0-14, depending on the level of acidity or alkalinity of the solution. We commenced the data augmentation by selecting  $\alpha$ , the number of augmentations. Then, for each augmentation, we determined a random value  $\psi$  in the range of [0,1] to multiply by the original  $X$  and  $Y$ , equally

modifying the pH values while maintaining the result within the original boundaries [0,14]. Finally, we maintained the original samples and added each augmentation to return the augmented data  $X$  and  $Y$ , as detailed in Algorithm 1. It is important to note that we employed 30 augmentations of the entire training dataset, or  $\alpha = 30$ , and that the augmented dataset can also be employed to test the IIR filters.

Algorithm 1: Data augmentation for pH measurements	
	Input: $X, Y, \alpha$
	Output: $\hat{X}, \hat{Y}$
1	$\hat{X} = [X]$
2	$\hat{Y} = [Y]$
3	<b>For</b> $i = [2, 3, \dots, \alpha + 1]$ <b>do</b>
4	$\psi \sim [0, 1]$
5	$\hat{X}_i = [\hat{X}_{i-1} \cap \psi \otimes X]$
6	$\hat{Y}_i = [\hat{Y}_{i-1} \cap \psi \otimes Y]$
7	<b>Return</b> $\hat{X}, \hat{Y}$

Considering that we must train a deep-learning neural network, the dataset must be split to avoid overfitting and to ensure reliable results. In this work, we utilized 60% of the dataset for training, 20% for validation, and 20% for testing. Thereafter, we configured the model to generate extra data with the training augmentation data, as described in Algorithm 1.

### 2.2.2.3 Training Datasets

The pH values utilized to assess the performance of RNN and IIR digital filters were 4 and 7 units for signal and reference waveforms, respectively. However, before commencing pH measurements, the instrument must be calibrated. Thus, for calibration purposes, we included a third pH value of 10.00 of a standardized buffer solution (Mallinckrodt Baker, Hampton, New Jersey, USA). Finally, the calibration procedure can be improved if a fourth solution, outside of the calibrated substance range in our case [3.99, 10.00], is utilized. Hence, a final substance of 2.5 pH units was employed to perform the calibration procedure. Thereafter, the periodic signal needed for VF was generated. Figure 7 depicts the training dataset (a) without mechanical perturbations, and (b) with intrinsic and extrinsic disturbances. Moreover, in Figure 7, we separate into two phases the required steps, calibration and measurement, needed to sense pH with the portable instrumentation. The datasets consisting of 21723 temporal samples,  $t_i$ , ADC voltages,  $v_i$ , and pH values,  $pH_i$ , for scenarios with present and absent perturbations are available in the Supplementary Materials section of this work, in Annex 2.

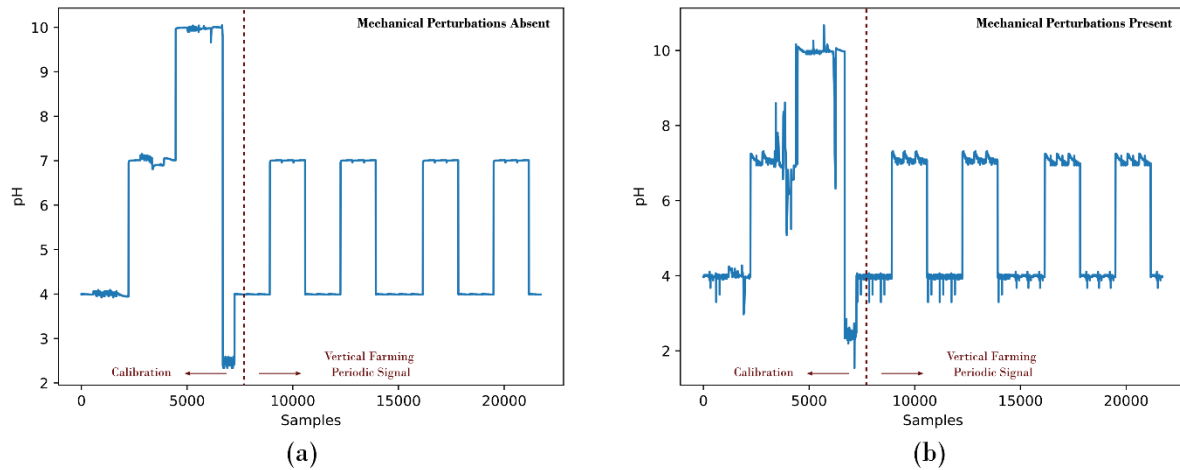


**Figure 7.** The training dataset (a) without mechanical perturbations and (b) exhibiting intrinsic and extrinsic disturbances were generated to mimic the conditions that are common in real-life VF applications. The two phases, Calibration and VF Periodic Signal generation, needed to employ the pH instrument are respectively depicted in the left and right portions of each illustration.

As seen in Figure 7, once the instrument is duly calibrated, we generate the periodic signals, which are identical to the control waveforms of Figure 5. During calibration, the instrument is more prone to exhibit mechanical perturbations because buffer solution, electrode, and detection electronics have to be manipulated frequently (i.e. electrode and container cleaning is mandatory after each calibration measurement) In this work, we consider these unpredictable fluctuations to demonstrate that a RNN filter is more resilient in real scenarios, as opposed to IIR filtering.

#### 2.2.2.4 IIR Digital Filter Designs

The portable and precise pH instrument that we describe in this work can implement well-established (analog or digital) electronic filters, such as Butterworth, Chebyshev, and Elliptic arrangements. Furthermore, a salient feature of IIR filters is that they can be based on these electronic configurations. In order to assess the usability of such filters in real-life VF applications, we designed (a) Butterworth, (b) Chebyshev I, (c) Chebyshev II, and (d) Elliptic digital IIR configurations. As commented previously, the pH input function is periodic with a rather slow varying frequency. Therefore, the low-pass filters specifications have to consider this expected behavior. We defined a passband frequency of 1Hz with a maximum 1dB attenuation. Additionally, the stopband frequency was specified to be 10Hz for a 60dB attenuation. The sampling frequency was assumed to be one order of magnitude greater than the stopband frequency.

**Table 1.** IIR digital filter designs for the Butterworth, Chebyshev I, Chebyshev II, and Elliptic configurations employed in this work.

Filter	Order	a Coefficients	b Coefficients	Transfer Function
Butterworth	4	{ 1, -3.836, 5.521, -3.534, 0.8486 }	{ $8.985 \times 10^{-7}$ , $3.594 \times 10^{-6}$ , $5.391 \times 10^{-6}$ , $3.594 \times 10^{-6}$ , $8.985 \times 10^{-7}$ }	$\frac{8.985 \times 10^{-7} z^4 + 3.594 \times 10^{-6} z^3 + 5.391 \times 10^{-6} z^2 + 3.594 \times 10^{-6} z + 8.985 \times 10^{-7}}{z^4 - 3.836 z^3 + 5.521 z^2 - 3.534 z + 0.8486}$
Chebyshev I	3	{ 1, -2.935, 2.875, -0.939 }	{ $1.47 \times 10^{-5}$ , $4.431 \times 10^{-5}$ , $4.431 \times 10^{-5}$ , $1.477 \times 10^{-5}$ }	$\frac{1.477 \times 10^{-5} z^3 + 4.431 \times 10^{-5} z^2 + 4.431 \times 10^{-5} z + 1.477 \times 10^{-5}}{z^3 - 2.935 z^2 + 2.875 z - 0.9398}$
Chebyshev II	3	{ 1, -2.98, 2.96, -0.9803 }	{ $9.347 \times 10^{-5}$ , $-9.298 \times 10^{-5}$ , $-9.298 \times 10^{-5}$ , $9.347 \times 10^{-5}$ }	$\frac{9.347 \times 10^{-5} z^3 - 9.298 \times 10^{-5} z^2 - 9.298 \times 10^{-5} z + 9.347 \times 10^{-5}}{z^3 - 2.98 z^2 + 2.96 z - 0.9803}$
Elliptic	3	{ 1, -2.935, 2.875, -0.939 }	{ $4.69 \times 10^{-4}$ , $-4.09 \times 10^{-4}$ , $-4.09 \times 10^{-4}$ , $4.69 \times 10^{-4}$ }	$\frac{4.69 \times 10^{-4} z^3 - 4.09 \times 10^{-4} z^2 - 4.09 \times 10^{-4} z + 4.69 \times 10^{-4}}{z^3 - 2.935 z^2 + 2.875 z - 0.9399}$

Utilizing the Signal Processing Toolbox of MATLAB, we determined filter orders, as well as the corresponding transfer functions of the filters, including the  $a$  and  $b$  coefficients. Table 1 presents the orders, coefficients, and transfer functions of the digital filters. Finally, Figure 8 illustrates the digital filter designs for (a) Butterworth, (b) Chebyshev I, (c) Chebyshev II, and (d) Elliptic digital IIR configurations. The IIR digital filter MATLAB scripts are available in the Supplementary Materials section in Annex 2..

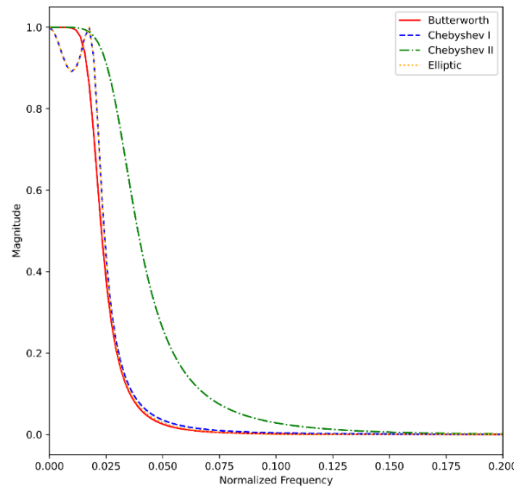


**Figure 8.** The Butterworth, Chebyshev I, Chebyshev II, and Elliptic IIR digital filter designs consider a  $-1\text{dB}$  passband frequency of  $1\text{Hz}$ , and a  $-60\text{dB}$  stopband frequency of  $10\text{Hz}$ .

### 2.2.2.5 RNN Digital Filter Design

The RNN-based digital filter proposed in this work implements the advanced structure depicted in Figure 2 in Annex 2. In order to optimize the design of the RNN digital filter, we determined the number of neurons per layer by testing multiple configurations. The tested layouts included various  $l1=l2=[10,20,30,40,50,60,70,80,90,100]$



LSTM neurons; three different  $l3=[1,5,7]$  GRU arrangements; as well as single RNN and output segments,  $l4=[1]$  and  $l5=[1]$ . Furthermore, we also varied the number of prior samples. We tested  $psamples=[500, 1000, 1500, 2500, 3000, 3500]$ . We assessed 2101 different configurations of the model with the MSE loss function, which we decided to employ because it is the most utilized metric to train regression models in ANNs. For the 2101 configurations, we trained the model with 500 epochs and a batch size of 5000. This approach requires different steps per epoch depending on the size of the training set, which is variable because, as commented above, we allowed changing the prior samples required as inputs. Moreover, we adjusted the learning rate according to Equation 1, increasing the effect of error and modifying the learning rate across epochs.

$$l_r = 1.0 \times 10^{-5} \times 10^{\frac{epoch}{100}} \quad (1)$$

The training mechanism utilized in this work stops after twenty steps without improvement of the validation loss. Furthermore, we configured the training process to solely save the best model. After assessing the 2101 configurations with the dataset containing 21723 samples with 30 augmentations for training, we obtained that the best model, as determined by the MSE loss function, ensues when  $l_1 = 90$ ,  $l_2 = 90$ ,  $l_3 = 1$ ,  $l_4 = 1$ ,  $l_5 = 1$ , and  $psamples = 2000$ . In Figure 9, we depict the logarithmic parallel coordinates for all the configurations trained with the MSE loss function based on the testing of MSE results. The best model is highlighted in red, MSE Test = 0.002017. Meanwhile, blue and gray are variations of models exhibiting better and worse performance, respectively. Lastly, in black we present the model with the worst outcome, MSE Test = 0.207638994.

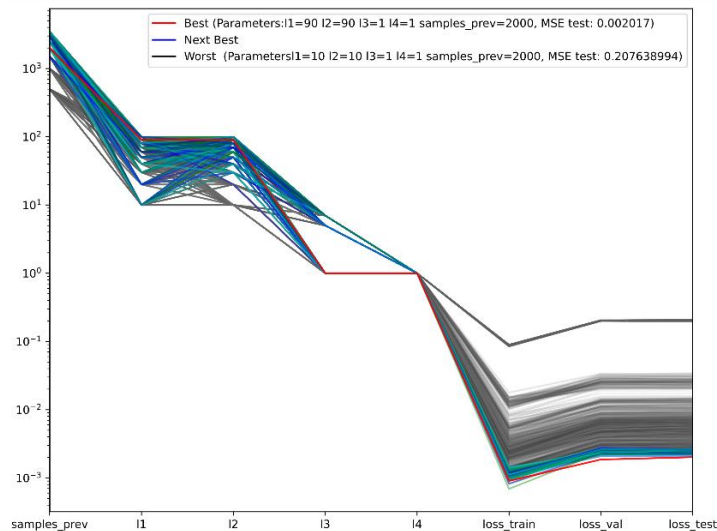


**Figure 9.** The outcome of the advanced digital filter structure of Figure 2 in Annex 2 is shown as the logarithmic parallel coordinates for all the configurations trained with the MSE loss function based on the testing of MSE

results; best model is in red; next best models are in blue variations; next in performance are in gray hues; and worst is depicted in black.

The training metrics obtained for the best model trained with the MSE loss function at the maximum step reached before stopping due to no loss validation improvement are depicted in Table 2.

**Table 2.** Training metrics for the best model trained with MSE loss function at the maximum step reached.

Step	Epoch MAE	Epoch MSE	Epoch MAPE	Epoch lr
317	0.0364	0.0053	53.3455	0.0145

The validation metrics for the best model trained with the MSE loss function obtained at the maximum stage reached are enumerated in Table 3.

**Table 3.** Validation metrics for the best model trained with MSE loss function at the maximum step reached.

Step	Epoch MAE	Epoch MSE	Epoch MAPE	Epoch lr
317	0.0415	0.0030	8.3354	0.0145

The test metrics obtained for the best model trained with the MSE loss function are enlisted in Table 4.

**Table 4.** Testing metrics in the test dataset for the best model trained with MSE loss function.

Model	Test MAE	Test MSE	Test MAPE	R-squared
RNN	0.0337	0.0020	6.8970	0.9076
k-RNN*	0.0254	0.0013	5.4111	0.9406

\* The RNN model was optimized by using a multiplying constant, k, of value 1.030

Once the digital filters were fully characterized, we assessed their implementation in a VF setting, as described in annex 2.

## 2.3 Design of a fuzzy inference system to compensate for the effect of temperature on pH measurements using genetic algorithms.

### 2.3.1 Methods

The fuzzy inference machine considers the voltage delivered by the electrode (AgCl) measured with five samples of known pH, 4, 6.86, 7, 9.18, 10 at different temperatures (15°C to 30°C), thus obtaining a small database with 80 readings for the genetic algorithm. These experiments define the values of the input and output universes specific to the electrode used. The rule used in the controller is the Mamdani rule. The aggregation was done through the max operation and defuzzification by a centroid of gravity.

The fuzzy models presented here have two input variables: the value of the voltage measured by the electrode  $V$  and the value of the temperature of the solution  $T$ . The output variable, pH, describes the temperature of the solution. The output variable, pH, describes the actual pH value at a given temperature. The inputs are the voltage represented by the set  $V$  with five terms:

$$V = \{V_{pH10}, V_{pH9.18}, V_{pH7}, V_{pH6.86}, V_{pH4}\}$$

Where each value represents the approximate pH value corresponding to the voltage levels measured by the electrode.

And the temperature represented with the set  $T$  with five terms:

$$T = \{TVL, TL, TA, TH, TVH\}$$

VL represents the Very low, L set as Low, A is the Average, H equal to High, VH denominated Very High.

The expected output in the experiment is a pH level between 4 to 10. Thus, we let the genetic algorithm tune the fuzzy inference system for obtaining the appropriate output sets for the centroid defuzzification.

Then, the output is given by pH with five terms:

$$pH = \{pH4, pH6.86, pH7, pH9.18, pH10\}$$

Where each value represents the real pH value taking into account the temperature. The universe considered for the voltage ranges that the sensor can deliver is  $UV = \{x \in \mathbb{Z}: -200 \leq x \leq 200\}$ , for temperature is  $UT = \{y \in \mathbb{Z}: 15 \leq y \leq 30\}$  and for pH value  $UpH = \{z \in \mathbb{Z}: 4 \leq z \leq 10\}$ .

Maestría en Ciencias en Ingeniería Mecatrónica  
Design and characterization of an advanced pH instrument using *Artificial Intelligence* algorithms for  
*Vertical Farming* applications

---

The objective function (equation (2)) uses the genetic algorithm in the fuzzy inference machine to fit the vertices of the Gaussian functions (5 input sets, 5 output sets, and 25 rules).

$$y = \left( \sum_{i=1}^{80} |Ai - Bi| \right) + \frac{0.1}{|M-m|} \quad (2)$$

where  $A_i$  is the value obtained with the fuzzy inference machine using the vertices tuned by the genetic algorithm,  $B_i$  is the desired value for the dataset values.  $M$  is the maximum, and  $m$  is the minimum of the values obtained. The objective is to minimize the function given in equation (6). As the problem to be optimized is dimension 105, we used an initial population of 500 individuals, each with 1155 alleles, where every 11 alleles form a bit string representing a real number, with a resolution of 1000 decimals. The selection method is by tournament, the tournament size applied here is 100, the number of crossover points is a random number, the mutation rate is 5%, and 30000 generations. Table 5 represents the values of the voltage (mV) at different temperatures ( $^{\circ}\text{C}$ ), and different pH.

**Table 5.** Electrode voltage values at different temperatures.

$^{\circ}\text{C}$	pH=4	pH=6.86	pH=7	pH=9.18	pH=10
	mV	mV	mV	mV	mV
15	161.51	8	4.95	-119.63	-163.53
16	162.11	8.03	5.12	-121.06	-163.11
17	162.71	8.05	5.23	-121.5	-163.8
18	163.31	8.08	5.67	-121.99	-164.31
19	163.88	8.1	5.75	-122.63	-164.88
20	164.48	8.16	5.86	-122.78	-164.48
21	165.08	8.19	6.09	-123.01	-166.08
22	165.68	8.23	6.2	-123.22	-166.68
23	166.28	8.26	6.25	-124.09	-167.28
24	166.88	8.27	6.43	-124.53	-167.85
25	168.55	8.28	6.53	-124.96	-169.08
26	176.05	8.31	6.73	-125.38	-169.3
27	176.65	8.33	6.86	-125.78	-169.85
28	178.25	8.37	7.03	-125.24	-170.25
29	179.90	8.42	7.26	-125.7	-170.85
30	180.13	8.39	7.67	-126.12	-172.45

### III. CONCLUSIONS

In this work, the implementation of a cost-effective and portable instrument, which enables accurate pH measurements for global Vertical Farming applications, has been described. By performing a well-designed calibration of the sensor, near Nernstian response, in this case 57.56 [mV/pH], was demonstrated. The instrumentation was compared to a laboratory gold standard, which is at least ten times more expensive, and was shown to be accurate in determining the pH of substances in the 2–14 range. Furthermore, the instrument yields precise pH results with an average absolute deviation of 0.06 pH units and a standard deviation of 0.03 pH units. Compared to previous research efforts, the instrumentation is unique because it incorporates a three-layer IoT

architecture with Perception, Network, and Application Layers. Additionally, the design is optimal for worldwide adoption by consisting of four modular stages: sensing, signal conditioning, signal acquisition, and communications. The design of the instrument was shown to be ADC-limited, with a minimum detectable value of 0.028 pH units, and a typical absolute accuracy of  $\pm 0.062$  pH units. In order to overcome this limitation, a means to improve performance was presented by meticulously designing the bias and amplification circuitry of the signal conditioning stage, and by optimizing the signal acquisition section of the instrument.

We have proposed an advanced filtering scheme based on Recurrent Neural Networks (RNNs) and Deep Learning to enable efficient control strategies for Vertical Farming (VF) applications. We demonstrated that the best RNN model incorporates five neuron layers. The first and second of the segments contain ninety LSTM neurons. The third layer implements one GRU neuron. The fourth segment incorporates one RNN network, while the output layer was designed by using a single neuron exhibiting a rectified linear activation function. By utilizing this RNN digital filter two variations were introduced: (1) A scaled RNN model to tune the filter to the signal(s) of interest, and (2) A moving average filter to eliminate harmonic oscillations of the output waveforms. The RNN models were contrasted with conventional Butterworth, Chebyshev I, Chebyshev II, and Elliptic digital IIR configurations. The RNN digital filtering schemes avoid introducing unwanted oscillations, which makes them more suitable for VF than their IIR counterparts. Furthermore, by utilizing the advanced features of scaling of the RNN model, we demonstrated that the RNN digital filter is pH selective, as opposed to conventional IIR filters. In real VF settings, the features of tuning (or selecting) an instrument to detect variable pH values, as well as ensuring that such device is resilient to dynamic (i.e., unpredictable) perturbations are of utmost importance. Hence, the use of advanced filtering schemes such as those based on RNN and Deep Learning is preferable as opposed to employing IIR filtering for VF.

Finally, a Mamdani fuzzy logic system auto-tuned through genetic algorithms was explored to obtain the real pH value without considering the slight variation of temperature. The system can identify the correct pH values considering the possible changes in voltage that can influence the electrode due to temperature. At the same time, an important fact is that the performance of the pH electrode deteriorates due to its useful life or external factors. With the application of the fuzzy system, it is possible to approximate a sensor's behavior to another in optimal or more sophisticated conditions with ATC. It would be enough to build a dataset with the voltage measurements provided by the sensor at certain temperatures and the correct pH value that corresponds to the readings of the already calibrated sensor. The genetic algorithm function will tune the fittest vertices for the fuzzy interference system sets in the defuzzification to obtain the correct pH value. For this work, the system only operates within the range of data used (pH4 to pH10), and future work will create a more extensive dataset. In addition, the incorporation of fuzzy logic in a control mechanism for monitoring nutrients in water in a multilevel hydroponic growing system considering parameters such as pH, conductivity, and temperature was explored. By considering these variables, dosing pumps could control the modification of nutrients in the water.

---

## VI. BIBLIOGRAPHY

- (1) Liu, X.; Zhai, Y.; Li, S.; Wang, B.; Wang, T.; Liu, Y.; Qiu, Z.; Li, C. Hydrothermal carbonization of sewage sludge: Effect of feed-water pH on hydrochar's physicochemical properties, organic component and thermal behavior. *J. Hazard. Mater.* 2020, 388, 122084. [CrossRef] [PubMed]
- (2) Abdel Daiem, M.M.; Said, N.; Negm, A.M. Potential energy from residual biomass of rice straw and sewage sludge in Egypt. *Procedia Manuf.* 2018, 22, 818–825. [CrossRef]
- (3) Esteban-Gutiérrez, M.; Garcia-Aguirre, J.; Irizar, I.; Aymerich, E. From sewage sludge and agri-food waste to VFA: Individual acid production potential and up-scaling. *Waste Manag.* 2018, 77, 203–212. [CrossRef]
- (4) Ruqing, N.; Fengyuan, H.; Yunfei, J.; Xinjing, T. Cycle and Harm of Main Pollutants in Thermal System of Gas Turbine. *IOP Conf. Ser. Earth Environ. Sci.* 2020, 546, 32028. [CrossRef]
- (5) Li, Y.; Liu, C.; He, F.; Wang, F. Analysis on Water Wall Tube Explosion in a Power Plant. *IOP Conf. Ser. Earth Environ. Sci.* 2020, 526, 12162. [CrossRef]
- (6) Muncan, J.; Tei, K.; Tsenkova, R. Real-Time Monitoring of Yogurt Fermentation Process by Aquaphotomics Near-Infrared Spectroscopy. *Sensors* 2020, 21, 177. [CrossRef]
- (7) Jiang, J.; Sun, Y.F.; Tang, X.; He, C.N.; Shao, Y.L.; Tang, Y.J.; Zhou, W.W. Alkaline pH shock enhanced production of validamycin A in fermentation of *Streptomyces hygroscopicus*. *Bioresour. Technol.* 2018, 249, 234–240. [CrossRef]
- (8) Grzelak, J.; Åšle, zak, R.; Krzystek, L.; Ledakowicz, S. Effect of pH on the production of volatile fatty acids in dark fermentation process of organic waste. *Ecol. Chem. Eng. S* 2018, 25, 295–306. [CrossRef] *Appl. Sci.* 2022, 12, 7038 16 of 17
- (9) Nunes Filho, R.C.; Galvan, D.; Efftig, L.; Terhaag, M.M.; Yamashita, F.; Benassi, M.d.T.; Spinosa, W.A. Effects of adding spices with antioxidants compounds in red ale style craft beer: A simplex-centroid mixture design approach. *Food Chem.* 2021, 365, 130478. [CrossRef]
- (10) Lehnhardt, F.; Nobis, A.; Skornia, A.; Becker, T.; Gastl, M. A Comprehensive Evaluation of Flavor Instability of Beer (Part 1): Influence of Release of Bound State Aldehydes. *Foods* 2021, 10, 2432. [CrossRef]
- (11) Guimarães, B.P.; Neves, L.E.P.; Guimarães, M.G.; Ghesti, G.F. Evaluation of maturation congeners in beer aged with Brazilian woods. *J. Brew. Distill.* 2020, 9, 1–7. [CrossRef]
- (12) Nakazawa, N.; Wada, R.; Fukushima, H.; Tanaka, R.; Kono, S.; Okazaki, E. Effect of long-term storage, ultra-low temperature, and freshness on the quality characteristics of frozen tuna meat. *Int. J. Refrig.* 2020, 112, 270–280. [CrossRef]
- (13) Ezati, P.; Bang, Y.J.; Rhim, J.W. Preparation of a shikonin-based pH-sensitive color indicator for monitoring the freshness of fish and pork. *Food Chem.* 2021, 337, 127995. [CrossRef] [PubMed]

- (14) Ezati, P.; Priyadarshi, R.; Bang, Y.J.; Rhim, J.W. CMC and CNF-based intelligent pH-responsive color indicator films integrated with shikonin to monitor fish freshness. *Food Control* 2021, 126, 108046. [CrossRef]
- (15) Ezati, P.; Tajik, H.; Moradi, M.; Molaei, R. Intelligent pH-sensitive indicator based on starch-cellulose and alizarin dye to track freshness of rainbow trout fillet. *Int. J. Biol. Macromol.* 2019, 132, 157–165. [CrossRef]
- (16) Ogunniyi, A.D.; Tenzin, S.; Ferro, S.; Venter, H.; Pi, H.; Amorico, T.; Deo, P.; Trott, D.J. A pH-neutral electrolyzed oxidizing water significantly reduces microbial contamination of fresh spinach leaves. *Food Microbiol.* 2021, 93, 103614. [CrossRef]
- (17) Ding, Z.; Johanningsmeier, S.D.; Price, R.; Reynolds, R.; Truong, V.D.; Payton, S.C.; Breidt, F. Evaluation of nitrate and nitrite contents in pickled fruit and vegetable products. *Food Control* 2018, 90, 304–311. [CrossRef]
- (18) Alegbeleye, O.O.; Singleton, I.; Sant’Ana, A.S. Sources and contamination routes of microbial pathogens to fresh produce during field cultivation: A review. *Food Microbiol.* 2018, 73, 177–208. [CrossRef]
- (19) Jin, H.; Qin, Y.; Pan, S.; Alam, A.U.; Dong, S.; Ghosh, R.; Deen, M.J. Open-Source Low-Cost Wireless Potentiometric Instrument for pH Determination Experiments. *J. Chem. Educ.* 2018, 95, 326–330. [CrossRef]
- (20) Inserra, B.; Hayashi, K.; Marchisio, A.; Tulliani, J.M. Sol–gel-entrapped pH indicator for monitoring pH variations in cementitious materials. *J. Appl. Biomater. Funct. Mater.* 2020, 18, 2280800020936540. [CrossRef] [PubMed]
- (21) Ghoneim, M.T.; Nguyen, A.; Dereje, N.; Huang, J.; Moore, G.C.; Murzynowski, P.J.; Dagdeviren, C. Recent Progress in Electrochemical pH-Sensing Materials and Configurations for Biomedical Applications. *Chem. Rev.* 2019, 119, 5248–5297. [CrossRef] [PubMed]
- (22) Yoon, J.H.; Kim, S.M.; Park, H.J.; Kim, Y.K.; Oh, D.X.; Cho, H.W.; Lee, K.G.; Hwang, S.Y.; Park, J.; Choi, B.G. Highly self-healable and flexible cable-type pH sensors for real-time monitoring of human fluids. *Biosens. Bioelectron.* 2020, 150, 111946. [CrossRef][PubMed]
- (23) Manjakkal, L.; Sakthivel, B.; Gopalakrishnan, N.; Dahiya, R. Printed flexible electrochemical pH sensors based on CuO nanorods. *Sens. Actuators B Chem.* 2018, 263, 50–58. [CrossRef]
- (24) Dang, W.; Manjakkal, L.; Navaraj, W.T.; Lorenzelli, L.; Vinciguerra, V.; Dahiya, R. Stretchable wireless system for sweat pH monitoring. *Biosens. Bioelectron.* 2018, 107, 192–202. [CrossRef]
- (25) Córdoba, C.; Mera, J.; Paredes, O.; Benavides, J. Sensor óptico para mediciones de PH obtenido por el método sol-gel con moléculas orgánicas dopadas en matriz vítrea. *Rev. Soc. Química México* 2004, 48, 203–207.
- (26) Rasheed, H.S.; Ahmed, N.M.; Matjafri, M.Z. Ag metal mid layer based on new sensing multilayers structure extended gate field effect transistor (EG-FET) for pH sensor. *Mater. Sci. Semicond. Process.* 2018, 74, 51–56. [CrossRef]
- (27) Sinha, S.; Pal, T.; Kumar, D.; Sharma, R.; Kharbanda, D.; Khanna, P.K.; Mukhiya, R. Design, fabrication and characterization of TiN sensing film-based ISFET pH sensor. *Mater. Lett.* 2021, 304, 130556. [CrossRef]



- Rader, C.M.; Gold, B. Digital Filter Design Techniques in the Frequency Domain. Proceedings of the IEEE 1967, 55, 149–171, doi:10.1109/PROC.1967.5434.
- (28) Pilipović, R.; Risojević, V.; Bulić, P. On the Design of an Energy Efficient Digital IIR A-Weighting Filter Using Approximate Multiplication. Sensors 2021, Vol. 21, Page 732 2021, 21, 732, doi:10.3390/S21030732.
- (29) Dilmi, S. Calcium Soft Sensor Based on the Combination of Support Vector Regression and 1-D Digital Filter for Water Quality Monitoring. Arab J Sci Eng 2022, doi:10.1007/S13369-022-07263-W.
- (30) Stanciu, L.; Stanciu, V.; Badea, R. Digital Filters with Small Transition Frequency Bands. ISSCS 2019 - International Symposium on Signals, Circuits and Systems 2019, doi:10.1109/ISSCS.2019.8801801.
- (31) Kimmel, J.C.; McDole, A.D.; Abdelsalam, M.; Gupta, M.; Sandhu, R. Recurrent Neural Networks Based Online Behavioural Malware Detection Techniques for Cloud Infrastructure. IEEE Access 2021, 9, 68066–68080, doi:10.1109/ACCESS.2021.3077498.
- (32) Bendarkar, D.; Somase, P.; Rebari, P.; Paturkar, R.; Khan, A. Web Based Recognition and Translation of American Sign Language with CNN and RNN. International Journal of Online and Biomedical Engineering (iJOE) 2021, 17, 34– 50, doi:10.3991/IJOE.V17I01.18585.
- (33) Kang, T.; Lim, D.Y.; Tayara, H.; Chong, K.T. Forecasting of Power Demands Using Deep Learning. Applied Sciences 2020, Vol. 10, Page 7241 2020, 10, 7241, doi:10.3390/APP10207241.
- (34) Yang, D.; Gu, C.; Zhu, Y.; Dai, B.; Zhang, K.; Zhang, Z.; Li, B. A Concrete Dam Deformation Prediction Method Based on Lstm with Attention Mechanism. IEEE Access 2020, 8, 185177–185186, doi:10.1109/ACCESS.2020.3029562.



# ANNEX 1

## Article

# Cost-Effective and Portable Instrumentation to Enable Accurate pH Measurements for Global *Industry 4.0* and *Vertical Farming* Applications

Rolando Hinojosa-Meza <sup>1</sup>, Ernesto Olvera-Gonzalez <sup>1,\*</sup>, Nivia Escalante-Garcia <sup>1</sup>, José Alonso Dena-Aguilar <sup>2</sup>, Martín Montes Rivera <sup>3</sup> and Paulino Vacas-Jacques <sup>1,2,\*</sup>

<sup>1</sup> Laboratorio de Iluminación Artificial, Tecnológico Nacional de México/IT de Pabellón de Arteaga, Carretera a la Estación de Rincón Km. 1, Aguascalientes 20670, Mexico; rolando.hm@pabellon.tecnm.mx (R.H.-M.); nivia.eg@pabellon.tecnm.mx (N.E.-G.)

<sup>2</sup> Departamento de Ingenierías, Tecnológico Nacional de México/IT de Pabellón de Arteaga, Carretera a la Estación de Rincón Km. 1, Aguascalientes 20670, Mexico; jose.da@pabellon.tecnm.mx

<sup>3</sup> Dirección de Posgrados e Investigación, Universidad Politécnica de Aguascalientes, Calle Paseo San Gerardo #201, Fracc. San Gerardo, Aguascalientes 20342, Mexico; martin.montes@upa.edu.mx

\* Correspondence: jose.og@pabellon.tecnm.mx (E.O.-G.); paulino.vj@pabellon.tecnm.mx (P.V.-J.)

**Abstract:** Global *Vertical Farming* (VF) applications with characteristic *Industry 4.0* connectivity will become more and more relevant as the challenges of food supply continue to increase worldwide. In this work, a cost-effective and portable instrument that enables accurate pH measurements for VF applications is presented. We demonstrate that by performing a well-designed calibration of the sensor, a near Nernstian response, 57.56 [mV/pH], ensues. The system is compared to a ten-fold more expensive laboratory gold standard, and is shown to be accurate in determining the pH of substances in the 2–14 range. The instrument yields precise pH results with an average absolute deviation of 0.06 pH units and a standard deviation of 0.03 pH units. The performance of the instrument is ADC-limited, with a minimum detectable value of 0.028 pH units, and a typical absolute accuracy of  $\pm 0.062$  pH units. By meticulously designing bias and amplification circuitry of the signal conditioning stage, and by optimizing the signal acquisition section of the instrument, a (minimum) four-fold improvement in performance is expected.

**Keywords:** pH-instrument; *Vertical Farming*; *Industry 4.0*; Nernstian response; cost-effective; portable; instrumentation



**Citation:** Hinojosa-Meza, R.; Olvera-Gonzalez, E.; Escalante-Garcia, N.; Dena-Aguilar, J.A.; Montes Rivera, M.; Vacas-Jacques, P. Cost-Effective and Portable Instrumentation to Enable Accurate pH Measurements for Global *Industry 4.0* and *Vertical Farming* Applications. *Appl. Sci.* **2022**, *12*, 7038. <https://doi.org/10.3390/app12147038>

Academic Editor: Amy J. C. Trappey

Received: 11 June 2022

Accepted: 5 July 2022

Published: 12 July 2022

**Publisher's Note:** MDPI stays neutral with regard to jurisdictional claims in published maps and institutional affiliations.



**Copyright:** © 2022 by the authors. Licensee MDPI, Basel, Switzerland. This article is an open access article distributed under the terms and conditions of the Creative Commons Attribution (CC BY) license (<https://creativecommons.org/licenses/by/4.0/>).

## 1. Introduction

Globally, numerous industries employ the pH level for multiple purposes. For instance, the pH is recurrently used as a central metric to determine the alkalinity. Furthermore, by controlling the pH, an efficient coagulation of sludge in wastewater can be guaranteed [1–3]. Similarly, pH serves as a reference to monitor and prevent corrosion in pipes and boilers [4,5]. In fermentation processes, continuous quantification of the pH is relevant to avoid the generation of unwanted and harmful by-products [6–8]. In the brewing industry, the pH serves to determine aging, increments in hop hardness, and bittering concentrations [9–11]. For perishable products, such as meat and fish, the pH level reveals shelf life and freshness [12–15]. Finally, the pH is central to determine ripening stage, as a function of ethylene concentration, of fruits and vegetables [16–18].

Our laboratory specializes in applied research and technology development in the field of *Precision Farming* (PF). PF is defined as the optimal utilization of technology to accurately assess: planting density, fertilizer quantity, and farming supplies, as needed to precisely predict crop production and yield [19].

Of particular interest to our group is the important field of *Vertical Farming* (VF). VF refers to systems of agriculture where salads, microgreens, herbs, etc. are grown

under artificial light as supplemental irradiation, and sensing technology is integrated to continuously improve quality and yield. VF ensures sustainability by addressing the problem of food security for the growing population around the world [20]. In VF solutions, plants are produced in *Closed Plant Production Systems*, which are generally hydroponic, aeroponic, or aquaponic [21]. In particular, a VF hydroponic system is being constructed in our laboratory, which consists of three distinct vertical racks where various plants can be grown. Each variety is exposed to a specific light recipe depending on the plant characteristics. Ambient humidity and temperature sensors are distributed along the racks to monitor plant parameters. The nutrients come from a reservoir that incorporates a pump, as well as water level, temperature, *total dissolved solids*, and pH sensors. Finally, these sensors communicate wirelessly with a gateway, which transmits the data to a dashboard.

In the field of VF, the pH is called a *main soil parameter*, because its measurement generates *main* or primary information for soil fertilization and bioremediation processes. Moreover, the pH level is central to VF, since it influences the chemical, physical, and biological soil properties, affecting factors such as plant growth, de-nitrification, plant toxicity, bacterial activity, and soil nutrients [22,23]. In the past, several groups have reported the construction of instrumentation to enable pH measurements. For example, Jin et al. [24] developed a pH potentiometer applicable to teaching in a chemistry laboratory setting. Moreover, a pH sensor to assess the changes in cementitious materials, through a sol-gel process with an alizarin yellow as meter, has been developed [25]. Additionally, portable chemical sensors, requiring specialized processes for manufacturing, have been reported for non-invasive real-time monitoring of parameters for medical care and disease diagnosis [26,27]. Manjakkal et al. [28] integrated an electrochemical pH sensor, applicable to several industries, with a screen printed on flexible substrates through CuO nanostructures exhibiting nanorods morphology. The measurement range was established to be 5–8.5 pH units. Dang et al. [29] developed a wireless system for monitoring pH of sweat, integrated by a pair of serpentine-shaped stretchable interconnects. The authors constructed a reference electrode using graphite-polyurethane composites for biological applications. Cordoba et al. [30] reported the development of an optical sensor, which requires a high-cost external instrument to determine the pH level. Rasheed et al. [31] designed a multilayer (ZnO/Ag/ZnO) film pH sensor, which was tested as an extended gate field effect transistor. The pH detection range was demonstrated to be 2–12 pH units. Lastly, solutions using ISFET (Sensitive Field Effect Transistors) sensors, which have the advantage of being small, have been proposed. Nonetheless, with ISFET sensors, samples under study must be small, and the measuring range is limited to 10 pH units (1.5 to 11.5 pH) [32].

An essential aspect of any instrument intended for VF use is that such instrumentation must meet availability, portability, and cost-effectiveness constraints to enable global adoption. Furthermore, the global food supply chain, which by 2050 will have to increase its capacity by 60–70% due to the growth of the world population [33], would benefit greatly if connected (characteristic of *Industry 4.0* solutions) pH sensors were available. Thus, the goal of this article is to describe the implementation of a portable, cost-effective, and connected instrument that enables accurate pH measurements for VF and, more generally, *Industry 4.0* applications.

This work is divided into six sections. Section 2 deals with the theoretical background, as required to address pH sensing for global *Vertical Farming* applications. In Section 3, the instrument is described in the context of a three-layer Internet of Things architecture. Here, the circuit design for pH measurements is presented. In Section 4, the results of sensor characterization and pH measurements are presented. The discussion section, presented in Section 5, describes two modifications that can be implemented to the circuitry, in order to increase the precision of the instrument. Finally, the results of this work and future research directions are summarized in Section 6.

## 2. Theoretical Background

### *pH Sensing Aspects: Considerations for Global Industry 4.0 Applications*

The term *Potentia Hydrogenii*, commonly known as pH, was originally proposed by Sørensen to describe the solution pressure of hydrogen-ions in aqueous solutions. Nowadays, the pH is conceived as a metric to quantify the activity of hydrogen-ions,  $a_{H^+}$ , in any solution. Mathematically, the pH is defined as shown in Equation (1) [34]:

$$\text{pH} = -\log a_{H^+} \quad (1)$$

The most common materials utilized for constructing electrochemical pH sensors include: 1. Glass Electrodes, 2. Metal Oxides, 3. Polymer/Carbon, and 4. Metal/Metal Oxide-Metal Composites [35]. The suitability of any of the aforementioned sensors to address global *Industry 4.0* challenges, including *Vertical Farming*, depends on worldwide availability, accessibility, and cost-efficiency of the constituting materials. Unquestionably, the *Glass Electrode* is a front-runner by fulfilling the requirements needed for global adoption of pH sensing. Glass electrodes [36], including the well-known *silver | silver-chloride* (Ag | AgCl) arrangement, implement a two electrode setup. These potentiometric systems consist of working and reference electrodes. Furthermore, the main working concept of these pH sensors relies on measuring equilibrium conditions at the surface of the working electrode. Under equilibrium conditions, *Nernst's Law*, shown in Equation (2) applies, and describes the (half) cell potential in terms of the activity of the electroactive species [37]:

$$E_{eq} = E^0 + \left(\frac{RT}{nF}\right) \ln\left(\frac{a_0}{a_R}\right) = E^0 + 2.303\left(\frac{RT}{nF}\right) \log\left(\frac{a_0}{a_R}\right) \quad (2)$$

where

$E_{eq}$  represents the electric potential at equilibrium [V],

$E^0$  denotes standard potential [V],

$R$  is the universal gas constant;  $8.314 \text{ [J mol}^{-1} \text{ K}^{-1}]$ ,

$T$  represents the temperature [K],

$n$  denotes the electrons number,

$F$  is the Faraday constant;  $96,485 \text{ [C mol}^{-1}]$ ,

$a_0$  represents the activity of the oxidizing agent,

$a_R$  denotes the activity of the reducing agent.

In a practical setting, on one side of the sensor, the reference electrode is exposed to a well-known and constant solution of hydrogen-ion activity, e.g., a buffer solution. On the other side of the sensor, the electrode is in contact with the pH solution under study. Due to the aforementioned sensor design, the contribution of one (i.e., the reference) of the electrodes is known, and Equation (2) can be rewritten as a function of the pH under study, as expressed in Equation (3):

$$E = E^0 - \left(\frac{2.303 \times RT}{nF}\right) \text{pH} \quad (3)$$

Detection electronics, signal conditioning and acquisition, as well as wireless communications of the electrical signal are critical aspects in sensing (pH) variables for global VF (and *Industry 4.0*) applications, especially due to the fact that a majority of the (farming) operations occur in places with scarce access to technology. Therefore, the instrumentation required to accurately measure pH for global *Industry 4.0* applications is far from trivial, requiring accurate characterization of the expected signals and a suitable design that is applicable to the setting where the technology will be implemented.

Taking these considerations for global VF applications into account, an accurate characterization of the expected signal is indispensable. For a standard and globally available *silver | silver-chloride* reference electrode configuration, the electrochemical redox response is well known (Ag | AgCl standard potential being 220 mV [38]) and involves the

generation of only one electron. Consequently, the relationship between electric potential and pH is linear, and the slope is a function of temperature (refer to Equation (3)). Assuming a working temperature of 25 °C, the ideal Nernst response is shown in Equation (4):

$$E = E^0 - 59.16 \times \text{pH} [\text{mV}] \quad (4)$$

As presented in this section, novel materials have been proposed and developed to measure the pH for various applications. Some of these materials exhibit a sensitivity (i.e., the slope in the last expression) metric that is greater than the value of the Nernstian response, described in Equation (4). Nevertheless, despite material and manufacturing complexities, most sensitivity values oscillate around 40 to 80 [mV/pH]. Furthermore, in global *Industry 4.0* applications, including VF for developing countries, access to electrodes made with novel materials is scarce, limiting sensitivity to values below the Nernstian response, 59.16 [mV/pH]. Therefore, the design and implementation of portable and cost-efficient solutions to accurately measure pH in global *Industry 4.0* applications represent a challenge.

In this work, we present a potentiometric pH measurement instrument that is compatible with readily available glass electrodes (as well as other less conventional sensors), and that implements an optimal electronic design by being accurate, portable, cost-efficient, and *Industry 4.0* ready for global applications.

### 3. Materials and Methods

Internet of Things (IoT) is a key enabling technology for *Industry 4.0* applications. No unified or standardized agreement has been reached with respect to IoT architectures. Nonetheless, every IoT architecture should implement at least three layers [39]. More complex architectures, including four- or five-layered ones, have also been proposed [40]. The instrument described in this work is unique, compared to other pH sensing devices, because it incorporates a three-layer IoT architecture with *Perception*, *Network*, and *Application Layers*.

#### 3.1. Materials

In Figure 1, we depict the block diagram of the cost-effective and portable instrument to enable accurate pH measurements for global VF and, more generally, *Industry 4.0* applications, as proposed and implemented by our group. The instrument described in this work is unique, compared to other pH sensing devices, because it incorporates a three-layer IoT architecture with *Perception*, *Network*, and *Application Layers*.

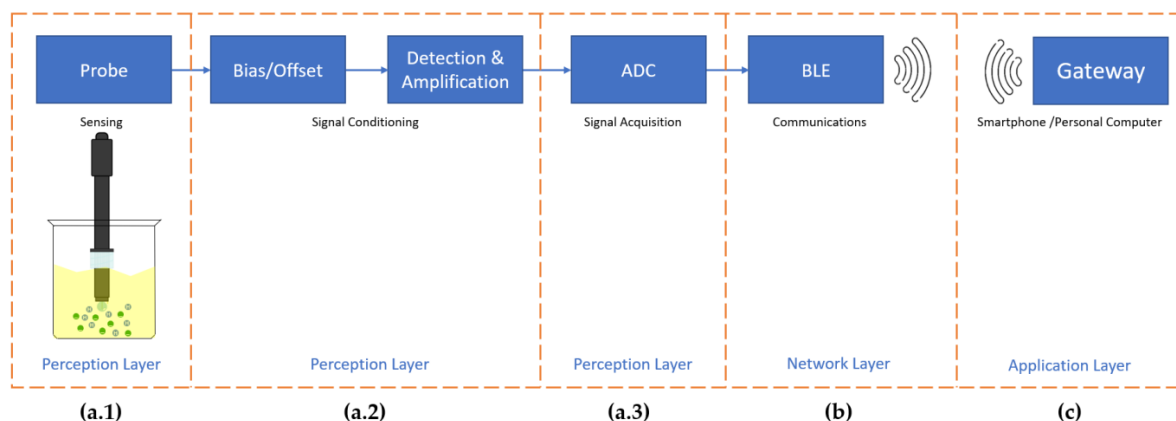


**Figure 1.** The cost-effective and portable pH instrument has been implemented in a three-layer IoT architecture, consisting of (a) *Perception*, (b) *Network*, and (c) *Application Layers*. The *Perception Layer* is further divided into: (a.1) *Sensing*, (a.2) *Signal Conditioning*, and (a.3) *Signal Acquisition* stages. The *Network Layer* has been enabled by means of a Bluetooth (BLE) *Communications* stage. The *Application Layer* utilizes a gateway, in the form of a *Smartphone* or a *Personal Computer*, for user interaction.

As illustrated in Figure 1, the three-layer architecture of the instrument incorporates: (a) *Perception Layer*, (b) *Network Layer*, and (c) *Application Layer*. The *Perception* or *Physical Sensor Layer* is further divided into: (a.1) *Sensing*, (a.2) *Signal Conditioning*, and (a.3) *Signal Acquisition* stages. Meanwhile, the *Network Layer*, used to connect the pH sensor to other sensors, network devices, or servers, is implemented through a *Wireless Bluetooth (BLE) Communications* stage. Finally, the *Instrument Application Layer*, which is in charge of providing useful information to the user, is enabled by means of a smartphone or a personal computer. Hereafter, we describe the materials necessary to implement the sections of the accurate, cost-effective, and portable instrumentation for pH measurements.

### 3.1.1. Perception Layer—Sensing Stage

We employ a *silver | silver-chloride, Ag | AgCl*, glass electrode in a potentiometric arrangement, which is readily available and cost-effective. The implemented sensor (Hinotek, Ningbo, China, E201-BNC) consists of a working electrode in the form of a glass ball, filled with a well-known buffer solution, which is in contact with the sample under study. The reference electrode also interacts with the solution of unknown pH. The sensor is protected by a cover and maintained in a storage solution, which is central to ensure sensor performance over time. A schematic of the pH sensor is depicted in Figure 2.

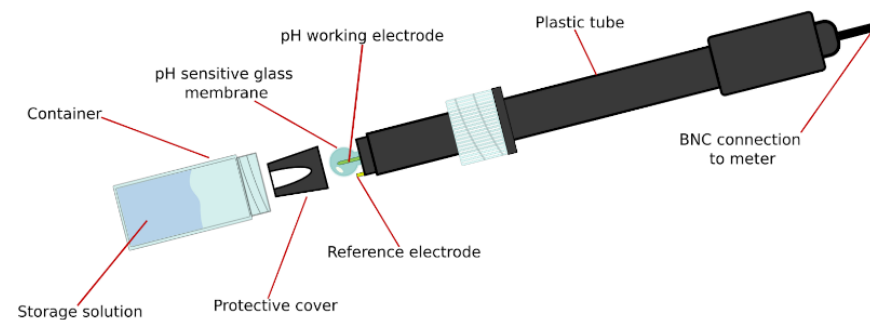


**Figure 2.** The implemented sensor consists of: a. Working electrode in contact with sample under study; b. Reference electrode interacting with solution of unknown pH; c. Protective cover; d. Storage solution; and e. Standard BNC connector for interoperability.

Any other pH detector (including those implementing novel materials) in a potentiometric arrangement would, despite accessibility and/or availability constraints, be compatible with the instrument described in this work, provided it has a standard BNC connector. Such a connector was selected to ensure interoperability and to facilitate signal conditioning interfacing.

### 3.1.2. Perception Layer—Signal Conditioning and Signal Acquisition Stages

As clearly seen from Equation (4), alkaline solutions tend to generate negative potential differences. Meanwhile, acidic solutions will have a positive trend, in terms of the voltage generated by the sensor. Therefore, in order to ensure that the electrical waveform is adequate for analog to digital conversion (ADC), an offset voltage must be implemented in the signal conditioning stage. As illustrated in Figure 3, a divider network with a stable voltage input (Texas Instruments, Dallas, TX, USA, TL431) of 2.5 V defines the bias voltage. This offset voltage can be varied by means of a potentiometer (RV1). In the discussion section, we present key modifications to the passive components of this bias stage of the signal conditioning circuitry, which serve to optimize pH detection.

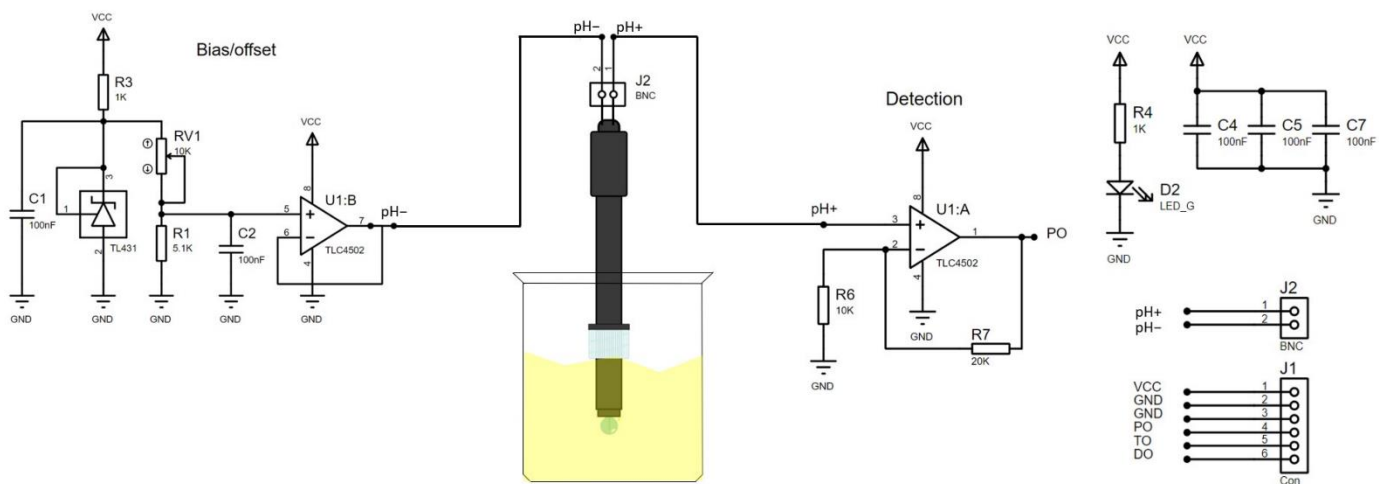


**Figure 3.** The signal conditioning stage is constructed by implementing an offset section, followed by a detection/amplification stage. The sensor is coupled using an array of precision op-amps in buffer and non-inverting amplifier configurations to ensure adequate performance.

Considering that a potentiometric system is in place, pH measurements should be ideally performed in equilibrium, as emphasized in Equation (2). Therefore, the electrical current generated between working and reference electrodes should be as negligible as possible. This implies that the impedance of offset and detection stages should be various orders of magnitude greater compared to the pH sensor impedance.

The instrument employs an array of precision operational amplifiers, op-amps (Texas Instruments, TLC4502), with an input impedance of  $1 \times 10^{12} [\Omega]$  and a typical bias current of 1 [pA]. Such a configuration ensures that negligible current flows through the sensor as required by the potentiometric design. Finally, the amplification section is configured as a conventional non-inverting amplifier with the gain determined by resistors R6 and R7, as depicted in Figure 3. In order to facilitate global VF applications, the complete signal conditioning stage can be implemented in a single electronic module (DIY More, Hong Kong, China PH-4502C). A thorough revision of such integrated modules is suggested, in order to determine expected offset, detection, and amplification performance. Finally, breadboard implementations can be constructed by following the schematic of Figure 3.

The electrical signal generated by the instrument proposed in this work is the sum of the bias voltage plus the potential difference generated by the pH sensor, as seen in Figure 3. This signal is amplified and acquired by the ADC of a microcontroller. In our case, an ATmega328P (Atmel Corporation, San Jose, CA, USA) microcontroller built into an Arduino UNO board (Smart projects, Ivrea, Italy, Arduino UNO) was used. It is important to note that, in order to enable global adoption, practically any standard microcontroller, such as those of the STM32 Family (STMicroelectronics, Grenoble, Auvergne-Rhône-Alpes, France), the nRF52 series (Nordic VLSI, Trondheim, Trondheim Fjord, Norway), or other member of the ATmega series (Atmel Corporation, San Jose, CA, USA), can be equally employed. Similarly, other integrated modules can be utilized to replicate this instrumentation locally.

### 3.1.3. Network Layer—Bluetooth Wireless Communications Stage

The *Network Layer* enables the pH sensor to connect to other devices such as gateways (e.g., in the form of smartphones or personal computers) or even other sensors. Such connectivity is characteristic of *Industry 4.0* applications. In the instrument described in this work, a Bluetooth radio version 2.0 (Linvor, Jinan city, Shandong, China, LV-BC-2.0) enables wireless transmission of pH data, and serves as the *Network Layer*. The radio, implemented in a breadboard (Olimex, Plovdiv, Bulgaria, BLE HC-06) for ease of integration, is a Class 2 device, and exhibits a maximum communication range of 10 m [39]. This range is sufficient for isolated VF applications. However, for distributed VF applications or, more generally, other *Industry 4.0* applications, a Class 1 Bluetooth device can be employed to yield a

range of 100 m. In fact, for conventional farming, the Bluetooth technology enables a very desirable feature: *Mesh Networks* [40]. In such a topology, a rather large area (e.g., 1000 m<sup>2</sup>) can be covered with a handful of Bluetooth radios. Any gateway, functioning as part of the *Application Layer*, which supports Bluetooth communications, as specified in this section, can interface with the instrumentation, potentially minimizing deployment challenges encountered in global *Industry 4.0* applications.

### 3.1.4. Integration of the Portable pH Instrument

Figure 4 displays the layout and a representative picture of our portable pH instrument, as well as the integration required to enable accurate pH measurements for global VF applications. To integrate the overall solution six main components are needed: 1. Glass electrode for pH sensing with standard BNC connector; 2. Signal conditioning module; 3. Bluetooth communications module; 4. Integration breadboard; 5. Signal acquisition and processing module; and 6. Power supply.

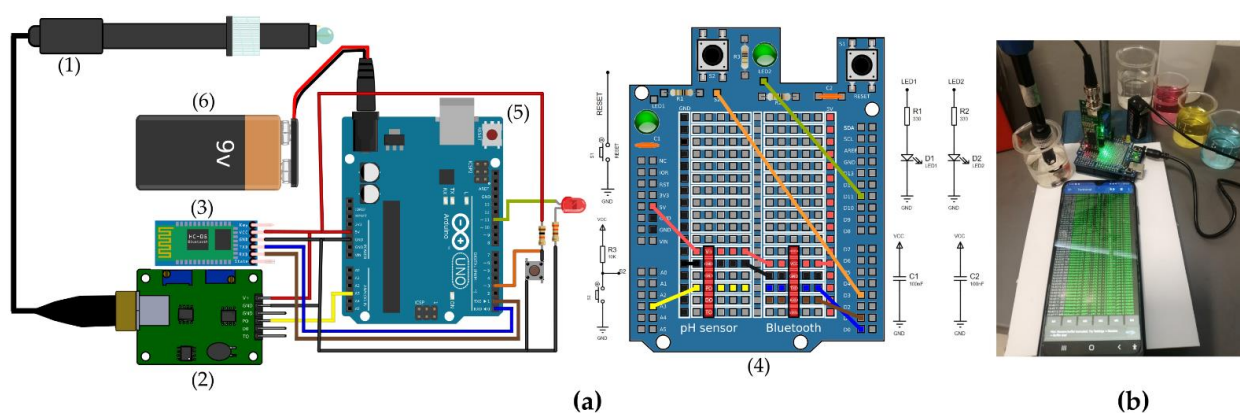


**Figure 4.** (a) The pH instrumentation for global VF applications consists of six main components: (1) Glass electrode; (2) Signal conditioning module; (3) Bluetooth communications module; (4) Integration breadboard; (5) Signal acquisition and processing module; and (6) Power supply. (b) Representative photo.

Figure 4a provides a detailed integration (i.e., wiring) diagram to ensure adequate signal processing, as well as the intermediate breadboard needed to assemble the components that constitute the instrument. Finally, Figure 4b presents a representative picture of the portable instrument for pH measurements.

## 3.2. Methods

### 3.2.1. pH Sensor Characterization

The pH of a solution under study can be determined after a meticulous calibration. In order to characterize the pH sensor, the potential difference over the two electrodes must be measured, and related to the hydrogen-ion activity of reference solutions.

Three pH buffer solutions (Mallinckrodt Baker, Hampton, NJ, USA, manufacture date 31 August 2020) with a 2-year validity certification (at 25 °C) and traceable to NIST standards were used. The standard buffer solutions employed in the calibration of our instrument were: 1. Biphthalate; 2. Phosphate; and 3. Borate. Correspondingly, the pH and certified range values for the buffer solutions were 4 [3.96, 4.04]; 7 [6.96, 7.04]; and 10 [9.99, 10.01]. Utilizing the batch information of our buffer solutions, the pH reference values for our calibration procedure were: 3.99, 6.98, and 10.00.

The characterization method is divided into two phases. In phase one, the sensitivity of the pH sensor is determined with a conventional voltage meter, such as a multimeter. It is important to note that the instrument input impedance should be high, and the noise performance optimally below the mV range for accurate calibration. In phase two, the signal conditioning stage, as described in this work is employed, in order to quantify



the modified (i.e., including bias and amplification effects) sensitivity of the pH sensor. Hereafter, the methods for both phases are described.

Phase I does not include the signal conditioning stage. First, the pH sensor is attached to the measuring device using the BNC connector. For this phase, a multimeter (Steren, Ciudad de México, Mexico, MUL-605) is employed to determine the voltage, irrespective of polarity, as a function of buffer solution. Next, the calibration curve that describes the linear behavior of the sensor is calculated by using regression techniques. As seen from Equation (4), the derived slope will serve to relate pH as a function of (sensor) voltage.

In Phase II, the signal conditioning stage is included. Nonetheless, the above methodology remains practically the same. One of the differences is that in the first step, the pH sensor is attached to the signal conditioning module using the BNC connector. Then, the circuitry of Figure 3 is employed to measure the voltage as a function of buffer solution. Next, the calibration curve that describes the linear behavior of the sensor is obtained by employing regression techniques. Here another difference is in place. The pH is still related to a modified potential difference, which includes the effects of the signal conditioning stage: bias and amplification. The modified potential difference is obtained by dividing the output voltage by the gain and subtracting the bias voltage. The derived slope will serve to relate pH as a function of (instrument) voltage. Finally, it is important to note that, irrespective of the calibration method, the overall cleanliness and mechanical stability, while measuring, of the working electrode are key factors to obtain accurate calibration results.

### 3.2.2. Preparation of Signal Conditioning, Acquisition, and Transmission

The procedure implemented to utilize the signal conditioning, acquisition, and transmission stages is as follows. First, the wiring of the instrument is performed, as shown in Figure 4a. It is relevant to note that this step defines the performance of the signal acquisition stage, if an external voltage is used. In our case, this parameter was set to 5 V using the microcontroller code. Then, the offset voltage of the instrument is tuned by cautiously adjusting the potentiometer, RV1 in Figure 3, thus accounting for the ADC configuration previously mentioned. Finally, BLE transmission of sensed data is facilitated by means of the microcontroller code, which implements two modalities: *Calibration* and *Measurement*. In *calibration* mode, the user is enabled to characterize the sensor (refer to Section 3.2.1) by employing the three buffer solutions. The resulting parameters are stored in the instrument memory for future use. In *measurement* mode, the instrument acquires arbitrary voltage values, and converts such information to pH values. pH information is then sent serially to the Bluetooth radio, which transmits wirelessly the data to a gateway (i.e., personal computer or smartphone) for further processing.

### 3.2.3. Methodology to Assess the pH of Arbitrary Solutions

The first step to measure the pH of a selected sample is to perform the calibration of the probe, refer to Section 3.2.1. Here, sensor cleanliness is crucial. Second, the sensor is connected to the instrument, and the signal conditioning, acquisition, and transmission stages are prepared as mentioned in Section 3.2.2. Once this has been performed, the instrument is ready for measurements. Nevertheless, the sample must be prepared and the chemical integrity of the same must be ensured. In order to perform pH evaluation, mechanical stability must be guaranteed. In the discussion section, we elaborate further on the implications of unstable systems, which are likely to occur in global VF settings.

A *simple-to-use* interface was implemented, by means of a push-button (S2), to select the operation modality. A light emitting diode (LED2) is used to indicate operation mode, and for general user interaction. Once instrument and sample are ready, the user selects an operation mode, by means of S2, and performs the pH measurement. Such measurement is then transmitted to the gateway of interest. The microcontroller code and exemplary pH measurements are available upon request to the authors.

The microcontroller code and exemplary pH measurements are available upon request to the authors. Furthermore, calibration code may be found in the Supplementary Materials section of this work.

## 4. Results

### 4.1. Signal Conditioning Characterization

Potential differences with negative and positive polarities will ensue for alkaline and acidic solutions, respectively. Furthermore, in order to optimize performance, the full dynamic range of the ADC should be used. This condition implies that the minimum bias voltage should ideally match the potential difference for the most alkaline solution possible. Additionally, optimally, the maximum offset value would match the potential difference for the most acidic sample.

The minimum offset voltage is obtained by selecting the greatest resistance value of the potentiometer, RV1, in Figure 3. Recalling that a 2.5 V stable source feeds the voltage divider network, by simple inspection, the minimum bias voltage is determined to be 840 mV. The maximum offset, however, depends not only on the divider network (with a theoretical value of 2.5 V), but also on the amplifier and acquisition setup. From Figure 3, it is trivial to anticipate a three-fold gain for the amplification stage. Furthermore, assuming a conventional ADC configuration with an analog reference voltage  $V_{AREF}$  of 5 V, the maximum input signal will be given by  $V_{AREF}/GAIN$ , or quantitatively 1.67 V.

A device exhibiting Nernstian response would have a full detection range of  $\pm 414$  mV, centered ideally at 0 V for a neutral pH. In global VF applications, the aforementioned range denotes theoretical extrema of practically all available sensors.

Combining the effects of bias and electrode response, the signal conditioning characterization is obtained before and after the amplification stage. The minimum theoretical voltage should be 426 mV before amplification and 1.278 V after. Meanwhile, as stated above, the maxima have an additional restriction imposed by the ADC. Thus, the maximum voltage should be 1.67 V before amplification and 5 V after. This analysis serves to demarcate the working bias range of the signal conditioning stage. Assuming the Nernstian response, end users can select any offset voltage in the 840–1250 mV range. From this analysis, we detect an area of improvement; namely, the optimization of the ADC dynamic range. Such improvement is addressed in the discussion section.

### 4.2. Sensor Characterization

As described in Section 3.2.1, and shown quantitatively in Figure 5, the pH sensor is characterized in two phases: Figure 5a, using a multimeter and Figure 5b, employing the instrumentation described in this work. During the first ten seconds, refer to Figure 5, the sensor remains outside of the sample, and then the electrode is exposed (i.e., introduced) to the solution under test. It is important to note that this was performed for both configurations. Then, we let the sensor stabilize and perform the measurements for a period of 60 s, while acquiring data every 0.25 s. Table 1 presents, for both sensor characterization phases, the statistical measures obtained for voltage and pH after the aforementioned 60 s period.

**Table 1.** Statistical parameters derived from pH sensor characterizations: Phase I and Phase II.

pH *	Phase I. Multimeter **	Phase II. Instrumentation **	
	E{V} [mV] ***	E{V} [V]	$\sigma\{V\}$ [V]
4	164.74302	3.04761449	0.000487422
7	4.48031	2.5272936	0.000456076
10	−166.07790	2.01269855	0.000459554

\* The certified (Batch/Product Numbers: B38W00/5657, B35W06/5656, and B35W00/5655) pH values of the buffer solutions utilized in this work were 3.99, 6.98, and 10.00. The systematic uncertainty of the pH of buffer solutions establishes a limit in the precision (in the 0.01 range) of pH measurements that can be achieved with this method. \*\* Here, E{V} and  $\sigma\{V\}$  stand for expected value and standard deviation of random variable V, which represents the measured voltage or electrical potential in mV or V. \*\*\* The measurement range for the voltage meter was set to automatic, and did not surpass  $\pm 400$  mV. From the manufacturer datasheet, the precision of the readings is expected to be 0.5% within this range.

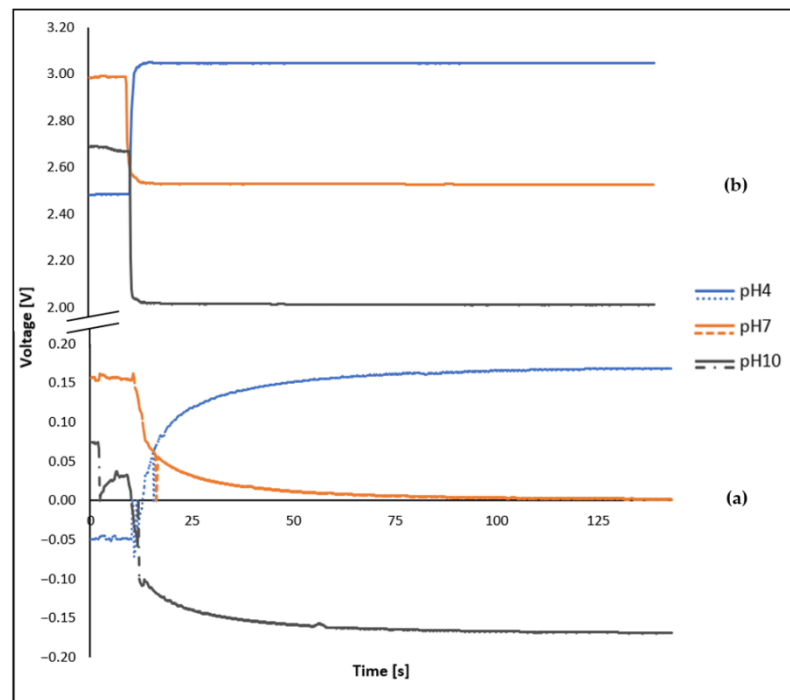


**Figure 5.** The sensor characterization is performed in two different phases: (a) utilizing a multimeter and (b) employing the instrumentation described in this proposal.

As noted in Section 4.1, from Table 1 and Figure 5, we confirm that, for our sensor, the response to neutral pH solutions is practically centered at 0 V. Additionally, for the configuration of the instrument, the bias voltage was measured to be 840 mV. Thus, the expected quantitative voltage for a neutral solution, at the instrument output, is straightforwardly determined to be 2.52 V, which matches precisely the measured value.

Considering that the instrument will bestow information comparable to that shown in Table 1, the calibration curve is obtained by performing a linear regression to this data. In Equation (5), the linear regression is presented. Furthermore, in Figure 6, we depict the calibration curve for our pH sensor.

$$\text{pH} = -5.791 V_{out} + 21.647 \tag{5}$$

where  $V_{out}$  represents the output instrument voltage in [V].

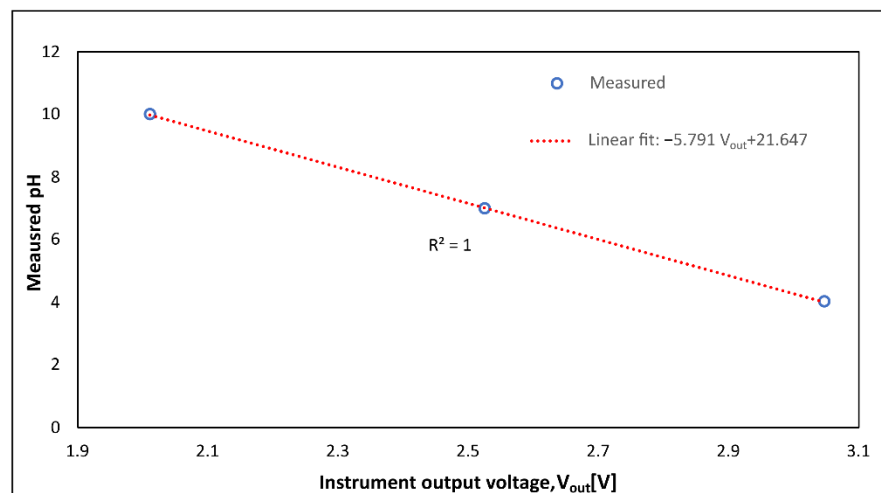


**Figure 6.** The calibration curve enables the direct measurement of pH from the instrument output.

In Section 3.1.2, the importance of the instrument impedance to obtain accurate measurements was emphasized. Additionally, in the design proposed in this work, we placed special emphasis on this respect. In fact, the multimeter datasheet (Steren, Ciudad de México, Mexico, MUL-605) reports an input impedance of 10 M $\Omega$ , which is significantly lower than the impedance in our proposal. By carefully following the procedure for Phase II, described in the preceding section, the instrument (without offset and amplification effects) sensitivity can be calculated. This information is shown in Table 2.

**Table 2.** Statistical sensitivity parameters derived from pH sensor characterization: Phase II.

Phase II. Instrumentation *	
pH	E{V} [mV]
4	173.666667
7	0
10	-171.666667

\* Here, E{V} is the expected value of a random variable V, which represents the measured voltage in mV.

A device exhibiting Nernstian response would have a detection range of  $\pm 177$  mV, ideally centered at 0 V, for a pH range of  $\pm 3$  units. Comparing the theoretical Nernstian response to the values presented in Table 2, a maximum deviation of 6 mV for the proposed instrument is observed. Moreover, translating the information presented in Table 2 to the sensitivity metric (i.e., voltage per single pH unit [mV/pH]), it is simple to demonstrate a measured (average) sensitivity of 57.56 [mV/pH]. Comparing this value to the Nernstian response, see Equation (3), the instrument sensitivity is 1.6 units below the reference parameter. By simple mathematical calculation this represents a 97.3% percent “compliance” with respect to the optimal Nernstian response. It is, thus, concluded that the proposed pH sensor characterization described in this work may enable the creation of a precise and portable instrument for global VF applications requiring pH measurements.

#### 4.3. Accurate pH Measurements for Global Industry 4.0 and Vertical Farming Applications

In order to validate the accuracy of our portable instrumentation, as intended for global VF (and *Industry 4.0*) applications, a laboratory grade pH device (Ohaus Corporation, Parsippany, NJ, USA, AB33M1) was selected as gold standard. Thirteen samples with varying pH values were utilized. For every measurement, a rigorous process involving cleanliness, temperature stability, calibration, and mechanical stability of the probe was implemented. Figure 7 depicts the results of the instrument presented in this work to enable accurate pH measurements for global *Industry 4.0* and VF applications. In order to ensure global VF applicability, the cost of the device is important. In our case, the cost (uelectronics) of the instrument was ~60 USD. In contrast, the gold standard costs ~715 USD (Viresa); i.e.,  $\sim 11.5\times$  more expensive. Thus, our solution is cost-effective, portable, and accurate.

Using the information depicted in Figure 7, the average and median absolute deviations (reference minus measured pH) are 0.057 and 0.063 pH units, respectively. Meanwhile, the standard deviation of the absolute deviation is 0.03 pH units. For the acidic substance exhibiting the lowest pH value, the maximum relative error is 5%. In contrast, alkaline substances have relative errors that are as low as 0.3%. Figure 7 depicts error bars that describe the absolute deviations of measured and reference data. As noted before, various error bars are not easily distinguishable due to instrumentation performance. In any case, the accuracy and applicability of the proposed instrument is clearly established.

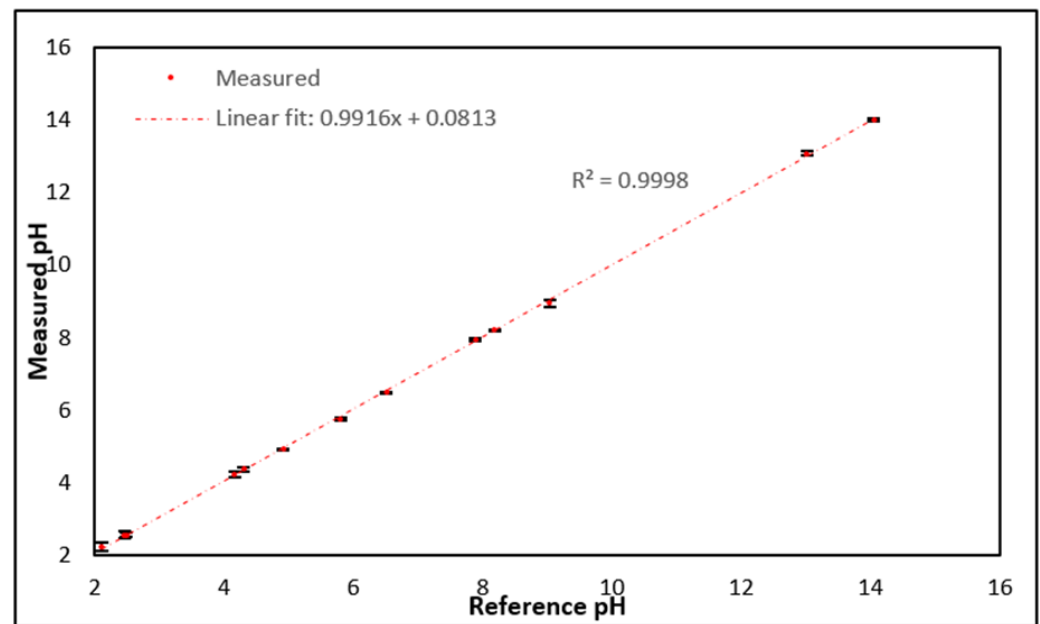


**Figure 7.** The performance of the portable instrumentation for pH measurements is established by comparing our results to those of a reference instrument (Ohaus, AB33M1). The solutions utilized for this experiment, in ascending order of pH value, commencing from the most acidic one, are given as follows: a. Lemon juice, b. Cola soda, c. Vinegar, d. Orange juice, e. Beer, f. Coffee, g. Tea, h. Milk, i. Tap water, j. Human saliva, k. Hand soap, l. Sodium hypochlorite, and m. Sodium hydroxide.

## 5. Discussion

Various research groups have proposed different systems for pH sensing. Table 3 presents a comparison of sensor features, including *pH sensitivity* and *range*, *application area*, *cost*, and *portability*, as required for global applications. This analysis serves to present the results of this work in the light of previous advances reported in the scientific literature. The features of the laboratory grade apparatus, which was employed as gold standard, are also included for completeness.

**Table 3.** Comparison of pH sensor features as required for global applications.

pH Sensing Materials	pH Range	pH Sensitivity	Application Area	Cost (USD)	Portable	Global Access	Ref.
CuO Nanorods	5–8.5	0.64 $\mu\text{F}/\text{pH}$ at 50 Hz	Biological, Food, Medicine, Agriculture	N/A	No	No	[28]
Graphite-polyurethane composite (Ag AgCl) EGFET (ZnO Ag ZnO)	5–9	$-11.13 \pm 5.8 \text{ mV}/\text{pH}$	Health Monitoring *	N/A	N/A	N/A	[29]
Glass electrode (Pd PdO)	2–12	0.62 $\mu\text{A}^{1/2}/\text{pH}$	Health Monitoring	N/A	N/A	N/A	[31]
Carbon fiber thread electrodes coated with self-healing polymers (Ag AgCl and Pt wire)	N/A	51 mV/pH	Laboratory Instruction	\$50 **	Yes	No **	[24]
Sol-gel-entrapped TiN-gate ISFET	3.89–10.09	58.28 mV/pH	Health Monitoring and Disease Diagnostics	N/A	Yes	No	[27]
Ohaus AB33M1 (Ag AgCl)	10.2–12	N/A	Cementitious materials	N/A	N/A	N/A	[25]
Glass electrode (Ag AgCl)	4–10	53.98 mV/pH	Medicine and Biological Industries	N/A	N/A	N/A	[41]
Glass electrode (Ag AgCl)	1–14	N/A	Not restricted	\$715	No	No	[TW] ***
Glass electrode (Ag AgCl)	2–14	57.56 mV/pH	Not restricted	\$60	Yes	Yes	[TW] ***

\* The device was originally reported for *sweat monitoring* applications. \*\* Reported cost refers to hardware electronics, the design of which is intended for a laboratory setting and would require modularity to enable global adoption. \*\*\* TW = This Work.

As seen from the data in Table 3, most of the end applications are related to biological areas. Additionally, a crucial aspect is that measurement range are limited, and that sensors have been designed, developed, and implemented for specific tasks. In contrast, it is clear from Table 3 that the instrumentation described in this work provides the features of *accuracy, measurement range, portability, cost-efficiency, and adaptability*, necessary to address global *Vertical Farming* and *Industry 4.0* pH sensing challenges. Nonetheless, some systems, such as those reported by Rasheed et al. [31] and Jin et al. [24], exhibit similar characteristics in terms of measuring range or cost (i.e., specific features needed for global adoption). Having a single instrument that can offer the complete set of features needed for global adoption is a key contribution of this work.

The instrumentation described in this work enables precise determination of the pH, with an expected absolute deviation of 0.06 pH units and a standard deviation of 0.03 pH units. The precision required of pH measurements is intrinsically related to the task under consideration. For instance, in the field of hydroponic farming (hydroponics is an advanced technique for plant and vegetable production that utilizes water instead of soil as growing matrix [42], implementable in a *Vertical Farming* setting), the pH level must be maintained in the 5.5 to 6.8 range [42]. Furthermore, the detection of minor changes in the pH level significantly impacts water quality, and thus, the main nutrients of these systems. The instrument presented in this work enables accurate detection of pH variations of 0.1 pH units, with a 68% confidence interval, for hydroponic farming. Hereafter, a brief discussion of the sources of uncertainty, within our instrument, is presented for those applications requiring more stringent pH control.

First, with respect to the actual sensor, the efficiency of the electrode can degrade due to the manufacturing process (better vs worse quality), glass membrane, reference cables (e.g., electrical interference or RF coupling), and especially maintenance. A decrease in performance has been validated, by our group, if the electrode is poorly maintained (i.e., cleaned). To counteract this problem, the calibration, as described in this work, was implemented. More concretely, in order to ensure accurate readings, the calculation of the *sensor “compliance”* metric, is advisable. For the case reported in this work, such a metric was demonstrated to be 97.3%.

Next, the impact of *Signal Conditioning* and *Acquisition* stages, which are closely interrelated, is addressed. In the current version of the pH instrument, refer to Section 4.1; the offset voltage is fixed to its minimum value of 840 mV. This places a restriction on the usable detection range of the ADC to 48%; namely, from 1.32 to 3.73 V (corresponding to pH values from 14 to 0 units). Figure 8 depicts a two-step approach to significantly improve the signal conditioning circuitry. First, the feedback resistor, R7, can be substituted (e.g., 10 k $\Omega$ ) to set the amplification factor to a different value (e.g., GAIN = 2), and the analog reference voltage can be set to 2.56 V. By implementing this first step, the usable detection range of the ADC becomes 65%; that is 0.83–2.51 V. Second, the minimum offset voltage of the divider network can be reduced to a different value (e.g., 420 mV). This is achieved by replacing the fixed resistor, R1, with a 2 k $\Omega$  component. By selecting the amplification factor correctly, the usable detection range can be optimized to 98% (i.e., in the 0–2.52 V range), which is approximately a two-fold improvement.

As noted throughout this work, the expected magnitude of the detected signal will approximate the Nernstian response, with a maximum of 59.16 mV per pH. For our instrument, the measured sensitivity was demonstrated to be 57.56 [mV/pH]. Thus, a difference of 10 mV in the sensor signal implies a variation of  $\sim 0.175$  pH units. Various sources can induce voltage variations of this magnitude, including the communications and ADC stages.

The *Network Layer*, or wireless communications stage, is not only necessary to enable transport of pH information, but rather indispensable to minimize coupling and/or layout effects in the instrumentation. In fact, pH information could also be sent to a personal computer (or smartphone) by means of wired (e.g., serial) communications. However, voltage variations on the 10 mV range due to coupling errors are commonly encountered

in wired communications. As noted before, such variations would induce an error that is almost twice the value of the instrument accuracy.

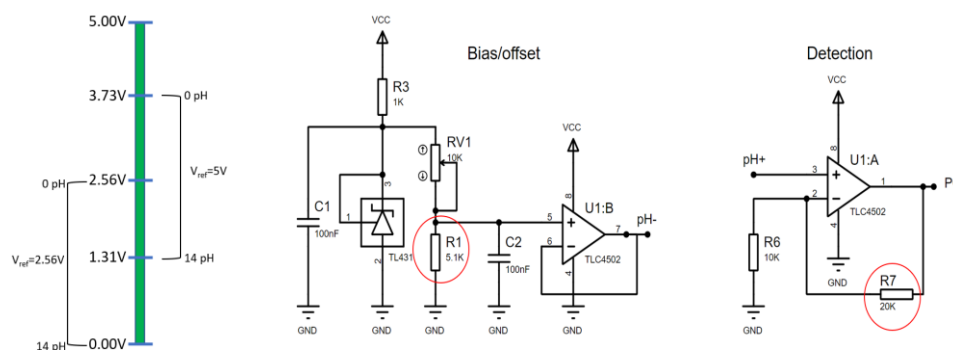


**Figure 8.** The signal conditioning stage can be improved by optimizing the usable detection range of the ADC. We propose to modify the feedback resistor and the (fixed) voltage divider network resistor to improve the performance by a two-fold factor: from 48 to 98% usable detection range.

Moreover, the evaluation of the dynamic range of the ADC is important because this establishes a minimum detectable voltage (i.e., pH). Thus, the measurement of potentials below a certain threshold is not plausible, and the system is said to be ADC-limited. Furthermore, various deviations inhibit ideal performance of ADCs. The absolute accuracy of an ADC serves to quantify: gain error, offset deviations, differential error, non-linearity, and quantization error. The ideal value of the absolute accuracy is  $\pm 0.5$  LSB.

In our instrument, a 10-bit ADC (Atmel Corporation, San José, CA, USA, ATmega328P) is utilized with a reference conversion voltage of 5 V and a typical absolute accuracy of  $\pm 2.2$  LSB. This implies a minimum detectable voltage of 4.88 mV, with ideal and typical absolute accuracies of  $\pm 2.44$  mV and  $\pm 10.74$  mV, respectively. As is the case with other deviation metrics, statistical methods can be utilized to reduce these errors.

The mean sensitivity of our instrument can be obtained from the absolute values of Table 2, and is equal to 172.67 [mV/pH]. This maps directly to the usable conversion range of the ADC, which is 2.41 V, over the full range of pH values. Therefore, we expect the minimum detectable pH value to be 0.028 units, with ideal and typical absolute accuracies of  $\pm 0.014$  pH units and  $\pm 0.062$  pH units, respectively. From this analysis and the results presented in this work, we can conclude that the current instrument design is ADC-limited. A straightforward improvement in the instrument can be implemented by using ADCs with greater dynamic ranges. For instance, the STM32L041 (STMicroelectronics, Grenoble, Auvergne-Rhône-Alpes, France) incorporates a 12-bit ADC, which would reduce by a four-fold factor the minimum detectable voltage, improving absolute accuracy proportionally. In such a setup, the minimum detectable pH increment would be 0.007 units, with ideal and typical absolute accuracies of  $\pm 0.0035$  pH units and  $\pm 0.015$  pH units, respectively.

Global (conventional and *Vertical Farming*) solutions are necessary worldwide. Such systems need to be robust in order to ensure adoption. Even in a controlled laboratory setting mechanical instabilities are readily recognized, refer to Figure 5. Due to the fact that minimal increments in sensor readings convert into significant pH variations, such instabilities impact significantly the recovered values. Our group has recently proposed an artificial intelligence (AI) approach to compensate for these types of scenarios [43,44].

## 6. Conclusions and Future Work

In this work, the implementation of a cost-effective and portable instrument, which enables accurate pH measurements for global *Vertical Farming* applications, has been described. By performing a well-designed calibration of the sensor, near Nernstian response, in this case 57.56 [mV/pH], was demonstrated. The instrumentation was compared to a laboratory gold standard, which is at least ten times more expensive, and was shown to be accurate in determining the pH of substances in the 2–14 range. Furthermore, the

instrument yields precise pH results with an average absolute deviation of 0.06 pH units and a standard deviation of 0.03 pH units. Compared to previous research efforts, the instrumentation is unique because it incorporates a three-layer IoT architecture with *Perception*, *Network*, and *Application* Layers. Additionally, the design is optimal for worldwide adoption by consisting of four modular stages: sensing, signal conditioning, signal acquisition, and communications. The design of the instrument was shown to be ADC-limited, with a minimum detectable value of 0.028 pH units, and a typical absolute accuracy of  $\pm 0.062$  pH units. In order to overcome this limitation, a means to improve performance was presented by meticulously designing the bias and amplification circuitry of the signal conditioning stage, and by optimizing the signal acquisition section of the instrument. The next steps in our research include the implementation of an AI algorithm to detect and compensate for mechanical instabilities of the instrument, and to incorporate other critical sensors, such as total dissolved solids meters, for VF applications.

**Supplementary Materials:** The calibration code information can be downloaded at: [https://pabellon.tecnm.mx/LIA/productos\\_generados.html#Trabajos\\_realizados](https://pabellon.tecnm.mx/LIA/productos_generados.html#Trabajos_realizados) (accessed on 30 June 2022).

**Author Contributions:** Conceptualization, R.H.-M., E.O.-G. and P.V.-J.; methodology, R.H.-M., E.O.-G. and P.V.-J.; software, R.H.-M., N.E.-G. and M.M.R.; validation, R.H.-M., E.O.-G. and P.V.-J.; formal analysis, R.H.-M., E.O.-G., N.E.-G., J.A.D.-A., M.M.R. and P.V.-J.; research, R.H.-M., N.E.-G. and P.V.-J.; resources, E.O.-G., J.A.D.-A. and P.V.-J.; data curation, R.H.-M., N.E.-G. and P.V.-J.; original drafting-drafting, R.H.-M., N.E.-G. and P.V.-J.; drafting-revising and editing, E.O.-G., M.M.R., J.A.D.-A. and P.V.-J.; visualization, R.H.-M., N.E.-G. and P.V.-J.; supervision, E.O.-G., N.E.-G., J.A.D.-A., M.M.R. and P.V.-J.; project management, R.H.-M., E.O.-G., N.E.-G. and P.V.-J.; fund raising, E.O.-G. and N.E.-G. All authors have read and agreed to the published version of the manuscript.

**Funding:** We acknowledge the support of the Consejo Nacional de Ciencia y Tecnología (CONACYT) in Mexico for supporting this work through funds for projects INFRA-2016-01, Project No. 270665. CB-2016-01, Project No. 287818. Additionally, we acknowledge the support to the Government of the State of Aguascalientes, and the Instituto para el Desarrollo de la Sociedad del Conocimiento del Estado de Aguascalientes (IDSCEA) through the Technological Innovation Fund for projects FEIT-AGS-2020-20-17, FEIT-AGS-2020-20-18 and 029-FEIT-2021.

**Institutional Review Board Statement:** Not applicable.

**Informed Consent Statement:** Not applicable.

**Data Availability Statement:** Not applicable.

**Conflicts of Interest:** The authors declare no conflict of interest.

## References

1. Liu, X.; Zhai, Y.; Li, S.; Wang, B.; Wang, T.; Liu, Y.; Qiu, Z.; Li, C. Hydrothermal carbonization of sewage sludge: Effect of feed-water pH on hydrochar's physicochemical properties, organic component and thermal behavior. *J. Hazard. Mater.* **2020**, *388*, 122084. [[CrossRef](#)] [[PubMed](#)]
2. Abdel Daiem, M.M.; Said, N.; Negm, A.M. Potential energy from residual biomass of rice straw and sewage sludge in Egypt. *Procedia Manuf.* **2018**, *22*, 818–825. [[CrossRef](#)]
3. Esteban-Gutiérrez, M.; Garcia-Aguirre, J.; Irizar, I.; Aymerich, E. From sewage sludge and agri-food waste to VFA: Individual acid production potential and up-scaling. *Waste Manag.* **2018**, *77*, 203–212. [[CrossRef](#)]
4. Ruqing, N.; Fengyuan, H.; Yunfei, J.; Xinjing, T. Cycle and Harm of Main Pollutants in Thermal System of Gas Turbiner. *IOP Conf. Ser. Earth Environ. Sci.* **2020**, *546*, 32028. [[CrossRef](#)]
5. Li, Y.; Liu, C.; He, F.; Wang, F. Analysis on Water Wall Tube Explosion in a Power Plant. *IOP Conf. Ser. Earth Environ. Sci.* **2020**, *526*, 12162. [[CrossRef](#)]
6. Muncan, J.; Tei, K.; Tsenkova, R. Real-Time Monitoring of Yogurt Fermentation Process by Aquaphotomics Near-Infrared Spectroscopy. *Sensors* **2020**, *21*, 177. [[CrossRef](#)]
7. Jiang, J.; Sun, Y.F.; Tang, X.; He, C.N.; Shao, Y.L.; Tang, Y.J.; Zhou, W.W. Alkaline pH shock enhanced production of validamycin A in fermentation of *Streptomyces hygroscopicus*. *Bioresour. Technol.* **2018**, *249*, 234–240. [[CrossRef](#)]
8. Grzelak, J.; Ąślęzak, R.; Krzystek, L.; Ledakowicz, S. Effect of pH on the production of volatile fatty acids in dark fermentation process of organic waste. *Ecol. Chem. Eng. S* **2018**, *25*, 295–306. [[CrossRef](#)]



9. Nunes Filho, R.C.; Galvan, D.; Effting, L.; Terhaag, M.M.; Yamashita, F.; Benassi, M.d.T.; Spinosa, W.A. Effects of adding spices with antioxidants compounds in red ale style craft beer: A simplex-centroid mixture design approach. *Food Chem.* **2021**, *365*, 130478. [[CrossRef](#)]
10. Lehnhardt, F.; Nobis, A.; Skornia, A.; Becker, T.; Gastl, M. A Comprehensive Evaluation of Flavor Instability of Beer (Part 1): Influence of Release of Bound State Aldehydes. *Foods* **2021**, *10*, 2432. [[CrossRef](#)]
11. Guimarães, B.P.; Neves, L.E.P.; Guimarães, M.G.; Ghesti, G.F. Evaluation of maturation congeners in beer aged with Brazilian woods. *J. Brew. Distill.* **2020**, *9*, 1–7. [[CrossRef](#)]
12. Nakazawa, N.; Wada, R.; Fukushima, H.; Tanaka, R.; Kono, S.; Okazaki, E. Effect of long-term storage, ultra-low temperature, and freshness on the quality characteristics of frozen tuna meat. *Int. J. Refrig.* **2020**, *112*, 270–280. [[CrossRef](#)]
13. Ezati, P.; Bang, Y.J.; Rhim, J.W. Preparation of a shikonin-based pH-sensitive color indicator for monitoring the freshness of fish and pork. *Food Chem.* **2021**, *337*, 127995. [[CrossRef](#)] [[PubMed](#)]
14. Ezati, P.; Priyadarshi, R.; Bang, Y.J.; Rhim, J.W. CMC and CNF-based intelligent pH-responsive color indicator films integrated with shikonin to monitor fish freshness. *Food Control* **2021**, *126*, 108046. [[CrossRef](#)]
15. Ezati, P.; Tajik, H.; Moradi, M.; Molaei, R. Intelligent pH-sensitive indicator based on starch-cellulose and alizarin dye to track freshness of rainbow trout fillet. *Int. J. Biol. Macromol.* **2019**, *132*, 157–165. [[CrossRef](#)]
16. Ogunniyi, A.D.; Tenzin, S.; Ferro, S.; Venter, H.; Pi, H.; Amorico, T.; Deo, P.; Trott, D.J. A pH-neutral electrolyzed oxidizing water significantly reduces microbial contamination of fresh spinach leaves. *Food Microbiol.* **2021**, *93*, 103614. [[CrossRef](#)]
17. Ding, Z.; Johanningsmeier, S.D.; Price, R.; Reynolds, R.; Truong, V.D.; Payton, S.C.; Breidt, F. Evaluation of nitrate and nitrite contents in pickled fruit and vegetable products. *Food Control* **2018**, *90*, 304–311. [[CrossRef](#)]
18. Alegbeleye, O.O.; Singleton, I.; Sant’Ana, A.S. Sources and contamination routes of microbial pathogens to fresh produce during field cultivation: A review. *Food Microbiol.* **2018**, *73*, 177–208. [[CrossRef](#)]
19. Kassim, M.R.M. IoT Applications in Smart Agriculture: Issues and Challenges. In Proceedings of the 2020 IEEE Conference on Open Systems (ICOS), Kota Kinabalu, Malaysia, 17–19 November 2020; pp. 19–24. [[CrossRef](#)]
20. Jürkenbeck, K.; Heumann, A.; Spiller, A. Sustainability Matters: Consumer Acceptance of Different Vertical Farming Systems. *Sustainability* **2019**, *11*, 4052. [[CrossRef](#)]
21. Al-Kodmany, K. The Vertical Farm: A Review of Developments and Implications for the Vertical City. *Buildings* **2018**, *8*, 24. [[CrossRef](#)]
22. Dagar, R.; Som, S.; Khatri, S.K. Smart Farming—IoT in Agriculture. In Proceedings of the 2018 International Conference on Inventive Research in Computing Applications (ICIRCA), Coimbatore, India, 11–12 July 2018; pp. 1052–1056. [[CrossRef](#)]
23. Penn, C.J.; Camberato, J.J. A Critical Review on Soil Chemical Processes that Control How Soil pH Affects Phosphorus Availability to Plants. *Agriculture* **2019**, *9*, 120. [[CrossRef](#)]
24. Jin, H.; Qin, Y.; Pan, S.; Alam, A.U.; Dong, S.; Ghosh, R.; Deen, M.J. Open-Source Low-Cost Wireless Potentiometric Instrument for pH Determination Experiments. *J. Chem. Educ.* **2018**, *95*, 326–330. [[CrossRef](#)]
25. Inserra, B.; Hayashi, K.; Marchisio, A.; Tulliani, J.M. Sol-gel-entrapped pH indicator for monitoring pH variations in cementitious materials. *J. Appl. Biomater. Funct. Mater.* **2020**, *18*, 2280800020936540. [[CrossRef](#)] [[PubMed](#)]
26. Ghoneim, M.T.; Nguyen, A.; Dereje, N.; Huang, J.; Moore, G.C.; Murzynowski, P.J.; Dagdeviren, C. Recent Progress in Electrochemical pH-Sensing Materials and Configurations for Biomedical Applications. *Chem. Rev.* **2019**, *119*, 5248–5297. [[CrossRef](#)] [[PubMed](#)]
27. Yoon, J.H.; Kim, S.M.; Park, H.J.; Kim, Y.K.; Oh, D.X.; Cho, H.W.; Lee, K.G.; Hwang, S.Y.; Park, J.; Choi, B.G. Highly self-healable and flexible cable-type pH sensors for real-time monitoring of human fluids. *Biosens. Bioelectron.* **2020**, *150*, 111946. [[CrossRef](#)] [[PubMed](#)]
28. Manjakkal, L.; Sakthivel, B.; Gopalakrishnan, N.; Dahiya, R. Printed flexible electrochemical pH sensors based on CuO nanorods. *Sens. Actuators B Chem.* **2018**, *263*, 50–58. [[CrossRef](#)]
29. Dang, W.; Manjakkal, L.; Navaraj, W.T.; Lorenzelli, L.; Vinciguerra, V.; Dahiya, R. Stretchable wireless system for sweat pH monitoring. *Biosens. Bioelectron.* **2018**, *107*, 192–202. [[CrossRef](#)]
30. Córdoba, C.; Mera, J.; Paredes, O.; Benavides, J. Sensor óptico para mediciones de PH obtenido por el método sol-gel con moléculas orgánicas dopadas en matriz vítrea. *Rev. Soc. Química México* **2004**, *48*, 203–207.
31. Rasheed, H.S.; Ahmed, N.M.; Matjafri, M.Z. Ag metal mid layer based on new sensing multilayers structure extended gate field effect transistor (EG-FET) for pH sensor. *Mater. Sci. Semicond. Process.* **2018**, *74*, 51–56. [[CrossRef](#)]
32. Sinha, S.; Pal, T.; Kumar, D.; Sharma, R.; Kharbanda, D.; Khanna, P.K.; Mukhiya, R. Design, fabrication and characterization of TiN sensing film-based ISFET pH sensor. *Mater. Lett.* **2021**, *304*, 130556. [[CrossRef](#)]
33. FAO. *El Estado Mundial de la Agricultura y la Alimentación 2021*; Food and Agriculture Organization of the United Nations: Rome, Italy, 2021. [[CrossRef](#)]
34. Kurzweil, P. Metal Oxides and Ion-Exchanging Surfaces as pH Sensors in Liquids: State-of-the-Art and Outlook. *Sensors* **2009**, *9*, 4955–4985. [[CrossRef](#)]
35. Manjakkal, L.; Szwagierczak, D.; Dahiya, R. Metal oxides based electrochemical pH sensors: Current progress and future perspectives. *Prog. Mater. Sci.* **2020**, *109*, 100635. [[CrossRef](#)]
36. Alva, S.; Binti Abdul Aziz, A.S.; Bin Syono, M.I.; Bin Wan Jamil, W.A. Ag/AgCl Reference Electrode Based on Thin Film of Arabic Gum Membrane. *Indones. J. Chem.* **2018**, *18*, 479–485. [[CrossRef](#)]

37. Westbroek, P. Electrochemical methods. *Anal. Electrochem. Text.* **2005**, 37–69. [[CrossRef](#)]
38. Levanov, A.V.; Isaikina, O.Y.; Lunin, V.V. Determining the Potential of a Silver/Silver Chloride Electrode at Different Temperatures. *Russ. J. Phys. Chem. A* **2019**, *93*, 770–773. [[CrossRef](#)]
39. Lonsetta, A.M.; Cope, P.; Campbell, J.; Mohd, B.J.; Hayajneh, T. Actuator Networks Sensor and Security Vulnerabilities in Bluetooth Technology as Used in IoT. *J. Sens. Actuator Netw.* **2018**, *7*, 28. [[CrossRef](#)]
40. Ghorri, M.R.; Wan, T.-C.; Sodhy, G.C. Bluetooth Low Energy Mesh Networks: Survey of Communication and Security Protocols. *Sensors* **2020**, *20*, 3590. [[CrossRef](#)]
41. Shylendra, S.P.; Lonsdale, W.; Wajrak, M.; Nur-e-alam, M.; Alameh, K. Titanium Nitride Thin Film Based Low-Redox-Interference Potentiometric pH Sensing Electrodes. *Sensors* **2020**, *21*, 42. [[CrossRef](#)]
42. Sharma, N.; Acharya, S.; Kumar, K.; Singh, N.; Chaurasia, O.P. Hydroponics as an advanced technique for vegetable production: An overview. *J. Soil Water Conserv.* **2018**, *17*, 364–371. [[CrossRef](#)]
43. Montes Rivera, M.; Escalante-Garcia, N.; Dena-Aguilar, J.A.; Olvera-Gonzalez, E.; Vacas-Jacques, P. Feature Selection to Predict LED Light Energy Consumption with Specific Light Recipes in Closed Plant Production Systems. *Appl. Sci.* **2022**, *12*, 5901. [[CrossRef](#)]
44. Olvera-Gonzalez, E.; Montes Rivera, M.; Escalante-Garcia, N.; Flores-Gallegos, E. Modeling Energy LED Light Consumption Based on an Artificial Intelligent Method Applied to Closed Plant Production System. *Appl. Sci.* **2021**, *11*, 2735. [[CrossRef](#)]

# ANNEX 2

Article

# Comparative analysis of RNN versus IIR digital filtering to optimize resilience to dynamic perturbations in pH sensing for *Vertical Farming*

Rolando Hinojosa-Meza <sup>1</sup>, Martín Montes Rivera <sup>2</sup>, Paulino Vacas-Jacques <sup>1,3\*</sup>, Nivia Escalante-García <sup>1\*</sup>, José Alonso Dena-Aguilar <sup>3</sup>, Aldonso Becerra Sanchez <sup>4</sup>, and Ernesto Olvera-Gonzalez <sup>1</sup>.

<sup>1</sup> Laboratorio de Iluminación Artificial, Tecnológico Nacional de México/IT de Pabellón de Arteaga, Carretera a la Estación de Rincón Km. 1, 20670, Aguascalientes, México; rolando.hm@pabellon.tecnm.mx (R. H.-M.); jose.og@pabellon.tecnm.mx (E. O.-G.).

<sup>2</sup> Universidad Politécnica de Aguascalientes, Calle Paseo San Gerardo #201, Fracc. San Gerardo, 20342 Aguascalientes, México; martin.montes@upa.edu.mx. (M. M. R.).

<sup>3</sup> Departamento de Ingenierías, Tecnológico Nacional de México /IT de Pabellón de Arteaga, Carretera a la Estación de Rincón Km. 1, 20670 Aguascalientes, México; jose.da@pabellon.tecnm.mx (J.A.D.-A.).

<sup>4</sup> Universidad Autónoma de Zacatecas, Campus Siglo XXI, Carr. Zacatecas-Guadalajara Km. 6, Ejido "La Escondida", 98610, Zacatecas, México; a7donso@uaz.edu.mx (A.B. S.).

\* Correspondence: paulino.vj@pabellon.tecnm.mx (P.V.-J.) and nivia.eg@pabellon.tecnm.mx (N.-E.-G.)

**Abstract:** We propose an advanced filtering scheme based on *Recurrent Neural Networks* (RNNs) and Deep Learning to enable efficient control strategies for *Vertical Farming* (VF) applications. We demonstrate that the best RNN model incorporates five neuron layers, with the first and second containing ninety Long Short-Term Memory neurons. The third layer implements one Gated Recurrent Units neuron. The fourth segment incorporates one RNN network, while the output layer is designed by using a single neuron exhibiting a rectified linear activation function. By utilizing this RNN digital filter, we introduce two variations: (1) A scaled RNN model to tune the filter to the signal of interest, and (2) A moving average filter to eliminate harmonic oscillations of the output waveforms. The RNN models are contrasted with conventional digital Butterworth, Chebyshev I, Chebyshev II, and Elliptic *Infinite Impulse Response* (IIR) configurations. The RNN digital filtering schemes avoid introducing unwanted oscillations, which makes them more suitable for VF than their IIR counterparts. Finally, by utilizing the advanced features of scaling of the RNN model, we demonstrate that the RNN digital filter can be pH selective, as opposed to conventional IIR filters.

**Keywords:** pH-instrument; Vertical Farming; Industry 4.0; IIR Filtering; Recurrent Neural Networks; RNN; Neural Networks; Digital Filtering; Butterworth Filter; Chebyshev Filter; Elliptic Filter.

## 1. Introduction

Recent predictions reveal that the world will not have the capacity to meet the requirements of food production and other alimentation products to ensure adequate nutrition for the entire population [1]. *Precision Agriculture* (PA) is the set of technological tools implemented to optimize crop-yield and -quality in plant production [2,3]. Also, an essential resource for sustainable agriculture is water.

Today, water use is inefficient: 65-70% of the freshwater is utilized for non-essential human activity [4]. Our research group focuses on developing novel PA techniques to maximize natural resources through *Vertical Farming* (VF). Furthermore, the effective use of this production style allows optimizing the space in which different crops, such as fruits, vegetables, fine herbs, and flowering plants, can be grown in the same area by locating them in different production levels. Hydroponic VF is the most common method to cultivate plants. The salient features of hydroponic VF systems

reside in their capacity to enable crop growth whilst minimizing water, CO<sub>2</sub>, energy, and fertilizer consumption. This is enabled by virtue of quantifying key growth parameters, such as conductivity, temperature, light exposure, and especially pH [5].

Generally speaking, plants are more vulnerable whenever alkalinity conditions are present. For example, crops are more susceptible to being attacked by insects when the alkalinity increases [6]. Meanwhile, whenever an acid behavior is present, plants tend to more frequently suffer diseases [7,8]. Furthermore, alkaline environments are correlated with deficiencies of nitrogen, phosphorus, and sulfur; whereas calcium, magnesium, potassium, and sodium deficiencies ensue in acidic conditions [9]. This implies that latent risks exist with respect to deficient ion distributions, vulnerability, and crop disease, which need to be detected and controlled. Therefore, depending on the plant or crop of interest, the pH must be controlled (normally in the range of 4 to 8 units [8,10–12]), in order to ensure optimal environments for growing and, thus, yield. We have recently proposed a portable and precise instrument to measure pH [13]. Utilizing such instrumentation, a pH control system can be conformed to ensure optimal crop yield. As a starting point to control pH for VF applications, an efficient and simple-to-implement *on-off* control scheme can be utilized.

Nonetheless, in order to implement such a control system, it is indispensable to have appropriately conditioned signals of the parameter of interest. Filtering signals when sensing variables with physical detectors implies suppressing wrong-scaled voltages, quantization variations, and harmonics, among other periodic perturbations found in specialized electronic circuitry. Such predictable filtering can be achieved, on the one hand, using traditional techniques such as Butterworth, Chebyshev, and Elliptic (analog or digital) filters [14–17].

On the other hand, when there are unpredictable perturbations, it is challenging to design an electronic circuit that can manage such imprecise and random behaviors. However, Artificial Intelligence (AI) has shown that it can deal with imprecise and unexpected conditions solving complex problems with no deterministic solution, especially when using Artificial Neural Networks (ANNs) and Deep Learning [18–21].

Recurrent Neural Networks (RNNs) are ANNs utilized when behaviors depend on time sequences, which allows the resolution of problems with unexpected behaviors, like detecting malware affecting cloud systems [22].

Natural language processing also employs RNNs for translation because these solutions must consider time sequences to maintain context [23]. Forecasting of power demand also uses RNNs to predict energy consumption depending on time sequences [24]. Finally, RNNs serve to predict concrete dam deformation based on previous deformation or time sequences [25].

In this work, we address the effect of temporal intrinsic and extrinsic (mechanical) perturbations, as applicable to the sensing and controlling of pH values, by using conventional digital filtering, and comparing it to a more resilient solution based on RNN. A main objective of this work is to evaluate the performance of an advanced signal conditioning and filtering stage, utilizing RNN and Deep Learning, to account for intrinsic and extrinsic temporal perturbations that ensue in real-world VF settings.

The following work is divided into six sections. The second section presents the theoretical background of the control system, focusing on advanced RNN and traditional digital filtering techniques, as applied to pH sensing. The third part of this work addresses the methodology and computing infrastructure needed to implement the IIR and RNN digital filters. We describe the transfer functions of IIR filters, as well as the optimal design of the RNN. Section four presents a comparison between traditional digital filtering and recurrent neural networks, as applicable to VF. A special emphasis is placed on presenting two variations of the advanced RNN digital filtering scheme. In the fifth part, we discuss the findings of this work and present new research directions. Finally, in the last section, we summarize our comparative analysis.

## 2. Theoretical Background

As commented above, controlling the pH, within a particular species-dependent range, is critical to ensure that the crop of interest will exhibit the expected yield, as well as being protected against

plant vulnerability and diseases. Furthermore, real-life VF arrangements are bound to suffer mechanical perturbations that are unpredictable. Therefore, recurring to fundamental control theory, the challenge to ensure that a VF setup is exposed to appropriate pH values can be schematized as shown in Figure 1.

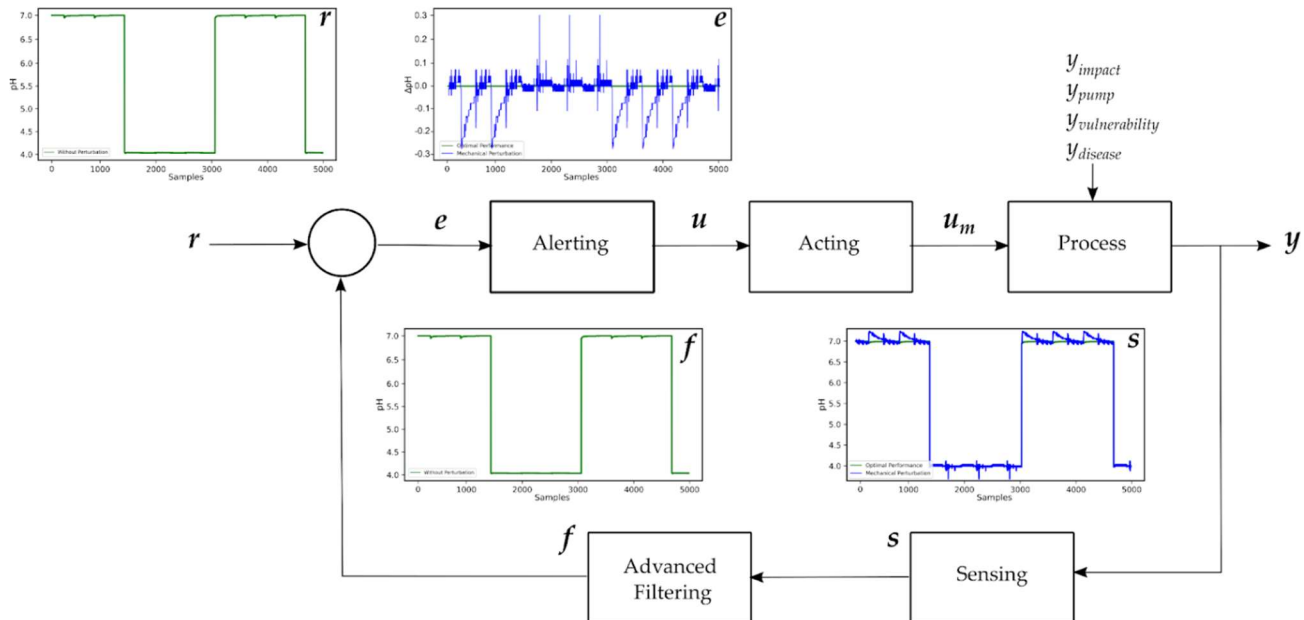


**Figure 1.** The operational block diagram of an optimal closed-loop control system to ensure that a VF setup is exposed to appropriate pH values includes: Sensing, (Advanced) Filtering, Alerting, Acting, and Processing sections. The most critical step of the control system is the filtering section because unpredictable perturbations occur in real-life VF implementations. In this diagram,  $r$  denotes reference signal,  $e = f - r$  and stands for error signal,  $u$  symbolizes process input,  $u_m$  is manipulated variable,  $y_{impact}$  demarcates extrinsic mechanical perturbations,  $y_{pump}$  represents intrinsic movement effects,  $y_{vulnerability}$  refers to intrinsic crop vulnerability,  $y_{disease}$  denotes intrinsic crop disease,  $s$  stands for sensed signal,  $f$  symbolizes filtered signal, and  $y$  is controlled output. .

The pH of a VF setup must be varied according to an *on-off* cycle, in order to ensure sufficient (avoiding overabundance) nutrients are delivered to the VF arrangement. This implies that the pH input function is periodic with a rather slow varying frequency. For example, orchids and blueberries need to be exposed to pH values close to 4 units [26–29] for a period of 8 hours, while optimally resting for 8 hours (when the pH of the reference substance in the container can be neutral as shown in Figure 1) before being exposed to another cycle. These application-dependent conditions enable us to predefine the expected waveforms (i.e., the reference signal,  $r$  in Figure 1) needed to enact the necessary control. However, as expected in any control system, perturbations occur, and it is of utmost importance to consider and address them appropriately.

As depicted in Figure 1, four distinct perturbations are bound to occur in VF systems: 1. Extrinsic unpredictable mechanical perturbations,  $y_{impact}$ , such as impacts; 2. Intrinsic random mechanical disturbances,  $y_{pump}$ , such as pump-induced effects; 3. Intrinsic crop vulnerabilities,  $y_{vulnerability}$ ; and 4. Intrinsic crop diseases,  $y_{disease}$ . The most challenging of these perturbations are the mechanical unpredictable ones. By implementing an Advanced Filtering stage, we demonstrate that such unpredictable behavior can be correctly addressed.

Two different types of digital filters exist: a. Fixed coefficient filters, including infinite impulse response (IIR) filters; and b. Variable coefficient filters, which include neural networks. Hereafter, we briefly present the theory of IIR filters (a cursory overview of digital filters has been recently reported in the literature, and newcomers are encouraged to refer to this material [30]) and delve into more detail on the theory of recursive neural networks as pertinent to this work.

### 2.1. Infinite Impulse Response Filters

Extensive literature exists to introduce the theory of infinite impulse response (IIR) digital filters [14–17]. IIR digital filters can be described by means of their transfer function  $H(z)$ , as shown in Equation (1) [31];

$$H(z) = \frac{Y(z)}{X(z)} = \frac{\sum_{k=0}^M b_k z^{-k}}{\sum_{l=0}^N a_l z^{-l}} \quad (1)$$

By rearranging, Equation (1) can be rewritten in the optimal form for inverse transformation,

$$\sum_{l=0}^N a_l z^{-l} Y(z) = \sum_{k=0}^M b_k z^{-k} X(z) \quad (2)$$

Here,  $z$  is the  $z$ -space variable. Meanwhile,  $a_l$  and  $b_k$  represent the IIR fixed filter coefficients. Additionally,  $M$  and  $N$  are the degrees of the numerator and denominator polynomials, respectively.

By setting the  $a_0$  coefficient to unity, as conventionally done, and rearranging Equation 2, we obtain the filter output in the time domain by means of the inverse  $z$ -transform.

$$y[n] = \sum_{k=0}^M b_k x[n-k] - \sum_{l=1}^N a_l y[n-l] \quad (3)$$

Finally, by determining the fixed coefficients of Equation 3, we can fully describe the output of arbitrary IIR digital filters.

### 2.2. Recurrent Neural Networks

Recurrent Neural Networks (RNNs) are artificial neural networks that differ from the most common Feedforward Neural Networks (FNNs) by introducing short memory effects, directional information cycles, and significant multicollinearity in the RNN variables, produced with weight connections between the same layer of neurons. RNNs add the possibility of changing the predicted behavior of the network depending on previous inputs. However, they are limited to short-time sequences because their updating gradients vanish or explode rapidly [25].

#### 2.2.1. Long Short-Term Memory Networks

Hochreiter and Schmidhuber proposed Long Short-Term Memory (LSTM) Networks in 1997. They have become the most popular RNNs. LSTMs predict long data sequences over a defined period, solving the vanishing problem in RNNs. An LSTM segment consists of blocks of cells. Each cell has its inputs, outputs, and memory. Cells that belong to the same block share input, output, and forget gates. The input gate decides whether the given information is worth remembering, and the forget gate decides how much of the given information is still worth remembering. The output gate decides whether the provided information is relevant at a given step. Each gate can be considered a neuron, and the LSTM cell is a hidden segment in a FNN [32].

In order to perform advanced filtering for the feedback signal depicted in Figure 1, we propose to suppress random pH perturbations (refer to signal  $s$  in Figure 1) with unpredictable behaviors for VF using neural networks. We perform such advanced filtering by utilizing the monitoring features of time sequences and of previous outputs that are characteristic of RNNs together with Deep Learning, aiming to obtain the response of the sensor (signal  $f$  in Figure 1) in the absence of unpredictable (mechanical) perturbations. As depicted in Figure 2, the Deep-Learning model tested in this work has five layers with neurons used to design RNNs. The first and second segments,  $l_1$  and  $l_2$ , only contain LSTM neurons, the third layer,  $l_3$ , contains Gated Recurrent Units (GRU) neurons, the fourth layer,  $l_4$ , contains simple RNN networks, and the final segment,  $l_5$ , is the output layer with a single neuron with a rectified linear activation function.

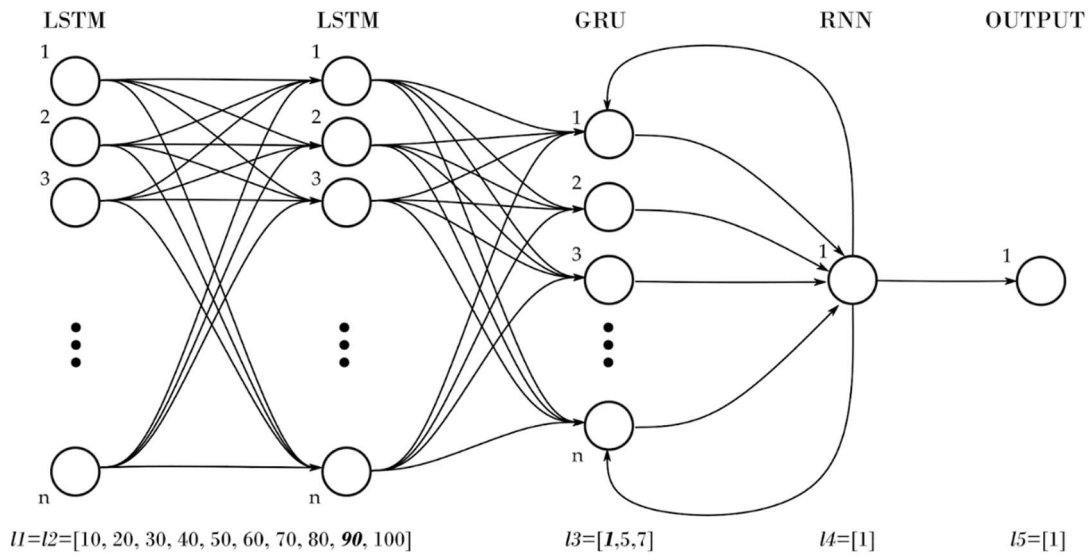


**Figure 2.** The advanced filter is based on a deep-learning model that incorporates five neuron layers to enable the Recurrent Neural Networks (RNNs). The first and second,  $l_1$  and  $l_2$ , layers solely contain LSTM neurons. The third segment,  $l_3$ , contains Gated Recurrent Units (GRU) neurons. The fourth layer,  $l_4$ , contains a simple RNN network, and the final segment,  $l_5$ , is the output layer with a single neuron exhibiting a rectified linear activation function. For each layer, the optimal number of neurons is highlighted in the square brackets of the diagram.

In the next section we present the materials used to generate the datasets, as well as the methods, such as filter designs including the frequency response of the IIR digital filters and the deep-learning RNN procedure, employed in this work.

### 3. Materials and Methods

#### 3.1. Materials

##### 3.1.1. Instrumentation

For the purpose of generating reference and output datasets ( $r$  and  $y$  in Figure 1), we utilized the pH instrumentation recently reported by our group. The instrument is conformed of a potentiometric *silver|silver-chloride* electrode (Hinotek, Ningbo, China, E201-BNC), which employs a dedicated electronic module (DIY More, Hong Kong, China PH-4502C) to detect the (analog) pH voltage signal. Signal digitization is achieved by a 10-bit ADC Arduino UNO (Smart projects, Ivrea, Italia, Arduino UNO), and the resulting (digital) pH voltage values are transmitted wirelessly by means of a Bluetooth (Olimex, Plovdiv, Bulgaria, BLE HC-06) radio [13].

Once the data is received, the computing entity performs the IIR and RNN digital filtering. For IIR digital filtering, we employed the Signal Processing Toolbox of *MATLAB* (MathWorks, Natick, United States, *MATLAB*) running on a Windows 10 Dell G3 3500 computer with a 4-core Intel i5-10300H 2.50GHz processor with 16GB of RAM. The RNN analysis was performed with the TensorFlow, Sklearn, and other conventional python libraries of *JupyterLab* (NumFOCUS, Austin, United States, Jupyter) running on a Windows 10 Desktop Computer with an Intel i7-6700 3.40GHz processor with 16GB of RAM and NVIDIA GeForce RTX 2060 GPU.

#### 3.2. Methods

Figure 3 displays (a) the block diagram and (b) the experimental setup that are needed to generate the training and testing waveforms, in order to assess the deep-learning RNN and IIR digital filters. The training dataset is created by using an ideal pH sensing setup without mechanical



perturbations, see the central section of Figure 3(b). Meanwhile, the intrinsic mechanical perturbations are enacted by exposing the instrument to a laboratory stirrer, refer to the left section of Figure 3(b), which mimics the use of conventional pumps in VF systems for circulation purposes [33,34]. Finally, the extrinsic mechanical perturbations were created by impacting the utilized setup, at different locations, as depicted in the right-most portion of Figure 3(b).

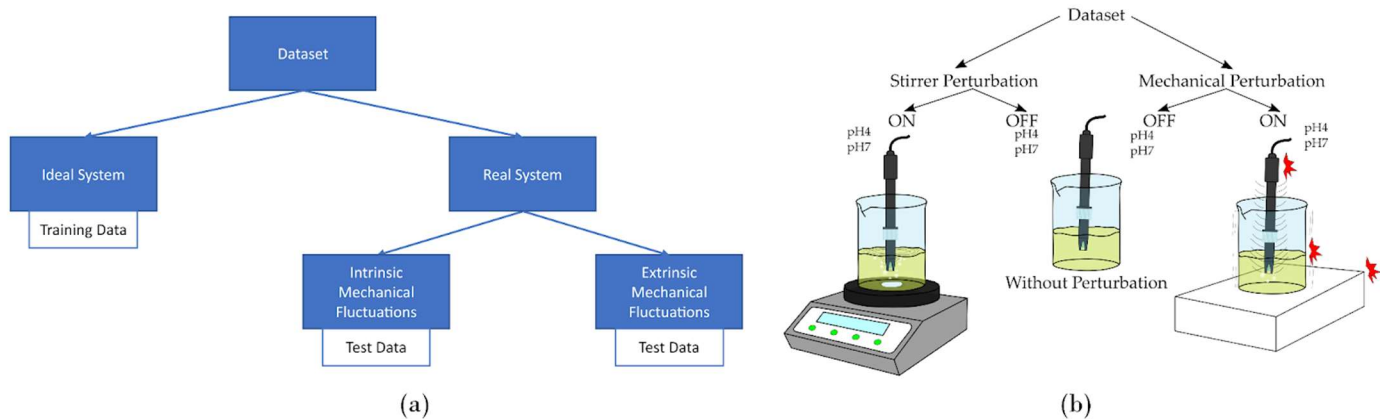


**Figure 3.** (a) Block diagram and (b) experimental setups of the pH instrumentation utilized to generate training and testing datasets, in order to assess the advanced filtering proposed in this work. We utilized different arrangements to create the intrinsic and extrinsic mechanical perturbations that are common in real-life VF applications.

### 3.2.1. Generation of Dataset

The objective of this study is to present a comparative analysis of advanced, RNN versus IIR, digital filters to optimize resilience to dynamic perturbations in pH sensing for VF applications. For this purpose, we need to generate the pH waveforms. Hereafter, we present the methodology followed to achieve this goal.

As reported recently by our group, to generate training and testing datasets, the instrumentation was first cleaned and calibrated. Reliable solutions (Mallinckrodt Baker, Hampton, New Jersey, USA) were utilized to ensure accurate pH values ( $pH_{signal} = 3.99$  and  $pH_{reference} = 6.98$ ) for the measurements [13].

We performed two sets of pH measurements for ideal and real scenarios, corresponding to mechanical perturbations being absent and present, respectively. In addition to pH values, we recorded the raw ADC temporal voltage values for redundancy and better control of the datasets. Thus, the dataset samples ( $n$ ) included: input temporal indices,  $t_i$ , ADC voltages,  $v_i$ , and pH values,  $pH_i$ , for (a) ideal  $input_i = (t_i, v_i, pH_i)$  and (b) real  $output_i = (t_i, v_i, pH_i)$  scenarios, for every sample  $i = [1 \dots n]$ . It is worth noting that the aforementioned datasets have a periodic behavior, in order to emulate the characteristic *on-off* cycle necessary to ensure optimal crop growth and yield.

### 3.2.2. Dataset Augmentation and Splitting

Specifically with respect to the RNN analysis, we utilized both datasets to train the model and suppress perturbations. As depicted in Figure 2, the RNN is based on a supervised-learning model, which requires knowledge of the input signals, as well as the desired output for training purposes. Since after RNN filtering, we are interested in obtaining pH signals free of perturbations, we solely utilized the signal without perturbations as the desired output dataset to train the model. Thus, the training input and output datasets were  $X = \{x_1, x_2, x_3, \dots, x_n\}$  and  $Y = \{y_1, y_2, y_3, \dots, y_n\}$ , where  $x_i$  and  $y_i$  were pH values for the signals with perturbations and without them, respectively.

Furthermore, we employed a data augmentation mechanism to increase the dataset samples and the representativity without the need for new measurements. The data augmentation in this work considered that the pH instrumentation will record values in the range 0-14, depending on the level of acidity or alkalinity of the solution. We commenced the data augmentation by selecting  $\alpha$ , the

number of augmentations. Then, for each augmentation, we determined a random value  $\psi$  in the range of  $[0,1]$  to multiply by the original  $X$  and  $Y$ , equally modifying the pH values while maintaining the result within the original boundaries  $[0,14]$ . Finally, we maintained the original samples and added each augmentation to return the augmented data  $\hat{X}$  and  $\hat{Y}$ , as detailed in Algorithm 1. It is important to note that we employed 30 augmentations of the entire training dataset, or  $\alpha = 30$ , and that the augmented dataset can also be employed to test the IIR filters.

Algorithm 1: Data augmentation for pH measurements	
	Input: $X, Y, \alpha$
	Output: $\hat{X}, \hat{Y}$
1	$\hat{X} = [X]$
2	$\hat{Y} = [Y]$
3	<b>For</b> $i = [2, 3, \dots, \alpha + 1]$ <b>do</b>
4	$\psi \sim [0, 1]$
5	$\hat{X}_i = [\hat{X}_{i-1} \cap \psi \otimes X]$
6	$\hat{Y}_i = [\hat{Y}_{i-1} \cap \psi \otimes Y]$
7	<b>Return</b> $\hat{X}, \hat{Y}$

Considering that we must train a deep-learning neural network, the dataset must be split to avoid overfitting and to ensure reliable results. In this work, we utilized 60% of the dataset for training, 20% for validation, and 20% for testing. Thereafter, we configured the model to generate extra data with the training augmentation data, as described in Algorithm 1.

### 3.2.3. Training Datasets

The pH values utilized to assess the performance of RNN and IIR digital filters were 4 and 7 units for signal and reference waveforms, respectively. However, before commencing pH measurements, the instrument must be calibrated[13]. Thus, for calibration purposes, we included a third pH value of 10.00 of a standardized buffer solution (Mallinckrodt Baker, Hampton, New Jersey, USA). Finally, the calibration procedure can be improved if a fourth solution, outside of the calibrated substance range in our case  $[3.99, 10.00]$ , is utilized. Hence, a final substance of 2.5 pH units was employed to perform the calibration procedure. Thereafter, the periodic signal needed for VF was generated. Figure 4 depicts the training dataset (a) without mechanical perturbations, and (b) with intrinsic and extrinsic disturbances. Moreover, in Figure 4, we separate into two phases the required steps, calibration and measurement, needed to sense pH with the portable instrumentation. The datasets consisting of 21723 temporal samples,  $t_i$ , ADC voltages,  $v_i$ , and pH values,  $pH_i$ , for scenarios with present and absent perturbations are available in the Supplementary Materials section of this work.

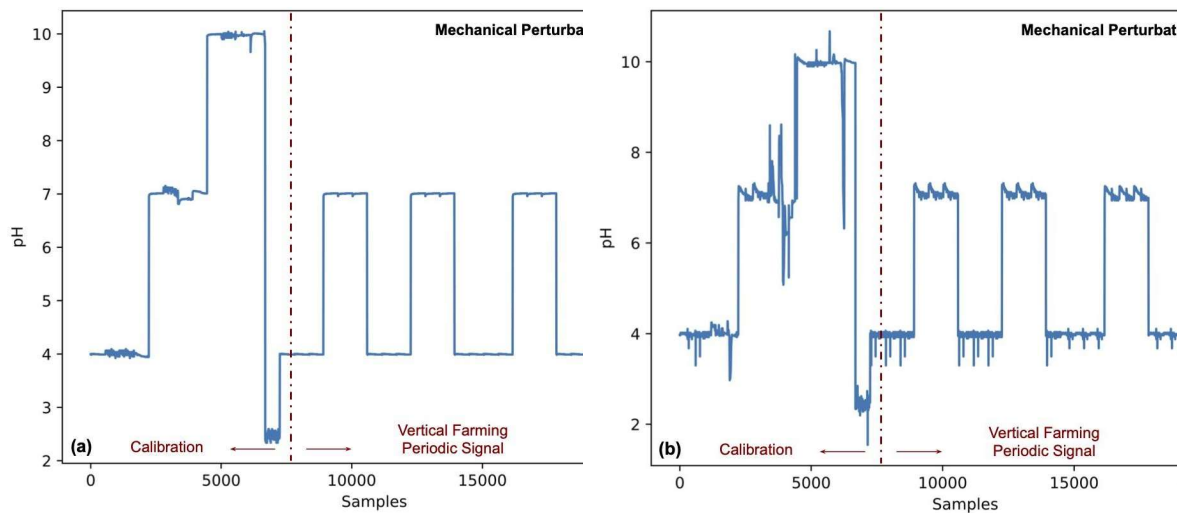


**Figure 4.** The training dataset (a) without mechanical perturbations and (b) exhibiting intrinsic and extrinsic disturbances were generated to mimic the conditions that are common in real-life VF applications. The two phases, *Calibration* and *VF Periodic Signal* generation, needed to employ the pH instrument are respectively depicted in the left and right portions of each illustration. .

As seen in Figure 4, once the instrument is duly calibrated, we generate the periodic signals, which are identical to the control waveforms of Figure 2. During calibration, the instrument is more prone to exhibit mechanical perturbations because buffer solution, electrode, and detection electronics have to be manipulated frequently (i.e. electrode and container cleaning is mandatory after each calibration measurement) In this work, we consider these unpredictable fluctuations to demonstrate that a RNN filter is more resilient in real scenarios, as opposed to IIR filtering.

### 3.2.4. IIR Digital Filter Designs

The portable and precise pH instrument that we recently proposed can implement well-established (analog or digital) electronic filters, such as Butterworth, Chebyshev, and Elliptic arrangements. Furthermore, a salient feature of IIR filters is that they can be based on these electronic configurations. In order to assess the usability of such filters in real-life VF applications, we designed (a) Butterworth, (b) Chebyshev I, (c) Chebyshev II, and (d) Elliptic digital IIR configurations. As commented previously, the pH input function is periodic with a rather slow varying frequency. Therefore, the low-pass filters specifications have to consider this expected behavior. We defined a passband frequency of 1Hz with a maximum 1dB attenuation. Additionally, the stopband frequency was specified to be 10Hz for a 60dB attenuation. The sampling frequency was assumed to be one order of magnitude greater than the stopband frequency.

**Table 1.** IIR digital filter designs for the Butterworth, Chebyshev I, Chebyshev II, and Elliptic configurations employed in this work.

Filter	Order	<i>a</i> Coefficients	<i>b</i> Coefficients	Transfer Function
Butterworth	4	{ 1, -3.836, 5.521, -3.534, 0.8486 }	{ $8.985 \times 10^{-7}$ , $3.594 \times 10^{-6}$ , $5.391 \times 10^{-6}$ , $3.594 \times 10^{-6}$ , $8.985 \times 10^{-7}$ }	$\frac{8.985 \times 10^{-7} z^4 + 3.594 \times 10^{-6} z^3 + 5.391 \times 10^{-6} z^2 + 3.594 \times 10^{-6} z + 8.985 \times 10^{-7}}{z^4 - 3.836 z^3 + 5.521 z^2 - 3.534 z + 0.8486}$
Chebyshev I	3	{ 1, -2.935, 2.875, -0.939 }	{ $1.47 \times 10^{-5}$ , $4.431 \times 10^{-5}$ , $4.431 \times 10^{-5}$ , $1.477 \times 10^{-5}$ }	$\frac{1.477 \times 10^{-5} z^3 + 4.431 \times 10^{-5} z^2 + 4.431 \times 10^{-5} z + 1.477 \times 10^{-5}}{z^3 - 2.935 z^2 + 2.875 z - 0.9398}$
Chebyshev II	3	{ 1, -2.98, 2.96, -0.9803 }	{ $9.347 \times 10^{-5}$ , $-9.298 \times 10^{-5}$ , $-9.298 \times 10^{-5}$ , $9.347 \times 10^{-5}$ }	$\frac{9.347 \times 10^{-5} z^3 - 9.298 \times 10^{-5} z^2 - 9.298 \times 10^{-5} z + 9.347 \times 10^{-5}}{z^3 - 2.98 z^2 + 2.96 z - 0.9803}$
Elliptic	3	{ 1, -2.935, 2.875, -0.939 }	{ $4.69 \times 10^{-4}$ , $-4.09 \times 10^{-4}$ , $-4.09 \times 10^{-4}$ , $4.69 \times 10^{-4}$ }	$\frac{4.69 \times 10^{-4} z^3 - 4.09 \times 10^{-4} z^2 - 4.09 \times 10^{-4} z + 4.69 \times 10^{-4}}{z^3 - 2.935 z^2 + 2.875 z - 0.9399}$

Utilizing the Signal Processing Toolbox of *MATLAB*, we determined filter orders, as well as the corresponding transfer functions of the filters, including the *a* and *b* coefficients of Equation 2. Table

1 presents the orders, coefficients, and transfer functions of the digital filters. Finally, Figure 5 illustrates the digital filter designs for (a) Butterworth, (b) Chebyshev I, (c) Chebyshev II, and (d) Elliptic digital IIR configurations. The IIR digital filter *MATLAB* scripts are available in the Supplementary Materials section of this work.

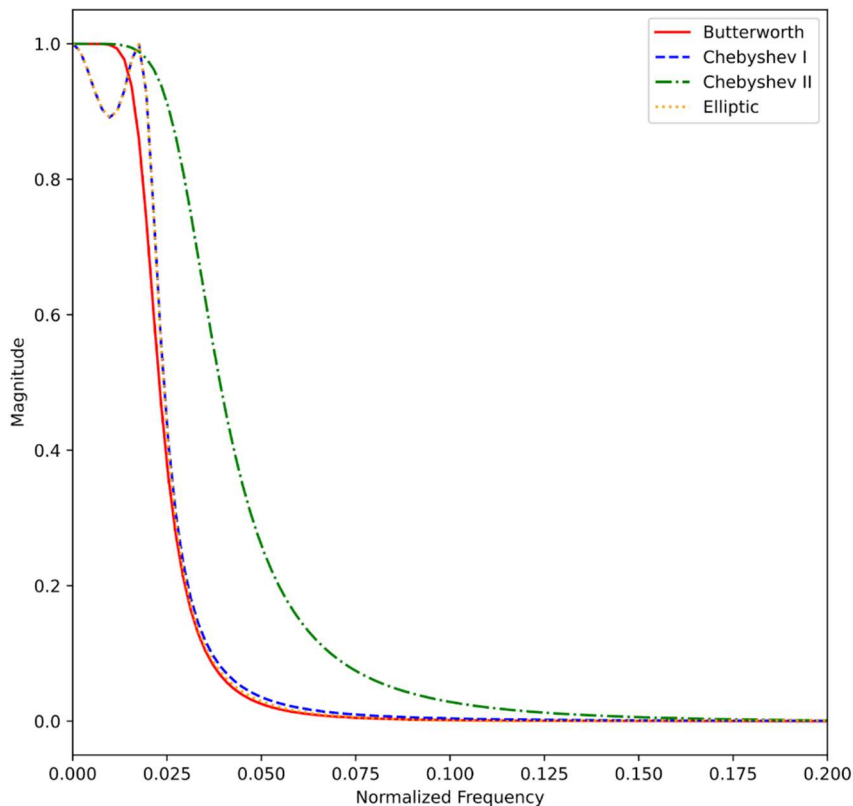


**Figure 5.** The Butterworth, Chebyshev I, Chebyshev II, and Elliptic IIR digital filter designs consider a -1dB passband frequency of 1Hz, and a -60dB stopband frequency of 10Hz.

### 3.2.5. RNN Digital Filter Design

The RNN-based digital filter proposed in this work implements the advanced structure depicted in Figure 2. In order to optimize the design of the RNN digital filter, we determined the number of neurons per layer by testing multiple configurations. The tested layouts included various  $l_1 = l_2 = [10, 20, 30, 40, 50, 60, 70, 80, 90, 100]$  LSTM neurons; three different  $l_3 = [1, 5, 7]$  GRU arrangements; as well as single RNN and output segments,  $l_4 = [1]$  and  $l_5 = [1]$ .

Furthermore, we also varied the number of prior samples. We tested  $psamples = [500, 1000, 1500, 2500, 3000, 3500]$ . We assessed 2101 different configurations of the model with the MSE loss function, which we decided to employ because it is the most utilized metric to train regression models in ANNs [35]. For the 2101 configurations, we trained the model with 500 epochs and a batch size of 5000. This approach requires different steps per epoch depending on the size of the training set, which is variable because, as commented above, we allowed changing the prior samples required as inputs. Moreover, we adjusted the learning rate according to Equation 4, increasing the effect of error and modifying the learning rate across epochs.

$$l_r = 1.0 \times 10^{-5} \times 10^{\frac{epoch}{100}} . \quad (4)$$

The training mechanism utilized in this work stops after twenty steps without improvement of the validation loss. Furthermore, we configured the training process to solely save the best model. After assessing the 2101 configurations with the dataset containing 21723 samples with 30 augmentations for training, we obtained that the best model, as determined by the MSE loss function,

ensues when  $l_1 = 90$ ,  $l_2 = 90$ ,  $l_3 = 1$ ,  $l_4 = 1$ ,  $l_5 = 1$ , and  $psamples = 2000$ . In Figure 6, we depict the logarithmic parallel coordinates for all the configurations trained with the MSE loss function based on the testing of MSE results. The best model is highlighted in red,  $MSE_{Test} = 0.002017$ . Meanwhile, blue and gray are variations of models exhibiting better and worse performance, respectively. Lastly, in black we present the model with the worst outcome,  $MSE_{Test} = 0.207638994$ .

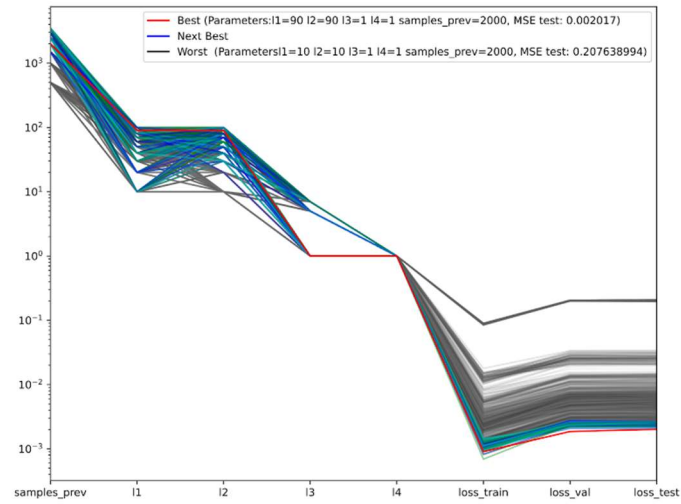


**Figure 6.** The outcome of the advanced digital filter structure of Figure 2 is shown as the logarithmic parallel coordinates for all the configurations trained with the MSE loss function based on the testing of MSE results; best model is in red; next best models are in blue variations; next in performance are in gray hues; and worst is depicted in black.

The training metrics obtained for the best model trained with the MSE loss function at the maximum step reached before stopping due to no loss validation improvement are depicted in Table 2.

**Table 2.** Training metrics for the best model trained with MSE loss function at the maximum step reached.

Step	Epoch MAE	Epoch MSE	Epoch MAPE	Epoch $l_r$
317	0.0364	0.0053	53.3455	0.0145

The validation metrics for the best model trained with the MSE loss function obtained at the maximum stage reached are enumerated in Table 3.

**Table 3.** Validation metrics for the best model trained with MSE loss function at the maximum step reached.

Step	Validation MAE	Validation MSE	Validation MAPE	Validation $l_r$
317	0.0415	0.0030	8.3354	0.0145

The test metrics obtained for the best model trained with the MSE loss function are enlisted in Table 4.

**Table 4.** Testing metrics in the test dataset for the best model trained with MSE loss function.

Model	Test MAE	Test MSE	Test MAPE	$R$ -squared
-------	-------------	-------------	--------------	--------------

RNN	0.0337	0.0020	6.8970	0.9076
$k$ -RNN*	0.0254	0.0013	5.4111	0.9406

\* The RNN model was optimized by using a multiplying constant,  $k$ , of value 1.030 (see Figure 9)

Once the digital filters were fully characterized, we assessed their implementation in a VF setting, as described next.

#### 4. Results

In real-life VF settings, the pH instrument will be calibrated and utilized to generate periodic signals exhibiting unpredictable patterns depending on multiple factors. Thus, the expected output of a pH instrument should include both phases, although the most prevalent one will be the periodic one. We utilized the waveforms of Figure 4 to quantify the performance of IIR and RNN digital filters for VF applications.

We commenced our assessment of both sets of digital filters by utilizing as test waveforms those of extrinsic (mechanical) perturbations enacted by impacting the container. Hereafter, we present the data with perturbations, without disturbances, and the output of the IIR models, as well as the RNNs trained model to filter the perturbations. In Figure 7, we show the obtained results for (a) IIR and (b) RNN.

**Table 5.** Testing metrics for the IIR and RNN models while assessing the external impact perturbation waveform.

Model	Test MAE	Test MSE	Test MAPE	$R$ -squared
Butterworth	0.1286	0.2003	0.0248	0.9077
Chebyshev I	0.1182	0.1684	0.0228	0.9224
Chebyshev II	0.4334	0.8926	0.0902	0.5889
Elliptic	0.1177	0.1657	0.0227	0.9236
RNN	0.0285	0.0014	6.1418	0.8804
$k$ -RNN*	0.0206	0.0008	4.5467	0.9302

\* The RNN model was optimized by using a multiplying constant,  $k$ , of value 1.030 (see Figure 9).

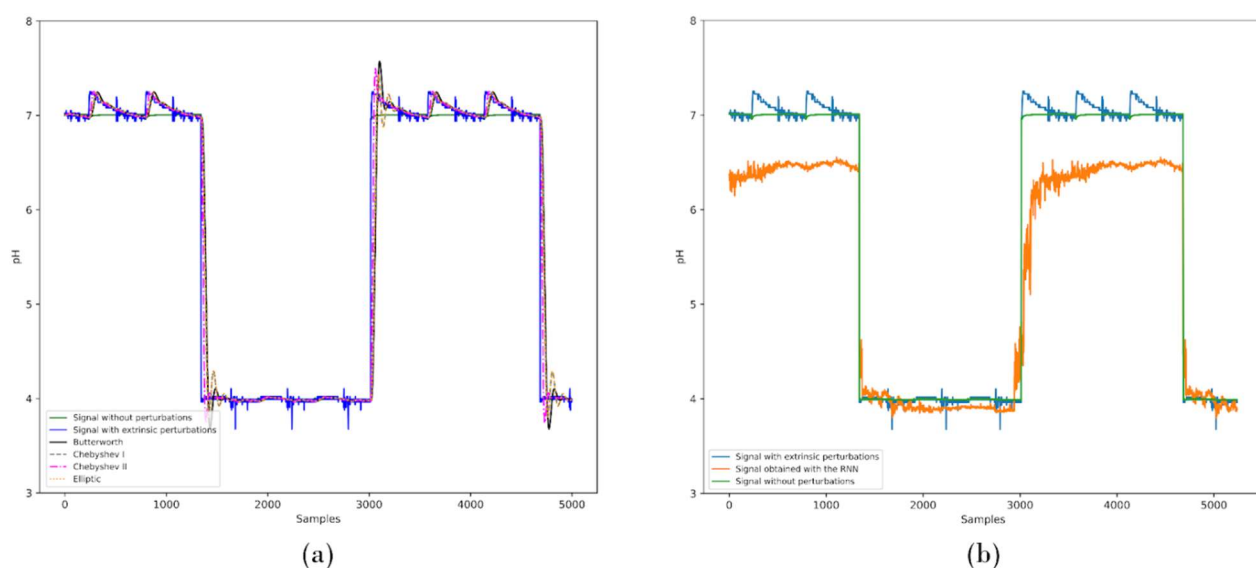


**Figure 7.** Comparative analysis of (a) IIR and (b) RNN digital filtering to assess the performance of the models to extrinsic mechanical perturbations for VF applications. Shown in the illustration are signals without perturbations, with disturbances, and with the IIR and RNN models applied to the external impact perturbation waveform.

The test metrics obtained for the IIR and the best trained RNN digital filters, employing the MSE loss function, while exposed to extrinsic mechanical perturbations, are enlisted in Table 5.

We continued the analysis by using as test signals the waveform of intrinsic perturbations, generated by means of the mechanical stirrer (refer to Figure 3), which mimics the recurrent pump variations encountered in VF settings. In Figure 8, we depict the results of the IIR and RNN models when exposed to intrinsic perturbations. In turn, in Table 6 we present the loss function MSE evaluation for IIR and RNN models as applicable to intrinsic disturbance.

**Table 6.** Testing metrics for the IIR and RNN models while assessing the internal impact perturbation waveform.

Model	Test MAE	Test MSE	Test MAPE	<i>R-squared</i>
Butterworth	0.1465	0.2079	0.0276	0.9042
Chebyshev I	0.1352	0.1748	0.0254	0.9194
Chebyshev II	0.4524	0.9072	0.0935	0.5821
Elliptic	0.1347	0.1720	0.0253	0.9207
RNN	0.0283	0.0013	6.1107	0.8812
<i>k</i> -RNN*	0.0207	0.0008	4.6574	0.9290

\* The RNN model was optimized by using a multiplying constant, *k*, of value 1.030 (see Figure 9).

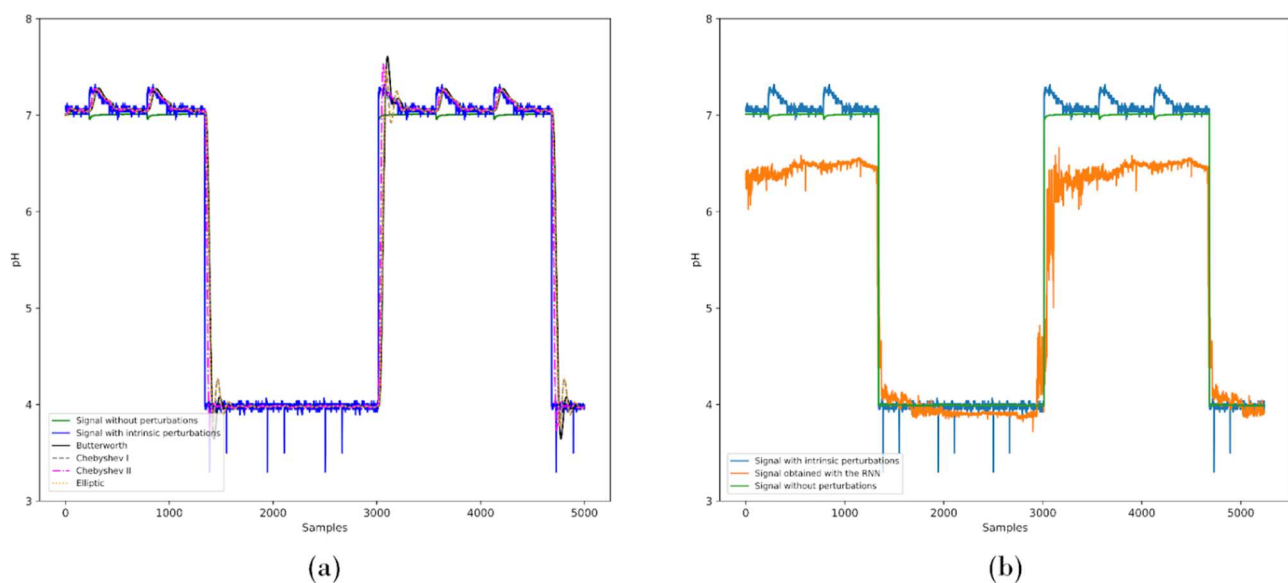


**Figure 8.** Comparative analysis of (a) IIR and (b) RNN digital filtering to assess the performance of the models to intrinsic mechanical perturbations in VF applications. Shown in the graph are signals without disturbances, with perturbations, and with the IIR and RNN models applied to the stirrer disturbance waveform.

Continuing our analysis of the advanced digital filter based on the RNN model described in this work, we assessed the extrinsic, i.e., Figure 7(b) and Table 5, as well as the intrinsic, i.e., Figure 8(b) and Table 6, mechanical perturbation results to determine if the RNN model performance could be improved by utilizing a rescaling constant, *k*. Thus, we returned to the training dataset and optimized a scaling parameter, *k*, in ranges [0.8,1.3] with steps of 0.001 (500 tests), multiplying the model output to improve the *R-squared* metric without changing the previously trained model. The obtained constant was  $k = 1.030$ , as shown in the optimization results of Figure 9. Using the aforementioned constant, we computed again the test metrics obtained for the test dataset in the best

model trained with the MSE loss function but now using the output scaling constant. The corresponding results are depicted in the last entry of Table 4.

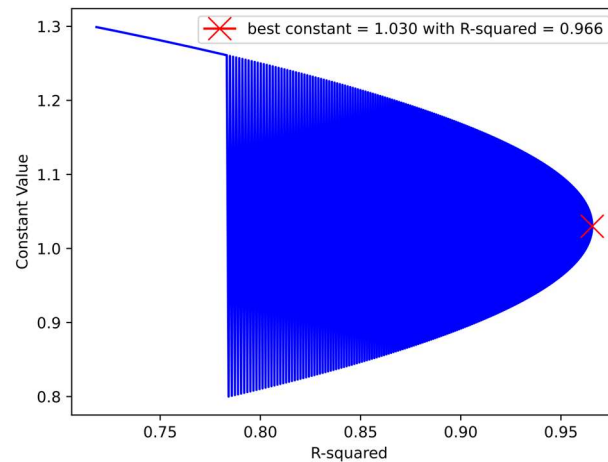


**Figure 9.** The MSE loss function optimization of the RNN digital filter model is based on the utilization of a scaling constant with the training dataset. After testing 500 different values, the optimal constant,  $k$ , was found to be 1.030; R-squared equaling 0.966.

Thereafter, we tested the scaled RNN, in short  $k$ -RNN, digital filter employing the extrinsic mechanical perturbations. Furthermore, in order to remove the harmonic oscillations of the  $k$ -RNN digital filter, we applied a moving average filter (MAF) with 300 samples to obtain the output waveform. Figure 10 depicts the results obtained for (a)  $k$ -RNN and (b) MAF-RNN digital filters while exposed to waveforms with extrinsic perturbations. In Table 5, we demonstrate that an *R-squared* metric of 0.9302 is obtained for the  $k$ -RNN model when exposed to unpredictable extrinsic mechanical perturbations.

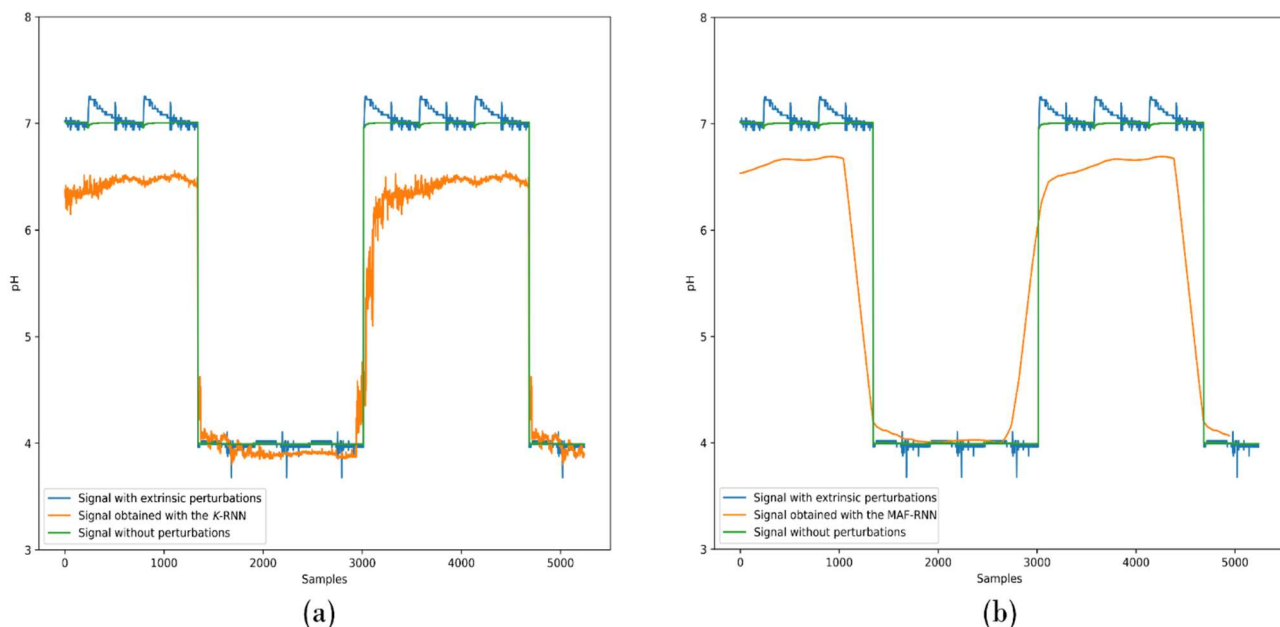


**Figure 10.** Comparative analysis of (a)  $k$ -RNN and (b) MAF-RNN digital filtering to assess the performance of the models to extrinsic mechanical perturbations for VF applications. Shown in the illustration are signals without perturbations, with disturbances, and with the  $k$ -RNN and MAF-RNN models applied to the external impact perturbation waveform.



Finally, we calculated the  $k$ -RNN and MAF-RNN digital filter performance when exposed to intrinsic mechanical perturbations. In Figure 11, we show the digital filtering performance for (a)  $k$ -RNN and (b) MAF-RNN models when exposed to waveforms with intrinsic perturbations. The corresponding test metrics when exposing the  $k$ -RNN filter to intrinsic mechanical perturbations are illustrated in the last entry of Table 6.

In the next section, we discuss the results and demonstrate how the RNN digital filter can be tuned to suit other VF applications.

## 5. Discussion and Future Work

In real-life VF settings, unpredictable mechanical perturbations hinder the implementation of efficient control strategies. Furthermore, as shown in this work, the use of conventional IIR digital filters introduces unwanted oscillations, which would impede the control process. Thus, the construction of robust solutions to address the filtering challenge is of utmost importance.

In this work, we have focused on providing an advanced digital filtering scheme based on RNN. As depicted in Figure 1, we assessed the RNN schemes for a signal centered at 4 pH units, while the reference signal was centered at 7. As commented before, such a configuration is pertinent to grow orchids and blueberries, pH ~4, and to maintain the electrode in good condition with a reference substance (in Figure 1 reference pH ~7, representative of water) whilst not administering nutrients.

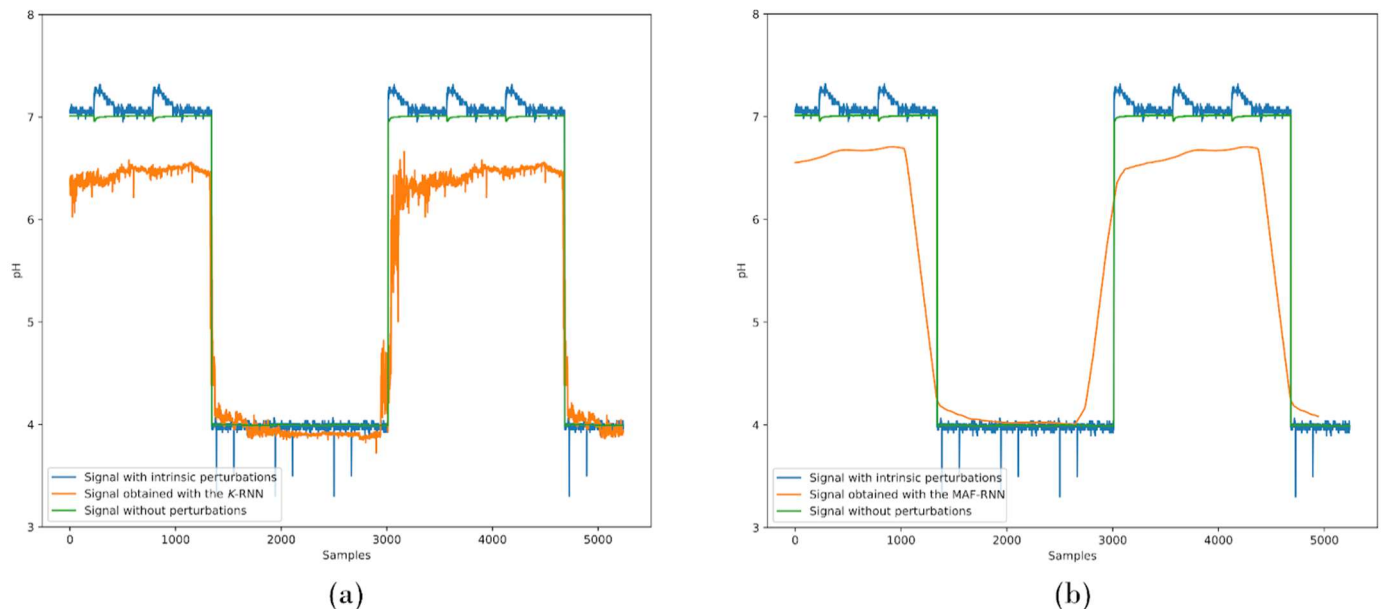


**Figure 11.** Comparative analysis of (a)  $k$ -RNN and (b) MAF-RNN digital filtering to assess the performance of the models to intrinsic mechanical perturbations in VF applications. Shown in the graph are signals without disturbances, with perturbations, and with the  $k$ -RNN and MAF-RNN models applied to the stirrer disturbance waveform.

The filtered signals,  $f$  in Figure 1, obtained with the RNN schemes, and depicted in Figure 7(b), Figure 8(b), Figure 10, and Figure 11 share several important features. First, we tuned the design of the RNN, including the multiplicative constant, to accurately filter the nutrition signal; centered at pH ~4. Second, the RNN signals do not exhibit considerable lags, which is relevant to avoid overexposing (i.e., to control) the crop to the nutrient substance. With respect to this last feature, it is worth noting that by modifying the MAF window size, we can control the lag exhibited in Figure 10(b) and Figure 11(b).

A salient feature of our RNN scheme has to do with the tuning of the digital filter. It is widely known that many crops require a nutrient substance with a pH close to 7 units [36,37]. A set of representative crops needing a pH close to 7 include lettuce, tomatoes, spinach, eggplants, and more

[38]. Hereafter, we present a modification of the RNN proposal to suit a signal centered close to 7 units, whilst assuming the reference pH is close to 4.

The RNN performance can be tuned by modifying the optimization constant,  $k$ . As before, we optimized the constant utilizing the  $R$ -squared metric with the signal dataset.

This yields a particularly flexible digital filtering approach, because the constant does not change the behavior of the RNN model, rather it serves to tune the RNN to tackle different specific challenges. We performed an optimization procedure similar to the one shown in Figure 9 and obtained new values for optimization constant and  $R$ -squared metrics; namely  $k = 1.076$  and  $R$ -squared = 0.959.

Afterwards, we tested the newly scaled  $k$ -RNN digital filter, assuming the same configuration of the MAF to eliminate harmonic oscillations of the output waveforms. Figure 12 depicts the results obtained for the  $k$ -RNN and MAF-RNN digital filters, tuned for a different pH value (i.e., at a particular constant  $k = 1.076$ ), while exposed to waveforms with (a) extrinsic and (b) intrinsic perturbations.

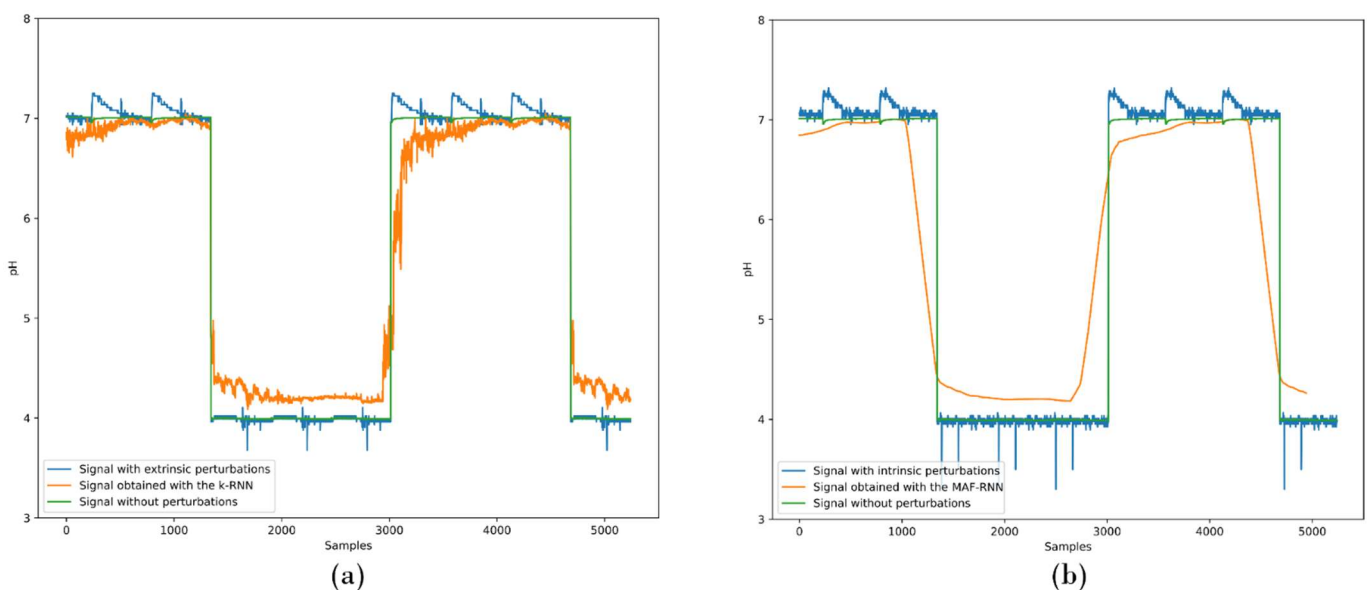


**Figure 12.** Comparative analysis of  $k$ -RNN and MAF-RNN digital filtering,  $k = 1.076$ , to assess the performance of the model to (a) extrinsic and (b) intrinsic unpredictable perturbations for VF applications. Shown in the illustration are signals without perturbations, with disturbances, and with the modified RNN models applied to the unpredictable perturbation waveforms.

As demonstrated in Figure 12, the RNN-based digital filters are particularly flexible for VF applications. Once the neural network has been adequately trained, we may tune the performance of the RNN digital filter by selecting the signal (i.e., pH) of interest. In a real VF setting, this feature is rather important because we can enact selective control depending on the crop of interest, without the need to re-train the neural network.

In the future, we will extend the analysis of the RNN model presented here to include the effects of vulnerability and disease in the detected signal. As commented before, both of these factors are critical to determine crop growth and yield.

## 6. Summary

In this work, we have proposed an advanced filtering scheme based on Recurrent Neural Networks (RNNs) and Deep Learning to enable efficient control strategies for *Vertical Farming* (VF) applications. We demonstrated that the best RNN model incorporates five neuron layers. The first and second of the segments contain ninety LSTM neurons. The third layer implements one GRU neuron. The fourth segment incorporates one RNN network, while the output layer was designed

by using a single neuron exhibiting a rectified linear activation function. By utilizing this RNN digital filter two variations were introduced: (1) A scaled RNN model to tune the filter to the signal(s) of interest, and (2) A moving average filter to eliminate harmonic oscillations of the output waveforms. The RNN models were contrasted with conventional Butterworth, Chebyshev I, Chebyshev II, and Elliptic digital IIR configurations. The RNN digital filtering schemes avoid introducing unwanted oscillations, which makes them more suitable for VF than their IIR counterparts. Furthermore, by utilizing the advanced features of scaling of the RNN model, we demonstrated that the RNN digital filter is pH selective, as opposed to conventional IIR filters. In real VF settings, the features of tuning (or selecting) an instrument to detect variable pH values, as well as ensuring that such device is resilient to dynamic (i.e., unpredictable) perturbations are of utmost importance. Hence, the use of advanced filtering schemes such as those based on RNN and Deep Learning is preferable as opposed to employing IIR filtering for VF.

**Supplementary Materials:** Advanced filtering code and datasets can be accessed at: [http://pabellon.tecnm.mx/LIA/productos\\_generados.html#Trabajos\\_realizados](http://pabellon.tecnm.mx/LIA/productos_generados.html#Trabajos_realizados) (accessed on 30 April 2023).

**Author Contributions:** Conceptualization, R.H.-M, M.M.R, P.V.-J, and N.E.-G; Methodology, M.M.R, P.V.-J, and E.O.-G; Software, R.H.-M, M.M.R, P.V.-J, and A.B.S; Validation, R.H.-M, A.B.S, and E.O.-G; formal analysis, R.H.-M, M.M.R, P.V.-J, and N.E.-G; investigation, R.H.-M, N.E.-G, J.A.D.-A, and A.B. S.; resources, M.M.R, P.V.-J, N.E.-G, and E.O.-G; data curation, R.H.-M, M.M.R, P.V.-J, and J.A.D.-A writing—original draft preparation, R.H.-M, M.M.R, P.V.-J, and N.E.-G; writing—review and editing, all authors; visualization, R.H.-M, P.V.-J, N.E.-G, J.A.D.-A, and A.B. S.; supervision, P.V.-J, N.E.-G, and E. O.-G.; project administration, M.M.R, P.V.-J, N.E.-G, and J.A.D.-A; funding acquisition, J.A.D.-A, A.B. S., and E.O.-G. fund raising, E.O.-G., N.E.-G.. All authors have read and accepted the published version of the manuscript.

**Funding:** We acknowledge the support of the Consejo Nacional de Ciencia y Tecnología (CONACYT) in Mexico for supporting this work through funds for projects INFRA-2016-01, Project No. 270665. CB-2016-01, Project No. 287818. Additionally, we acknowledge the support to the Government of the State of Aguascalientes, and the Instituto para el Desarrollo de la Sociedad del Conocimiento del Estado de Aguascalientes (IDSCEA) through the Technological Innovation Fund.

**Institutional Review Board Statement:** Not applicable.

**Informed Consent Statement:** Not applicable. Data Availability Statement: Not applicable.

**Conflicts of Interest:** The authors declare no conflict of interest.

## References

1. FOOD SECURITY AND NUTRITION IN THE WORLD THE STATE OF REPURPOSING FOOD AND AGRICULTURAL POLICIES TO MAKE HEALTHY DIETS MORE AFFORDABLE. **2022**, doi:10.4060/cc0639en.
2. Hurst, W.; Mendoza, F.R.; Tekinerdogan, B. Augmented Reality in Precision Farming: Concepts and Applications. *Smart Cities 2021*, Vol. 4, Pages 1454–1468 **2021**, 4, 1454–1468, doi:10.3390/SMARTCITIES4040077.
3. Raj, E.F.I.; Appadurai, M.; Athiappan, K. Precision Farming in Modern Agriculture. **2021**, 61–87, doi:10.1007/978-981-16-6124-2\_4.
4. Li, H.; Yang, H.; Zhan -, M.; Haruyama, S.; Darmawan, Z.; Kaminishi -, K.; Zheng, Y.; Yang, M.; Yao, L.; Chengming, L.; et al. Analysis on Water Wall Tube Explosion in a Power Plant. *IOP Conf Ser Earth Environ Sci* **2020**, 526, 012162, doi:10.1088/1755-1315/526/1/012162.
5. Van Gerrewey, T.; Boon, N.; Geelen, D. Vertical Farming: The Only Way Is Up? *Agronomy 2022*, Vol. 12, Page 2 **2021**, 12, 2, doi:10.3390/AGRONOMY12010002.
6. Yin, H.; Cao, Y.; Marelli, B.; Zeng, X.; Mason, A.J.; Cao, C. Soil Sensors and Plant Wearables for Smart and Precision Agriculture. *Advanced Materials* **2021**, 33, 2007764, doi:10.1002/ADMA.202007764.
7. Msimbira, L.A.; Smith, D.L. The Roles of Plant Growth Promoting Microbes in Enhancing Plant Tolerance to Acidity and Alkalinity Stresses. *Front Sustain Food Syst* **2020**, 4, 106, doi:10.3389/FSUFS.2020.0106/BIBTEX.
8. Penn, C.J.; Camberato, J.J. A Critical Review on Soil Chemical Processes That Control How Soil PH Affects Phosphorus Availability to Plants. *Agriculture 2019*, Vol. 9, Page 120 **2019**, 9, 120, doi:10.3390/AGRICULTURE9060120.

9. Liming Effects on Soil PH and Crop Yield Depend on Lime Material Type, Application Method and Rate, and Crop Species: A Global Meta-Analysis Available online: <https://agris.fao.org/agris-search/search.do?recordID=US201900294097> (accessed on 19 April 2023).
10. Adesina, I.; Bhowmik, A.; Sharma, H.; Shahbazi, A. A Review on the Current State of Knowledge of Growing Conditions, Agronomic Soil Health Practices and Utilities of Hemp in the United States. *Agriculture* **2020**, *Vol. 10*, Page 129 **2020**, *10*, 129, doi:10.3390/AGRICULTURE10040129.
11. Neina, D. The Role of Soil PH in Plant Nutrition and Soil Remediation. *Appl Environ Soil Sci* **2019**, *2* 019, doi:10.1155/2019/5794869.
12. Chandra, S.; Bhattacharya, J. Influence of Temperature and Duration of Pyrolysis on the Property Heterogeneity of Rice Straw Biochar and Optimization of Pyrolysis Conditions for Its Application in Soils. *J Clean Prod* **2019**, *215*, 1123–1139, doi:10.1016/J.JCLEPRO.2019.01.079.
13. Hinojosa-Meza, R.; Olvera-Gonzalez, E.; Escalante-Garcia, N.; Dena-Aguilar, J.A.; Montes Rivera, M.; Vacas-Jacques, P. Cost-Effective and Portable Instrumentation to Enable Accurate PH Measurements for Global Industry 4.0 and Vertical Farming Applications. *Applied Sciences* **2022**, *Vol. 12*, Page 7038 **2022**, *12*, 7038, doi:10.3390/APP12147038.
14. Rader, C.M.; Gold, B. Digital Filter Design Techniques in the Frequency Domain. *Proceedings of the IE EE* **1967**, *55*, 149–171, doi:10.1109/PROC.1967.5434.
15. Pilipović, R.; Risojević, V.; Bulić, P. On the Design of an Energy Efficient Digital IIR A-Weighting Filter Using Approximate Multiplication. *Sensors* **2021**, *Vol. 21*, Page 732 **2021**, *21*, 732, doi:10.3390/S21030732.
16. Dirmi, S. Calcium Soft Sensor Based on the Combination of Support Vector Regression and 1-D Digital Filter for Water Quality Monitoring. *Arab J Sci Eng* **2022**, doi:10.1007/S13369-022-07263-W.
17. Stanciu, L.; Stanciu, V.; Badea, R. Digital Filters with Small Transition Frequency Bands. *ISSCS 2019 - International Symposium on Signals, Circuits and Systems* **2019**, doi:10.1109/ISSCS.2019.8801801.
18. Ruospo, A.; Sanchez, E. On the Reliability Assessment of Artificial Neural Networks Running on AI-Oriented MPSoCs. *Applied Sciences* **2021**, *Vol. 11*, Page 6455 **2021**, *11*, 6455, doi:10.3390/APP11146455.
19. Sahu, S.K.; Mokhade, A.; Bokde, N.D. An Overview of Machine Learning, Deep Learning, and Reinforcement Learning-Based Techniques in Quantitative Finance: Recent Progress and Challenges. *Applied Sciences* **2023**, *Vol. 13*, Page 1956 **2023**, *13*, 1956, doi:10.3390/APP13031956.
20. Kim, T.; Vecchietti, L.F.; Choi, K.; Lee, S.; Har, D. Machine Learning for Advanced Wireless Sensor Networks: A Review. *IEEE Sens J* **2021**, *21*, 12379–12397, doi:10.1109/JSEN.2020.3035846.
21. Jospin, L.V.; Laga, H.; Boussaid, F.; Buntine, W.; Bennamoun, M. Hands-On Bayesian Neural Networks - A Tutorial for Deep Learning Users. *IEEE Comput Intell Mag* **2022**, *17*, 29–48, doi:10.1109/MCI.2022.3155327.
22. Kimmel, J.C.; McDole, A.D.; Abdelsalam, M.; Gupta, M.; Sandhu, R. Recurrent Neural Networks Based Online Behavioural Malware Detection Techniques for Cloud Infrastructure. *IEEE Access* **2021**, *9*, 68066–68080, doi:10.1109/ACCESS.2021.3077498.
23. Bendarkar, D.; Somase, P.; Rebari, P.; Paturkar, R.; Khan, A. Web Based Recognition and Translation of American Sign Language with CNN and RNN. *International Journal of Online and Biomedical Engineering (ijOE)* **2021**, *17*, 34–50, doi:10.3991/IJOE.V17I01.18585.
24. Kang, T.; Lim, D.Y.; Tayara, H.; Chong, K.T. Forecasting of Power Demands Using Deep Learning. *Applied Sciences* **2020**, *Vol. 10*, Page 7241 **2020**, *10*, 7241, doi:10.3390/APP10207241.
25. Yang, D.; Gu, C.; Zhu, Y.; Dai, B.; Zhang, K.; Zhang, Z.; Li, B. A Concrete Dam Deformation Prediction Method Based on Lstm with Attention Mechanism. *IEEE Access* **2020**, *8*, 185177–185186, doi:10.1109/ACCESS.2020.3029562.
26. Tasnim, R.; Calderwood, L.; Tooley, B.; Wang, L.; Zhang, Y.J. Are Foliar Fertilizers Beneficial to Growth and Yield of Wild Lowbush Blueberries? *Agronomy* **2022**, *Vol. 12*, Page 470 **2022**, *12*, 470, doi:10.3390/AGRONOMY12020470.
27. Song, X.; Li, Y.; Hu, Y.; Guo, W.; Wu, Z.; Zhang, Y.; Cao, Z. Endophytes from Blueberry Roots and Their Antifungal Activity and Plant Growth Enhancement Effects. *Rhizosphere* **2021**, *20*, doi:10.1016/J.RHISPH.2021.100454.
28. Sopalun, K.; Iamtham, S. Evaluation and Optimization of Pectinase Production by Endophytic Fungi Isolated from Thai Orchids Using Agrowaste Medium. *Journal of ISSAAS (International Society for Southeast Asian Agricultural Sciences)* **2020**, *26*, 86–98.
29. Schreiber, M.J.; Nunez, G.H. Calcium Carbonate Can Be Used to Manage Soilless Substrate Ph for Blueberry Production. *Horticulturae* **2021**, *7*, 74, doi:10.3390/HORTICULTURAE7040074/S1.
30. de Cheveigné, A.; Nelken, I. Filters: When, Why, and How (Not) to Use Them. *Neuron* **2019**, *102*, 280–293, doi:10.1016/J.NEURON.2019.02.039.
31. Borges, V.S.; Nepomuceno, E.G.; Duque, C.A.; Butusov, D.N. Some Remarks about Entropy of Digital Filtered Signals. *Entropy* **2020**, *Vol. 22*, Page 365 **2020**, *22*, 365, doi:10.3390/E22030365.

32. Hossain, G.M.S.; Rashid, Md.H.O.; Islam, Md.R.; Sarker, A.; Yasmin, Must.A.; Hossain, G.M.S.; Rashid, Md.H.O.; Islam, Md.R.; Sarker, A.; Yasmin, Must.A. Towards Mining Public Opinion: An Attention-Based Long Short Term Memory Network Using Transfer Learning. *Journal of Computer and Communications* **2022**, *10*, 112–131, doi:10.4236/JCC.2022.106010.
33. Vatistas, C.; Avgoustaki, D.D.; Bartzanas, T. A Systematic Literature Review on Controlled-Environment Agriculture: How Vertical Farms and Greenhouses Can Influence the Sustainability and Footprint of Urban Microclimate with Local Food Production. *Atmosphere* **2022**, *Vol. 13*, Page 1258 **2022**, *13*, 1258, doi:10.3390/ATMOS13081258.
34. Michael, G.W.; Tay, F.S.; Then, Y.L. Development of Automated Monitoring System for Hydroponics Vertical Farming. *ICoST) Journal of Physics: Conference Series* **2020**, *1844*, 12024, doi:10.1088/1742-6596/1844/1/012024.
35. Olvera-Gonzalez, E.; Rivera, M.M.; Escalante-Garcia, N.; Flores-Gallegos, E. Modeling Energy LED Light Consumption Based on an Artificial Intelligent Method Applied to Closed Plant Production System. *Applied Sciences* **2021**, *Vol. 11*, Page 2735 **2021**, *11*, 2735, doi:10.3390/APP11062735.
36. Holland, J.E.; White, P.J.; Glendinning, M.J.; Goulding, K.W.T.; McGrath, S.P. Yield Responses of Arable Crops to Liming – An Evaluation of Relationships between Yields and Soil PH from a Long-Term Liming Experiment. *European Journal of Agronomy* **2019**, *105*, 176–188, doi:10.1016/J.EJA.2019.02.016.
37. Li, Y.; Cui, S.; Chang, S.X.; Zhang, Q. Liming Effects on Soil PH and Crop Yield Depend on Lime Material Type, Application Method and Rate, and Crop Species: A Global Meta-Analysis. *J Soils Sediments* **2019**, *19*, 1393–1406, doi:10.1007/S11368-018-2120-2/METRICS.
38. Harinditha Ruchirawya, T.; Bandara, P.; Lanka Thilini Weerasooriya Assistant Lecturer, S.; Lanka Ruchirawya, S.T.; Nanayakkara, W.; Lanka Dimantha MAC, S.; Mgp, P. Crop Recommendation System. *Int J Comput Appl* **2020**, *175*, 975–8887.

# ANNEX 3

# Temperature compensation of pH measurements using a Fuzzy inference system and genetic algorithms

Rolando Hinojosa Meza<sup>1</sup>, Ernesto Olvera-Gonzalez<sup>1</sup>, Nivia Escalante-Garcia<sup>1</sup>, Martin Montes Rivera<sup>2</sup>

<sup>1</sup> Laboratorio de Iluminación Artificial, Tecnológico Nacional de México/IT de Pabellón de Arteaga, Carretera a la Estación de Rincón Km. 1, 20670 Aguascalientes, Mexico.

<sup>2</sup> Universidad Politécnica de Aguascalientes, Calle paseo San Gerardo #201, Fracc. San Gerardo, C.P. 20342, Aguascalientes, México.

rolandohinojosamz@outlook.com, e.olvera.itp@gmail.com,  
aivineg82@gmail.com, martin.montes@upa.edu.mx

## Abstract.

pH is a crucial variable in hydroponic crops that indicates the solution's acidity or alkalinity. It is necessary to control and adjust the pH in the nutrient solution of the crop since it affects the transference of nutrients to the root. The pH measurement compares the solution's potential with unknown  $[H^+]$  with a known reference. At the same time, the function of the pH meter is to convert the voltage ratio between a reference and a sensing half-cell into pH values. In acidic or alkaline solutions, the voltage at the outer membrane surface changes proportionally to changes in  $[H^+]$ . However, temperature affects the pH measurement, producing inaccurate measurements. The most complex sensors integrate Automatic Temperature Compensation (ATC) since they accurately adjust the electrode calibration for pH when the temperature changes. Nevertheless, ATC cannot correct for the pH/temperature effects of samples that are unknown. This research proposes a fuzzy interference system to compensate for the effects of temperature on pH measurement through a Mamdani interference system besides genetic algorithms to tune the vertices in the output arrays.

**Keywords:** fuzzy, genetic algorithms, artificial intelligence, instrumentation, pH variable.

## 1 Introduction

### 1.1 Description of Problem

Hydroponics is the technique of soilless cultivation, in which the water supplied to the plants dissolves a nutrient solution. When the nutrient solution is applied, the crops are not affected in their growth and development and obtain high yield potentials. A Key factor in hydroponic crops is the control and adjustment of the pH levels of the nutrient solution since it affects the availability of nutrients in the water and therefore

prevents root uptake. An element that can be found in different chemical forms depending on the pH of the solution. Soluble chemical forms will be directly assimilated by the roots, while other chemical forms will be insoluble and not assimilated, or even others may be toxic to the plant. In intensive crops, the pH of the substrate and/or nutrient solution must be within a narrow range. In addition, this pH value will increase slightly as the plants absorb the nutrients, so it should be monitored periodically and adjusted if necessary. The correct pH depends on the growing medium, the type of plant, and its age. The pH value is a measure that helps to control the nutrient dosing pumps when the pH value goes down or up. However, the pH measurement is no longer linear in behavior when the temperature changes. Automatic temperature compensation (ATC) is built into some sensors, allowing precise calibration adjustments of the pH electrode when the temperature changes. However, ATC cannot correct for unknown sample pH/temperature effects. When the behavior of a sensor is known, the ATC works adequately to perform the calibration of some sensors.

A problem to be solved with fuzzy inference systems is to find a structure and the type of rules for the implementation to reach an optimal behavior. Genetic algorithms have been implemented in the literature to optimize fuzzy systems applied to obtaining appropriate values for parameters measured in real problems.

A Fuzzy model was built based on a hybrid genetic algorithm adaptive network (GA-ANFIS) where the clustering as rule-based parameters is simultaneously optimized using Gas and Artificial Neural Networks (ANNs) [1]. Similarly, a neuro-fuzzy inference system (ANFIS) tuned by particle swarm optimization (PSO) algorithm monitors a nuclear power plant sensor [2].

Roy and Datta [3] proposed a hybrid model with a genetic algorithm and a fuzzy inference system used as a strategy in saltwater intrusion management. The genetic algorithm adjusts the parameters of the fuzzy system to obtain the optimal structure. Similarly, Genetic programming and artificial neural networks generate two nonlinear models to predict energy consumption in artificial lighting systems for closed plant production systems (CPPS) [4].

In this work, we use a fuzzy inference system to compensate for the temperature changes in pH measurements, using a genetic algorithm to tune the best vertices of the membership functions to obtain the desired behavior, specially adapted for the sensor used.

## 1.2 Theoretical Framework

The fuzzy inference systems rely on the concepts of fuzzy set theory (fuzzy if-then rules and fuzzy reasoning). Several researchers have successfully applied this theory in different areas, such as automatic control, data classification, decision analysis, expert systems, time series prediction, robotics, and pattern recognition. A rule base integrates the selection of fuzzy rules, the database (dictionary) defines the membership functions used in the fuzzy rules and the reasoning mechanism that runs the inference procedure on the given commands and facts to derive a reasonable output or conclusion [5].



The fuzzy set enumerates the degree of membership of an element that refers to a set. Therefore, the characteristic function of a fuzzy set can have values between 0 and 1, which denotes the degree of membership of an element to a given set [6].

If  $X$  is a collection of objects denoted generically by  $x$ , then a fuzzy set  $A$  in  $X$  is defined as a set of order pairs:

$$A = \{(x, \mu_A(x)) / x \in X\} \quad (1)$$

Where  $\mu_A(x)$  is the membership function for the fuzzy set  $A$ . The MF assigns to each element of  $X$  a degree of membership among 0 and 1. A fuzzy set is an extension of the classical set definition in which the characteristic function is allowed to have any value between 0 and 1.

A linguistic variable is a concept that qualified in a fuzzy way. Examples are height, age, error, error variance, among others. This variable is called "linguistic" due to its features defined in spoken language.

The discourse universe contains all the possible values taken by the elements that possess a property expressed by the linguistic variable. For example, in linguistic variables "height of a human," a set of values would be given between 1.4 and 2.3 m.

The different classifications made on the linguistic variable are called linguistic values, like the case of height. Thus, the universe of discourse could match different linguistic values such as low, medium, and high.

A linguistic value (name of the fuzzy set) together with a membership function (maps the elements of the universe of discourse) is a fuzzy set.

The union operation of two fuzzy sets  $A$  and  $B$  is a fuzzy set  $C$ , denoted as  $C = A \cup B$  or  $C = A \text{ OR } B$ . The membership function is related to that of  $A$  and  $B$  defined by Jantzen [7].

$$\mu_C(x) = \max(\mu_A(x), \mu_B(x)) = \mu_A(x) \vee \mu_B(x) \quad (2)$$

The intersection of fuzzy sets can be defined analogously. The intersection of two fuzzy sets  $A$  and  $B$  is a fuzzy set  $C$ , written as  $C = A \cap B$  or  $C = A \text{ AND } B$ , whose MF is related to those of  $A$  and  $B$  by

$$\mu_C(x) = \min(\mu_A(x), \mu_B(x)) = \mu_A(x) \wedge \mu_B(x) \quad (3)$$

Although in principle, any function would be valid for defining fuzzy sets. The most common functions used in practice are:

- GAMMA function:
- L function:
- LAMBDA or triangular function:
- PI or trapezoidal function:
- Smooth trapezoidal function
- Gaussian function

The fuzzy set theory allows us to represent vague (imprecise) facts and relations. Fuzzy reasoning is making inferences from fuzzy facts and relationships, combining fuzzy evidence, and updating the accuracy of beliefs.

Mamdani fuzzy systems mimic the performance of human operators in charge of controlling specific industrial processes. The goal was to summarize the operator's experience into a set of IF-THEN (linguistic) rules that a machine uses for automatically controlling the process. Specifically, using such a set of IF-THEN rules, a Mamdani fuzzy system defines a function  $f$  that generates numerical outputs  $y=f(x)$  from (generally numerical) input values  $x$ .

$$p \rightarrow q \equiv p \wedge q \rightarrow \mu_{p \rightarrow q}(u, v) = \min(\mu_A(u), \mu_B(v)) \quad (4)$$

Defuzzification refers to an operation for transforming a fuzzy set into a crisp representative value. For example, with the centroid defuzzification method, the fuzzy output is transformed into a number. This defuzzification is the most widely adopted defuzzification strategy, reminiscent of the calculation of expected values of probability distributions.

$$Z_{CG} = \frac{\sum_{k=1}^l z_k \mu(z_k)}{\sum_{k=1}^l \mu(z_k)} \quad (5)$$

Genetic algorithms simulate the process of natural selection based on Darwin's theory of evolution. Those species that can adapt to changes in their environment can survive and reproduce and pass on to the next generation. This algorithm simulates the "survival of the fittest" among individuals of consecutive generations to solve a problem. Each generation consists of a population of individuals where each individual represents a possible solution. The name given to each individual in the population is chromosome; within each chromosome are  $n$  number of genes which are the set of bits that make up a solution.

Genetic algorithms make the analogy with the genetic structure and behavior of chromosomes in the population. The basics of GAs include the natural selection principles listed below:

1. Individuals in the population compete for resources and mates.
2. Those individuals that are successful (fittest) then mate to create more offspring than others.
3. The genes of the "fittest" parents survive throughout the generation, i.e., sometimes parents create offspring that are better than either parent.
4. Therefore, each successive generation is better suited for its environment.

The summarized algorithm is below:

1. Randomly initialize the population.
2. Determine the fitness of the population.
3. Until convergence repeat:
  - a) Select the parents of the population.

- b) Crossover and generate a new population.
- c) Perform the mutation in the new population.
- d) Calculate the fitness of the new population.

## 2 Methodology

The fuzzy inference machine considers the voltage delivered by the electrode (AgCl) measured with five samples of known pH, 4, 6.86, 7, 9.18, 10 at different temperatures (15°C to 30°C), thus obtaining a small database with 80 readings for the genetic algorithm. These experiments define the values of the input and output universes specific to the electrode used. The rule used in the controller is the Mamdani rule. The aggregation was done through the max operation and defuzzification by a centroid of gravity.

The fuzzy models presented here have two input variables: the value of the voltage measured by the electrode  $V$  and the value of the temperature of the solution  $T$ . The output variable, pH, describes the temperature of the solution. The output variable, pH, describes the actual pH value at a given temperature. The inputs are the voltage represented by the set  $V$  with five terms:

$$V = \{V_{pH10}, V_{pH9.18}, V_{pH7}, V_{pH6.86}, V_{pH4}\},$$

Where each value represents the approximate pH value corresponding to the voltage levels measured by the electrode.

And the temperature represented with the set  $T$  with five terms:

$$T = \{TVL, TL, TA, TH, TVH\}$$

VL represents the Very low, L set as Low, A is the Average, H equal to High, VH denominated Very High.

The expected output in the experiment is a pH level between 4 to 10. Thus, we let the genetic algorithm tune the fuzzy inference system for obtaining the appropriate output sets for the centroid defuzzification.

Then, the output is given by pH with five terms:

$$pH = \{pH4, pH6.86, pH7, pH9.18, pH10\}$$

Where each value represents the real pH value taking into account the temperature. The universe considered for the voltage ranges that the sensor can deliver is  $UV = \{x \in \mathbb{Z}: -200 \leq x \leq 200\}$ , for temperature is  $UT = \{y \in \mathbb{Z}: 15 \leq y \leq 30\}$  and for pH value  $UpH = \{z \in \mathbb{Z}: 4 \leq z \leq 10\}$ .

The objective function (equation (6)) uses the genetic algorithm in the fuzzy inference machine to fit the vertices of the Gaussian functions (5 input sets, 5 output sets, and 25 rules) with the data in Tables 1 and 2.

$$y = (\sum_{i=1}^{80} |Ai - Bi|) + \frac{0.1}{|M-m|} \quad (6)$$

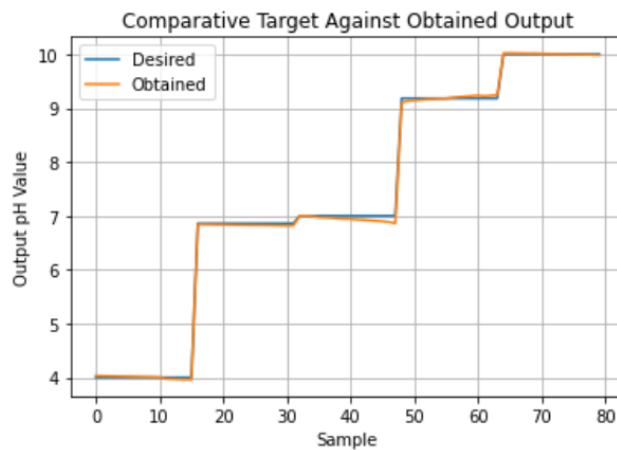
where  $Ai$  is the value obtained with the fuzzy inference machine using the vertices tuned by the genetic algorithm,  $Bi$  is the desired value for the dataset values.  $M$  is the maximum, and  $m$  is the minimum of the values obtained. The objective is to minimize the function given in equation (6). As the problem to be optimized is dimension 105, we used an initial population of 500 individuals, each with 1155 alleles, where every 11 alleles form a bit string representing a real number, with a resolution of 1000 decimals. The selection method is by tournament, the tournament size applied here is 100, the number of crossover points is a random number, the mutation rate is 5%, and 30000 generations. Table 1 represents the values of the voltage (mV) at different temperatures ( $^{\circ}\text{C}$ ), and different pH.

**Table 1.** Electrode voltage values at different temperatures.

	pH=4	pH=6.86	pH=7	pH=9.18	pH=10
$^{\circ}\text{C}$	mV	mV	mV	mV	mV
15	161.51	8	4.95	-119.63	-163.53
16	162.11	8.03	5.12	-121.06	-163.11
17	162.71	8.05	5.23	-121.5	-163.8
18	163.31	8.08	5.67	-121.99	-164.31
19	163.88	8.1	5.75	-122.63	-164.88
20	164.48	8.16	5.86	-122.78	-164.48
21	165.08	8.19	6.09	-123.01	-166.08
22	165.68	8.23	6.2	-123.22	-166.68
23	166.28	8.26	6.25	-124.09	-167.28
24	166.88	8.27	6.43	-124.53	-167.85
25	168.55	8.28	6.53	-124.96	-169.08
26	176.05	8.31	6.73	-125.38	-169.3
27	176.65	8.33	6.86	-125.78	-169.85
28	178.25	8.37	7.03	-125.24	-170.25
29	179.90	8.42	7.26	-125.7	-170.85
30	180.13	8.39	7.67	-126.12	-172.45

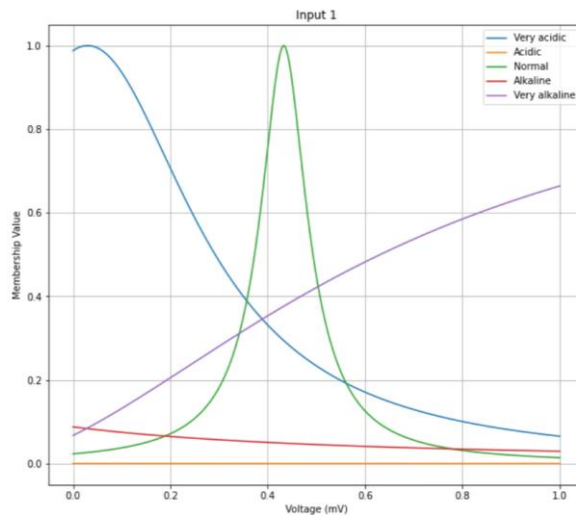
### 3 Results

The fuzzy inference system developed in Python can find a value that approximates the actual pH value. Figure 1 shows the fuzzy inference machine that corresponds the target pH values with the data set's input voltage and temperature values.



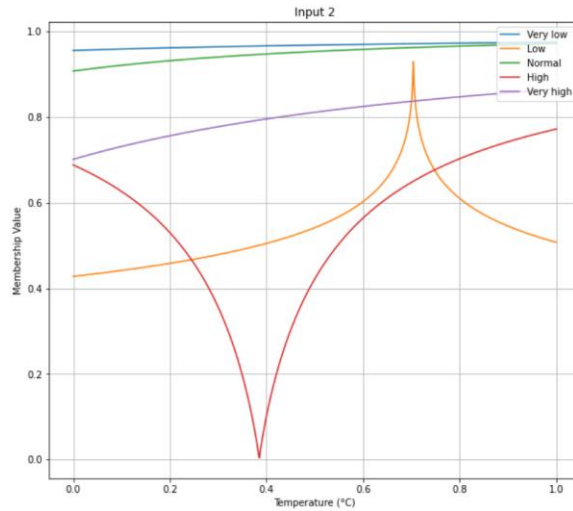
**Fig. 1.** Comparative graph between the output obtained and the desired output with the input data of the dataset.

Figure 2 shows the data sets for the different input voltages normalized-tuned by the genetic algorithm.



**Fig. 2.** Voltage (mV) input sets, tuned by the genetic algorithm.

The pH measurement with 16 different temperatures (from 15°C to 30°C) was divided into sets of 5 (total 3 data sets) to validate the sensor characterization. Figure 3 shows the element of the input normalized to two, where according to the temperature, the system infers the optimum pH value.



**Fig. 3.** Input sets for temperature (°C) tuned by the genetic algorithm.

The data set for the output universe is tuned by the generic algorithm and represented in Figure 4. The centroid defuzzification method obtained the appropriate pH value with the vertices of the Gaussian functions generated by the genetic algorithm.

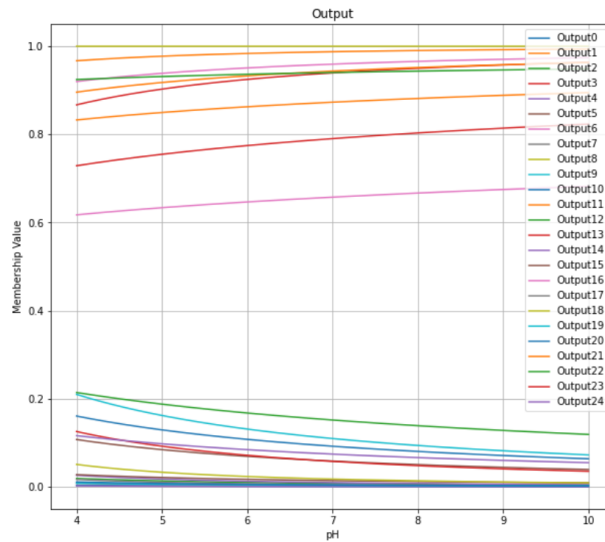


**Fig. 4.** Output sets tuned by the genetic algorithm.

## 4 Conclusions

The present investigation uses a Mamdani fuzzy logic system auto-tuned through genetic algorithms to obtain the real pH value without considering the slight variation of the temperature. The system can identify the correct pH values considering the possible changes in the voltage that can influence the electrode due to the temperature. At the same time, an important fact is that the performance of the pH electrode is deteriorated by the useful life or by external factors. With the application of the fuzzy system, it is possible to approximate a sensor's behavior to another in optimal conditions or more sophisticated with ATC. It would be enough to build a set of data with the voltage measurements given by the sensor at certain temperatures and the correct pH value that corresponds to the readings of the sensor already calibrated. The genetic algorithm function will tune the fittest vertices for the fuzzy inference system sets in the defuzzification to obtain the correct pH value. For this work, the system only works in the range of data we used (pH4 to pH10), as future work will create a more extensive data set. In addition, the incorporation of fuzzy logic in a control mechanism for monitoring nutrients in water in a multilevel hydroponic growing system considering parameters such as pH, conductivity, and temperature. By considering these variables, dosing pumps will activate for the modification of nutrients in the water.

## References

1. Morteza Zanaganeh, S. Jamshid Mousavi, Amir Farshad Etemad Shahidi: A hybrid genetic algorithm–adaptive network-based fuzzy inference system in prediction of wave parameters, *Engineering Applications of Artificial Intelligence*, 1194-1202, (2009)
2. Oliveira, M.V., Schirru, R. Applying particle swarm optimization algorithm for tuning a neuro-fuzzy inference system for sensor monitoring, *Progress in Nuclear Energy*, 177-183, (2009).
3. Roy, D.K., Datta, B. Genetic algorithm tuned fuzzy inference system to evolve optimal groundwater extraction strategies to control saltwater intrusion in multi-layered coastal aquifers under parameter uncertainty. *Model. Earth Syst. Environ.* 3, 1707–1725, (2017).
4. Gonzalez, O., Rivera, M., Escalante, N. & Flores, E.: Modeling Energy LED Light Consumption Based on an Artificial Intelligent Method Applied to Closed Plant Production System. *Applied Sciences*, 11(6), 2735, (2021).
5. Jang, J., Sun, C.: *Neuro-Fuzzy and Soft Computing*. 2nd Ed. Prentice-Hall, U.S.A. (1997).
6. Li, Y., Xiong, X., Qiu, C., Wang, Q., & Xu, J. Mining latent information in PTSD psychometrics with fuzziness for effective diagnoses. *Scientific reports*, 8(1), 1-8, (2018).
7. Jantzen, J.: *Foundations of Fuzzy Control*. 2nd Ed. Wiley, Denmark, (2007).
8. Grigorie, T. L., Botez, R. M., Lungu, M., Edu, R. I., & Obreja, R. Micro-electromechanical systems gyro performance improvement through bias correction over

- temperature using an adaptive neural network-trained fuzzy inference system. Proceedings of the Institution of Mechanical Engineers, Part G: Journal of Aerospace Engineering, 226(9), 1121-1138, (2012)
9. Yolanda, D., Hindersah, H., Hadiatna, F., & Triawan, M. A.: Implementation of real-time fuzzy logic control for NFT-based hydroponic system on Internet of Things environment. In 2016 6th International Conference on System Engineering and Technology (ICSET) (pp. 153-159). IEEE, (2016)
  10. Mitchell, M.: An Introduction to Genetic Algorithms. 1<sup>st</sup> edn. MIT press, U.S.A. (1999).
  11. Saucedo, M. Á. B.: MEDIDOR DE pH DE BAJO COSTO PARA APLICACIONES DIDÁCTICAS (LOW-COST pH-METER FOR DIDACTIC APPLICATIONS). Pistas Educativas, 42(137), (2020)
  12. Kulasekaran, A. & Gopal, Andal & Lakshimipathy, R. & Alexander, J.: Modification in pH measurements for getting accurate pH values with different pH meters irrespective of aging and drifts in the meters. International Journal of ChemTech Research. 8. 16-24, (2015)
  13. Christian A. Mejía Ramírez, Martín Montes Rivera: Optimization of a Production Process from Demand and Number of Defective Units through Diffused Logic and Genetic Algorithms. Research in Computing Science 147(2), 109–118, (2017)
  14. David Jesús Segura Cristino, Herón Molina Lozano, Elsa Rubio Espino, Víctor H. Ponce Ponce: Navigation and Obstacle Avoidance System Applying a Fuzzy Control System on an Arduino UNO. Research in Computing Science 148(10), 291–303, (2019)
  15. Camilo Morales Corral, Israel Soto: Control difuso para el seguimiento de trayectoria de un robot móvil. Research in Computing Science 149(8), 71–83, (2020)
  16. Westcott, C.: pH Measurements. Academic Press, (1978).



# ANNEX 4



The Mexican Society for Artificial Intelligence (SMIA)  
and the Centro de Investigación en Computación del Instituto Politécnico Nacional



Award this certificate to

**Rolando Hinojosa Meza, Ernesto Olvera Gonzales, Nivia Escalante Garcia, Martín Montes Rivera**

for 2nd place Best Paper Award with the work  
**Temperature compensation of pH measurements using a fuzzy inference system and genetic algorithms**  
at the workshop

**14th Workshop on Hybrid Intelligent Systems**

held in conjunction with the 20<sup>th</sup> Mexican International Conference on Artificial Intelligence, MICAI 2021.  
Mexico City, Mexico, October 25 - 30, 2021.



**Dr. Félix Castro Espinoza**  
SMIA President



**Dr. Ildar Batyrshin**  
Program Chair



**Dr. Alexander Gelbukh**  
Program Chair



**Dr. Grigori Sidorov**  
Program Chair

